SUBGAP ABSORPTION SPECTROSCOPY IN MICROCRYSTALLINE SILICON THIN FILMS

Oktay GÖKTAŞ

August, 2004

Subgap Absorption Spectroscopy in Microcrystalline Silicon Thin Films

By

Oktay GÖKTAŞ

A Dissertation Submitted to the
Graduate School in Partial Fulfillment of the
Requirements for the Degree of

MASTER OF SCIENCE

Department: Physics
Major: Physics

İzmir Institute of Technology

İzmir, Turkey

August, 2004

We approve the thesis of **Oktay GÖKTAŞ**

Date of Signature

.... **12.08.2004**

Assoc. Prof. Dr. Mehmet GÜNEŞ
Supervisor
Department of Physıcs

.... **12.08.2004**

Assoc. Prof. Dr. Metin TANOĞLU
Department of Mechanical Engineering

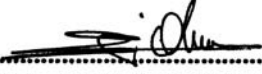

.... **12.08.2004**

Asst. Prof. Dr . Dr. Salih OKUR
Department of Physics

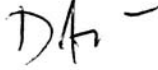

.... **12.08.2004**

Prof. Dr. Durmuş Ali DEMİR
Head of Department of Physics

ACKNOWLEDGMENTS

I am grateful to my advisor, Assoc. Prof. Dr. Mehmet Güneş for his help, support and scientific approach during this study.

I am also thankful to the other members of my thesis committee, Assoc. Prof. Dr. Metin Tanoğlu, and Asst. Prof. Dr. Salih Okur for their comments and suggestions.

I would like to thank İzmir Institute of Technology and department of physics for providing me a full time research assistantship during my master study.

I would like to thank The Scientific and Technical Research Council of Turkey (TÜBİTAK) and the International Bureau of the BMBF, Germany for their support to present work.

I am thankful to Dr. Reinhard Carius, Dr. Fridhelm Finger from Jülich Research Center, Germany, for their helpful discussion and contribution to present work and to Josef Klomfass for PDS measurements and calculations of fringe free absorption coefficient spectra of the films.

My special thanks go to my girlfriend and my family.

I would like to thank all my friends at Izmir Institute of Technolgy.

ABSTRACT

Intrinsic hydrogenated microcrystalline silicon thin films prepared by VHF-PECVD and HW-CVD methods under different deposition conditions have been investigated using steady state photoconductivity method (SSPC), photothermal deflection spectroscopy (PDS) and dual beam photoconductivity (DBP) method, and transmission spectroscopy. Absorption spectra of the investigated thin films were measured in a wide energy region using PDS and DBP. A procedure, for the firs time, was used to calculate fringe free absolute absorption coefficient of thin films from DBP yield spectrum and simultaneously measured transmission signal. The results were found to be in agreement with those of PDS above the bandgap energy. However, there are differences between below the bandgap energy in the spectra of both methods. The differences are discussed to be consistent with the underlying physics of these methods.

For some of investigated thin films there are remaining fringes in the $\alpha(h\nu)$ spectra measured using both methods. This is a strong indication of inhomogeneity present in the films in growth direction. DBP measurements were also performed for ac monochromatic light incident from substrate side in order to investigate the effect of inhomogeneous microstructure of the material on the absorption spectrum. It is found that some films have remaining fringes on their spectra for back ac measurements both for VHF-PECVD and HW-CVD grown thin films, whereas there is no remaining fringes observed for front ac measurements or vice versa. These findings are discussed to be an indication of inhomogeneity in growth direction which is already reported from TEM and Raman study.

Sub-bandgap absorption coefficients α(0.8 eV) were correlated with the silane concentration, which is main parameter to change the microstructure of these films. It is found that the thin films that deposited in the transition region, where a transition from a fully amorphous growth to full microcrystalline growth occurs, have smaller absorption coefficients indicating that the thin films deposited at transition region have less defect density. However, thin films deposited at the highly crystalline region have the highest defect density due to etching effect of H during the deposition. These results are also consistent with reported ESR studies.

ÖZ

VHF-PECVD ve HW-CVD metodları ile büyütülmüş katkısız mikrokrokristal silisyum ince filmler, durağan hal ışıl iletkenlik, ışıl ışın saptırma izgegözlem (PDS)ve iki demetli ışıl iletkenlik (DBP) methodları kulanılarak incelenmiş ve malzemenin mikroyapısının elektronik ve optik özeliklerine etkisi anlaşılmaya çalışılmıştır. Bu malzemelerin soğurma spekturumları geniş bir enerji aralığında elde edilmiştir. İki demetli ışıl iletkenlik (DBP) methodundan girişim saçaksız mutlak soğurma katsayisi izgesinin elde edilebilmesi için bir method, literatürde ilk kez, denenmiş ve elde edilen sonuçlar bağımsız olarak PDS deney düzeneğinden elde edilenlerle karşılaştırılmıştır. PDS ve DBP metodlarından elde edilen soğurma katsayısı izgesinin bant enerjisine kadar uyumlu olduğu gözlenmiş bant enerjisinin altında meydana gelen fark ise iki methodun farklı fiziksel temelere sahip olusuyla acıklanmıstır.

İncelenen fılmlerin bazıları için her iki metot ile elde edilen izgelerinde kalıcı saçaklar gözlenmiş olup bu saçakların varlığı malzemenin homojen olmayan yapısına bağlanmıştır. Bu etkiyi dahada derinlemesine incelemek için DBP deneyleri alışılagelmiş şeklinden hariç olarak, tekrenk ışık alttabaka cam (substrate) tarafından gelecek şekildede yapılmıştır. Bazı filmler için ön taraf ölçümlerinde saçak kalırken bazılarında da durum bunun tam tersidir. Elde edilen sonuçlar bu malzemelerin büyütme doğrultusunda kaydadeger sayılabilecek bir farklılık gösterdiği sonucuna işaret etmektedir.

Elde edilen bant içi sogurma degerleri, 0,8 eV için malzemenin mikroyapısını belirleyen temel parametre olan silane gazı konsantrasyonu ile ilişkilendirilmiştir. Eldeki veriler mikrokristal silisyum için bu film büyütme metodlarında, amorf fazdan mikrokristal faza geçişin gözlendiği kritik silane gazı konsantrasyon degeri civarında büyütülen filmlerin soğurma katsayılarının en düşük olduğunu göstermiştir. Bu degerler geçiş bolgesinde buyutulen ince fılm malzemelerde en az seviyede elektronık kusur bulundğunu göstermektedir. Buna karsılık, düşük silane gazı konsantrasyonlarında büyütülen ince filim malzamlerde cok yüksek yogunluklarda elektronik kusurlar oldugu anlaşılmıştır. Bu bulgular literatürde yayınlanan ESR sonuçları ile de uyumludur.

TABLE OF CONTENST

LIST OF FIGURES………………………………………………...………………vii

LIST OF TABLES………………………………………………………………………xii

Chapter 1. INTRODUCTION………...……………………………………………...1
1.1 Thesis Objectives……………………...……………………………………6

Chapter 2. EXPERIMENTAL…………………..…………………………………...8
2.1 Sample preparation…………………………………………………………...8
2.2 Characterization Techniques…………………………………………….....11
2.21 Steady State Photoconductivity…………………………………… 11
2.2.2 Dual Beam Spectroscopy……………………………………………..14
2.2.2.1 Flux Calibration………………………………………….18
2.2.2.2 Transmission Spectrum………………………………..19
2.2.2.3 Dual Beam Photoconductivity Spectrum………………...20
2.2.3 Photothermal Deflection spectroscopy…………………………….....24
2.2.4 Evaluation of Fringe Free Absorption Coefficients Spectrum from DBP Yield Spectrum………………………………………………….…26

Chapter 3. EXPERIMENTAL RESULTS IN HYDROGENATED MICROCRYSTALLINE SILICON THIN FILMS…………………………………...31
3.1 Introduction……………………………………………………………...31
3.2 Steady State Photoconductivity In Intrinsic μc-Si:H Thin Films……………31
3.3 Sub-Bandgap Absorption Spectra Of Intrinsic μc-Si:H Thin Films…………36
3.3.1 VHF-PECVD Grown Thin Films…………………………………….36
3.3.2 HW-CVD Grown Thin Films……………………………...……50
3.4 Conclusion…………………………………………………………...…71

Chapter 4. DISCUSSION AND CONCLUSSION………..……………………………73
4.1 Future Proposed Research…………………………………………….……..78

REFERENCES ………………………………………………………………………79

APPENDIXES. ……………………………………………………………………….83
Appendix A. Computer Program used for DBP Measurements…………………83
Appendix B. Computer Program For Calculation of α(hν) spectrum……………91

LIST OF FIGURES

Figure 2.1. Crystalline volume fraction of μc-Si:H thin films as a function of silane concentration……………………………………………………………………………..…9

Figure 2.2. Schematic diagram showing the prominent microstructural characteristics of μc-Si:H……………………………………………………………………………………..9

Figure 2.3. Schematic diagram of experimental setup of steady state photoconductivity system.…………………………..………………………………………….………….…12

Figure 2.4. Schematic diagram of dual beam photoconductivity system………… …...17

Figure 2.5. Flux spectrum of Quartz Tungsten Halogen (QTH) lamp obtained using pyroelectric detector……………………………………………………………….....19

Figure 2.6. Transmission spectrum of a μc-Si:H thin film…………………...…….…….…20

Figure 2.7. A typical row and normalized photocurrent spectra of a μc-Si:H thin films measured by DBP method…………………………………………………………...21

Figure 2.8. Power law dependency for ac and dc light…………………...…………..….22

Figure 2.9. Dual beam photoconductivity spectra for different intensities of bias light....23

Figure 2.10. Schematic diagram of photothermal deflection spectroscopy system…... ...25

Figure 2.11. a) Y_{DBP} spectrum normalized to PDS directly. In the inset, the transmission of the film is shown. b) Calculated fringe free absolute $\alpha(h\nu)$ spectrum of DBP and PDS measured independently…………………………………………………………..30

Figure 3.1. (a) σ_{ph} versus generation rate for intrinsic μc-Si:H films prepared using VHF-PECVD method. b) $\mu_n\tau_n$-product versus generation rate of the same intrinsic μc-Si:H thin films………………………………………………………………………….………33

Figure 3.2. (a) σ_{ph} versus generation rate for intrinsic μc-Si:H films prepared using HW-CVD method. b) $\mu_n\tau_n$-product versus generation rate of the same intrinsic μc-Si:H thin films………………………………………………………………………………….34

Figure 3.3. Summary of σ_{ph} (a) and $\mu_n\tau_n$ –product (b) versus generation rate of μc-Si:H thin films deposited by VHF-PECVD and HWCVD techniques…………………………35

Figure 3.4. a) DBP Yield spectrum measured with high and low bias light intensities for a μc-Si:H thin film deposited SC=4.3%. In the inset, phase of both measurements are shown. b) Transmission spectrum of the same sample.………………….…….…………37

Figure 3.5. a) Raw PDS and Y_{DBP} signals of a μc-Si:H thin film. In the inset transmission spectra of both methods are shown. b) Absolute α(hν) spectra of PDS and DBP measurements and that of c-Si and s-Si:H for comparison. In the inset, the phase of PDS and DBP are illustrated……………………………………………………………..39
Figure 3.6. a) Y_{DBP} spectra measured for ac light incident from film side and substrate side for intrinsic μc-Si:H film deposited by VHF-PECVD method with SC=4.3%. In the inset, transmission spectrum of the same sample is shown. b) Calculated α(hν) spectra of the same sample for both front and back ac illumination cases. In the inset, phase of both measurement signals are shown. ………………………………………………………41
Figure 3.7. a) Y_{DBP} spectra of a intrinsic μc-Si:H thin film deposited using VHF-PECVD with SC=6.25% for ac light incident from substrate side and film side. In the inset, transmission spectrum of the sample is shown. b) Calculated absolute α(hν) spectra of both DBP front and back ac illumination measurements. In the inset, phase of DBP signal are shown……………………………………………………………………………43
Figure 3.8. a) Raw PDS and Y_{DBP} spectra measured at high and low bias light intensities. In the inset, corresponding transmission spectra are given for a μc-Si:H sample deposited with SC=3.06 %. b) The calculated α(hν) spectra of PDS, phase corrected PDS, and those of DBP measurements. In the inset, the phase of PDS and DBP are given………..……45
Figure 3.9. a) Raw PDS and Y_{DBP} spectra measured at high and low bias light intensities. In the inset, corresponding transmission spectra are given for a μc-Si:H sample deposited with SC=3.69 %. b) The calculated α(hν) spectra of PDS, phase corrected PDS, and those of DBP measurements. In the inset, the phase of PDS and DBP are given…….………..46
Figure 3.10. a) Raw PDS and Y_{DBP} spectra measured at high and low bias light intensities. In the inset, corresponding transmission spectra are given for a μc-Si:H sample deposited with SC=4.96%. b) The calculated α(hν) spectra of PDS, phase corrected PDS, and those of DBP measurements. In the inset, the phase of PDS and DBP are given………………47

Figure 3.11. a) Raw PDS and Y_{DBP} spectra measured at high and low bias light intensities. In the inset, corresponding transmission spectra are given for a μc-Si:H sample deposited with SC=6.25 %. b) The calculated α(hν) spectra of PDS, phase corrected PDS, and those of DBP measurements. In the inset, the phase of PDS and DBP are given..……………..48
Figure 3.12. Comparison of the α(hν) values at sub-bandgap energy 0.8 eV independently measured by PDS and DBP front ac illumination for intrinsic μc-Si:H thin films deposited by VHF-PECVD. ……………………………………………………………………...49
Figure 3.13. a) Raw PDS and DBP Yield spectra of a μc-Si:H thin film deposited by HW-CVD method with SC=2.5%. In the inset, simultaneously measured corresponding transmission signal of PDS and DBP methods are shown. b) Corresponding absolute α(hν) spectra independently obtained from PDS and DBP measurements. In the inset the phase of PDS and DBP measurements are shown……………………………………..51
Figure 3.14. a) Raw PDS and DBP Yield spectra of a μc-Si:H thin film deposited by HW-CVD method with SC=2.5%. In the inset, simultaneously measured corresponding transmission signal of PDS and DBP methods are shown. b) Corresponding absolute α(hν) spectra independently obtained from PDS and DBP measurements. In the inset the phase of PDS and DBP measurements are shown…………………………………..…52
Figure 3.15. a) Raw PDS and DBP Yield spectra of a μc-Si:H thin film deposited by HW-CVD method with SC=2.5%. In the inset, simultaneously measured corresponding transmission signal of PDS and DBP methods are shown. b) Corresponding absolute α(hν) spectra independently obtained from PDS and DBP measurements. In the inset, the phase of PDS and DBP measurements are shown……………………………………..……54
Figure 3.16. a) DBP yield spectra of a a μc-Si:H thin film deposited by HW-CVD method with SC=4% for front and back ac illumination, which is shifted vertically for clarity together with raw PDS spectrum. In the inset, corresponding transmission signals of DBP front and back ac illuminations are shown. b) Calculated α(hν) spectra of DBP measurements for both front and back ac illuminations and that of PDS independently measured on the same sample. In the inset, phase of DBP and PDS are shown…………56

Figure 3.17. a) Raw PDS and DBP Yield spectra of a μc-Si:H thin film deposited by HW-CVD method with SC=2%. In the inset, simultaneously measured corresponding transmission signal of PDS and DBP methods. b) Corresponding absolute α(hν) spectra independently obtained from PDS and DBP measurements. In the inset the phase of PDS and DBP measurements are shown……………………………………………….………58
Figure 3.17. c) DBP yield spectra of a a μc-Si:H thin film deposited by HW-CVD method with SC=4% for front and back ac illumination, which is shifted vertically for clarity together with raw PDS spectrum. In the inset the transmission of the sample is shown. d) Calculated α(hν) spectra of DBP measurements for both front and back ac illuminations and that of PDS independently measured on the same sample. In the inset phase of DBP and PDS are shown……………………………………………………………………….59
Figure 3.18. a) Raw PDS and DBP Yield spectra of a μc-Si:H thin film deposited by HW-CVD method with SC=4.5%. In the inset, simultaneously measured corresponding transmission signal of PDS and DBP methods. b) Corresponding absolute α(hν) spectra independently obtained from PDS and DBP measurements. In the inset, the phase of PDS and DBP measurements are shown…………………………………………………………60
Figure 3.18 c) DBP yield spectra of a a μc-Si:H thin film deposited by HW-CVD method with SC=4.5% for front and back ac illumination, which is shifted vertically for clarity together with raw PDS spectrum. In the inset the transmission of the sample is shown. d) Calculated α(hν) spectra of DBP measurements for both front and back ac illuminations and that of PDS independently measured on the same sample. In the inset, phase of DBP and PDS are shown……………………………………………………………………….61
Figure 3.19 a) Raw PDS and DBP Yield spectra of a μc-Si:H thin film deposited by HW-CVD method with SC=5% for substrate temperature of 185 ^{o}C . In the inset, simultaneously measured corresponding transmission signal of PDS and DBP methods. b) Corresponding absolute α(hν) spectra independently obtained from PDS and DBP measurements. In the inset, the phase of PDS and DBP measurements are shown………62

Figure 3.19 c) DBP yield spectra of a a μc-Si:H thin film deposited by HW-CVD method with SC=5% (Substrate temperature is 185 ^{o}C) for front and back ac illumination, which is shifted vertically for clarity, together with raw PDS spectrum. In the inset, the transmission of the sample is shown. d) Calculated α(hν) spectra of DBP measurements for both front and back ac illuminations and that of PDS independently measured on the same sample. In the inset, phase of DBP and PDS are shown…………..……………….63
Figure 3.20 a) Raw PDS and DBP Yield spectra of a μc-Si:H thin film deposited by HW-CVD method with SC=5% for substrate temperature of 215 ^{o}C . In the inset, simultaneously measured corresponding transmission signal of PDS and DBP methods. b) Corresponding absolute α(hν) spectra independently obtained from PDS and DBP measurements. In the inset, the phase of PDS and DBP measurements are shown………64
Figure 3.20 c) DBP yield spectra of a a μc-Si:H thin film deposited by HW-CVD method with SC=5% (Substrate temperature is 215 ^{o}C) for front and back ac illumination, which is shifted vertically for clarity together with raw PDS spectrum. In the inset, the transmission of the sample is shown. d) Calculated α(hν) spectra of DBP measurements for both front and back ac illuminations and that of PDS independently measured on the same sample. In the inset, phase of DBP and PDS are shown…………………………………………...65
Figure 3.21 a) Raw PDS and DBP Yield spectra of a μc-Si:H thin film deposited by HW-CVD method with SC=6%. In the inset, simultaneously measured corresponding transmission signal of PDS and DBP methods. b) Corresponding absolute α(hν) spectra independently obtained from PDS and DBP measurements. In the inset, the phase of PDS and DBP measurements are shown……………………………………………………66
Figure 3.21 c) DBP yield spectra of a a μc-Si:H thin film deposited by HW-CVD method with SC=4.5% for front and back ac illumination, which is shifted vertically for clarity, together with raw PDS spectrum. In the inset the transmission of the sample is shown. d) Calculated α(hν) spectra of DBP measurements for both front and back ac illuminations and that of PDS independently measured on the same sample. In the inset, phase of DBP and PDS are shown……………………………………………………………………..…67

Figure 3.22 a) Raw PDS and DBP Yield spectra of a μc-Si:H thin film deposited by HW-CVD method with SC=7%. In the inset, simultaneously measured corresponding transmission signal of PDS and DBP methods. b) Corresponding absolute α(hν) spectra independently obtained from PDS and DBP measurements. In the inset, the phase of PDS and DBP measurements are shown……………………………………………………….68
Figure 3.22 c) DBP yield spectra of a a μc-Si:H thin film deposited by HW-CVD method with SC=7% for front and back ac illumination, which is shifted vertically for clarity, together with raw PDS spectrum. In the inset, the transmission of the sample is shown. d) Calculated α(hν) spectra of DBP measurements for both front and back ac illuminations and that of PDS independently measured on the same sample. In the inset, phase of DBP and PDS are shown…………………………………………………………….…………69
Fig 3.23 Comparison of the α(hν) values at sub-bandgap energy 0.8 eV independently measured by PDS and DBP front ac illumination for intrinsic μc-Si:H thin films deposited by HW-CVD. ……………………………………………………………………………70
Figure 4.1 The effect of microstructure characterized by the crystalline volume fraction I_C^{RS} on the sub-bandgap absorption coefficient α(0.8 eV) for both HW-CVD and VHF-PECVD μc-Si:H thin films…………………………………………………………..77

LIST OF TABLES

Table 2.1. Deposition parameters and thickness of μc-Si:H thin films used in this study..10

CHAPTER 1

INTRODUCTION

Intrinsic hydrogenated microcrystalline silicon (μc-Si:H) has recently become a very attractive material for thin film solar cells since, it is fully compatible with the existing thin film technology used for amorphous silicon based solar cells [1-3]. Thin films μc-Si:H materials can be deposited at low substrate temperatures on very cheap substrates and on large areas using plasma enhanced chemical vapor deposition methods (PECVD) [1, 4] and hot-wire chemical vapor deposition HW-CVD [5-7]. Intrinsic microcrystalline silicon thin films have also extended spectral response of crystalline silicon in the infrared region [2]. In addition to above advantages, much progress has been made to improve fabrication methods in order to achieve high deposition rates and high electronic quality.

Hydrogenated microcrystalline silicon, contrary to crystalline silicon, does not have homogenous structure. Its microstructure is much more complicated compared to crystalline and amorphous silicon. It is a composition of crystalline grains, grain boundaries, amorphous regions and voids in various amounts. Hydrogenated microcrystalline silicon was first deposited by Veprek and Marecek [8] in 1968. Here they used a special kind of plasma deposition technique. The deposition temperature was 600 ℃. Thereafter its first fabrication, deposition of μc-Si:H layers were reported using radio frequency glow discharge [9,10], using silane (SiH_4) as a source gas strongly diluted with hydrogen in order to induce formation of microcrystalline silicon rather than amorphous silicon. In these early works the deposition rates were well below 1 Å/s.

Having an indirect bandgap, μc-Si:H has a relatively low absorption coefficient, compared to that of amorphous silicon, in the visible region of solar spectrum. Therefore correspondingly ticker layers needed to achieve sufficient absorption and photogeneration. In addition to above reason, grain boundaries present in microcrystalline silicon were considered as an obstacle for electronic transport. Due to poor lifetime of electronic charge carriers and low deposition rates, several years passed for the first attempt of thin

film silicon solar cells consisting of μc-Si:H as a photovoltaically active layer [2]. Finally, in 1991 preliminary results were reported by Lucovsky et al. [11] and Faraji et al. [12]. Thereafter, entirely microcrystalline p-i-n and n-i-p type-silicon solar cells were reported [13, 14]. Meanwhile, significantly high deposition rates were achieved using very high frequency PECVD [15, 16, 1] , RF-PECVD [17] and Hot wire CVD [18, 6,4] methods. Intrinsic μc-Si:H thin film layers, fabricated by a variety of techniques, have been investigated widely as a potential material for optoelectronic thin film devices such as thin-film transistor, position sensors, color sensors, and especially for solar cells application. Microcrystalline silicon is also used in a tandem concept with amorphous silicon to form so called micromorph solar cells [19]. Recent recorded efficiency is about 10% and 14% for single junction and tandem junction solar cells, respectively [20]. Pilot production of large area modules has already been started by a Japanese company [5,2]. Thus, the potential of hydrogenated microcrystalline silicon for optoelectronic applications has gradually become important.

The most important feature of μc-Si:H is its microstructure. The volume fraction and spatial distribution of amorphous and crystalline phases throughout the material is an important parameter for its electronic and optical properties. It is well known from the first studies [21] that hydrogen dilution is an important parameter in determining the microstructure whatever deposition process is used such as VHF PECVD (Very High Frequency Plasma Enhanced Chemical Vapor Deposition) or HW CVD (Hot Wire Chemical Vapor Deposition). If hydrogen dilution is zero, the resulting layers are fully amorphous. If hydrogen is added to plasma, the layer quality is marginally altered but the layer remains amorphous until a threshold concentration is reached. If hydrogen concentration is further increased, at a certain value of SC ($SC=[SiH_4]/([Sih_4]+[H_2])$), the formation of crystalline regions begins. Then with the increasing SC, the crystalline volume fraction increases, and microcrystalline silicon layers wrapped by the amorphous tissue like regions are obtained. Several methods are used to characterize the structural properties of microcrystalline silicon thin films.

One of the most used technique to characterize structural properties of μc-Si:H thin films is Raman spectroscopy [1,21,23-26]. The technique is based on inelastic scattering of photon in the media because of interaction of photons and phonons (lattice vibrations).

The experiments are usually done in the back scattering geometry, where incident beam is perpendicular to the sample surface. A light beam of an Argon laser (λ_0=488 nm) or a HeNe laser of wavelength of 647 nm is often used for excitation [6,27]. Typical Raman peak of c-Si is symmetric and located at 520 cm^{-1} with a width (full width at half maximum) of about 3.5 cm^{-1}. As for a-Si:H films , a broad distribution is centered at 480 cm^{-1} with a typical width of about 60 cm^{-1}. The spectra of fully microcrystalline silicon thin films are asymmetric and located at 518 cm^{-1} with a width of 12 cm^{-1}. It has a tail extending towards low phonon frequencies. The tail is attributed to the presence of amorphous phase in the material. With increasing silane concentration the spectrum changes from a fully crystalline to almost fully amorphous phase. Between these two spectra, the spectra of films are superposition of these two peaks with different contribution. However, the Raman spectra can not provide a unique measure of the structure since the Raman cross sections and optical absorption coefficients of the amorphous and crystalline phases are generally different and may depend on the size of the crystallites, grain boundaries and strain in the crystallites [26, 27]. However, a semi-quantitative measure for the volume fraction of crystallites is generally evaluated from Raman spectra. The ratio of the scattering intensity of the crystalline phase to the total scattering intensity is used for such a measure where the area of the peaks determined from Gaussian fits to the spectra.

X-ray diffraction (XRD) is another measurement technique used for structural characterization of μc-Si:H thin films [28]. Crystalline silicon has diffraction patterns with sharp peaks at diffraction angels (2Θ) 28.4°, 47.3° and 56.1° for the <111>, <220> and <311> planes respectively. As for amorphous silicon, the peaks are broad. First peak is at about 27° and the second is at 52°. To determine the crystalline volume fraction of the films, the integrated intensities of the amorphous and crystalline peaks can be used with calibration of crystalline and amorphous powder spectra [27]. The crystalline peaks are broadened with increasing silane concentration. Finally, the amorphous phase dominates the spectra.

TEM is widely used as a characterization technique to obtain information about microstructure of μc-Si:H thin films. The TEM investigation of μc-Si:H thin films shows

that with the increasing hydrogen dilution crystalline volume fraction increases [1,28, 29]. At high SC, crystalline growth starts near the substrate surface and results in a columnar growth. The size of crystalline grains depends on deposition conditions. These crystalline regions are not perfectly crystalline but exhibit a large amount of twin defects [28]. The space between these grains is filled either by an amorphous network or by voids. The amorphous volume fraction is low. With increasing silane concentration, the volume fraction of crystalline phase decreases. The size of crystalline grains decrease and amorphous phase dominates the structure. The structural composition of microcrystalline silicon is highly sensitive to deposition parameters. Therefore, electronic and optical properties of microcrystalline silicon thin films are highly sensitive to deposition parameters such as silane concentration and substrate temperature. The main parameter is the SC, which changes electronic, optical and structural properties of the material. Having such a complicated structure, defect states present in the material has been a subject of ongoing research.

An important property of a photoactive material is its absorption coefficient spectrum. Microcrystalline silicon exhibits extended spectral response of crystalline silicon in infrared region and has absorption coefficient higher than that of crystalline silicon in the visible region [30,31]. Higher optical absorption is generally attributed to light scattering because of rough surface of μc-Si:H [32]. It might also be due to absorption of amorphous region, especially above 1.8 eV, present in the material since μc-Si:H is a composition of crystalline region , amorphous region and voids. Absorption enhancement bellow 1.8 eV down to 1.2 eV is attributed, in addition to light scattering [32], to strain effect in the grain and grain boundaries [33]. The absorption below 1.2 eV is called sub-bandgap absorption and is due to defect states present in the bandgap. Therefore, sub-bandgap absorption can be correlated with defect density present in the material.

These defect states on the surface and in the bulk of μc-Si:H are due to its inhomogeneous microstructure. These are due to broken Si bonds and unsatisfied bond in amorphous regions and also grain boundaries between crystalline regions. These defects are electronically active and play an important role in device performance. Several

methods have been used to characterize the defects such as electron spin resonance (ESR), steady state photoconductivity, dark conductivity, and optical absorption measurements.

Electron Spin Resonance (ESR) has widely been used to investigate defect states present in μc-Si:H. ESR is a powerful tool to probe defect states providing that they are paramagnetic. Many groups have performed ESR studies and several signals (g-values-gyromagnetic ratio) have been identified [34-37,24]. However, compared to a-Si:H , identification of such defects is less understood because of complicated structure of μc-Si:H. The g-value is defined as $g=h\nu/\mu_B B$. Here h is the Planck constant, ν is the microwave frequency at resonance, B is magnetic field at resonance and μ_B is the Bohr magneton. The resonance at 2.0052 is attributed to Si dangling bonds. The g value found for μc-Si:H is smaller than the g-value of a-Si:H [37]. When compared to polycrystalline silicon the spin densities are smaller which indicates an excellent hydrogen passivation. Another resonance is observed at g=1.996-1.998 and attributed to conduction electrons in the crystalline regions in the material. The third resonance is observed at 2.0043 and not identified yet.

Dark conductivity and steady state photoconductivity is widely used to obtain information about the nature of defects, transport, position of Fermi level, and recombination kinetics of photogenerated carriers in microcrystalline silicon thin films [34,29,38,39]. Intrinsic microcrystalline silicon has a slightly n-type conduction character [34]. In general, the dark conductivity tends to decrease with increasing silane concentration [29]. However, the conductivity versus reciprocal temperature curves can not be fit with a single activation energy [38].

Optical absorption measurements are also of great importance for characterization of optical properties of the photovoltaic materials. Photothermal deflection spectroscopy (PDS), originally established for amorphous silicon [40-42] has widely been used to measure absolute optical absorption coefficient spectrum of μc-Si:H thin films [6,43] in the visible and near infrared region. However, it suffers from substrate absorption effect since its contribution dominates the spectrum below 1.2 eV. Therefore, it is difficult to obtain accurate absorption coefficient below the bandgap energy of μc-Si:H using this techniques and it becomes rather difficult to compare different materials prepared with different deposition conditions. Alternatively photoconductivity techniques such as

constant photocurrent method (CPM), both in standard [44] and absolute mode [45] have been used to obtain absorption spectrum of μc-Si:H thin films [46]. However, in CPM technique, since low generation rate of monochromatic light is used, the lifetime of electrons is almost constant and therefore only occupied defect states below the Fermi level can be detected.

Another photoconductivity-based technique which has been extensively used for a-Si:H is dual beam photoconductivity method (DBP) [47-49]. The major advantage of DBP over CPM is that different bias light intensities can be used to detect more gap states since DBP has an intensity dependence on bias light intensity in the sub-bandgap region. Therefore by changing bias light intensity, additional information can be obtained about defect states in the gap of material. No study has been reported using DBP on μc-Si:H thin films until our recently reported study [50] where DBP yield spectrum was directly normalized to PDS results measured on the same sample. It was reported that DBP and PDS are complementary methods to investigate optical and electrical properties of microcrystalline silicon thin films.

As stated above μc-Si:H has a complicated structure and the parameters that lead to best device performance remains less understood. An extensive research has been carried out to better characterize the preparation of the intrinsic μc-Si:H that lead the best device performance depending on deposition parameters. However, there are many open questions to understand its physical properties and underlying physics involved.

1.1 Thesis Objectives

Since hydrogenated microcrystalline silicon is one of the most promising materials for large area solar cell application due to its unique properties, it is crucial to characterize material properties such as optical absorption spectra and defect states that present in the bandgap. This is important for describing best deposition parameters that leads best device performance.

The objective of this thesis is to obtain reliable absorption coefficient spectrum of intrinsic μc-Si:H thin films over a wide range of energy especially in the sub-bandgap region and to learn the effect of inhomogeneous structure of material on the absorption

coefficient spectra of the intrinsic μc-Si:H. Since absorption coefficient in the sub-bandgap is related to the defects states present in the gap of material, it is important to use a convenient characterization technique that is sensitive to the bulk defects states.

In this thesis, DBP method will be used to obtain absorption coefficients in a wide energy region, especially in the sub-bandgap energies, which are related to defect states present in the bandgap of μc-Si:H. For the first time, the interference fringe free absolute absorption coefficient spectrum is going to be calculated from the relative DBP yield spectrum and simultaneously measured transmission signal using procedure based on the Ritter-Weiser formula [51]. Then the resulting absolute absorption coefficient spectrum will be compared with that independently obtained from the PDS measurements. Finally, the absorption coefficients at sub-bandgap energy region will be taken as a comparison criterion to understand the effect of deposition conditions, especially the silane concentration and crystalline volume fraction, on the electronic and optical properties of intrinsic μc-Si:H thin films deposited by two different methods, VHF-PECVD and HW-CVD.

CHAPTER 2

EXPERIMENTAL

2.1 Sample Preparation

There are many deposition systems that used for deposition of μc-Si:H thin films. Intrinsic μc-Si:H thin films used in this study are deposited using very high frequency plasma enhanced chemical vapor deposition (VHF-PECVD) [29] and hot-wire chemical vapor deposition (HW-CVD) [6] methods in Jülich Research Center, Germany.

In PECVD, the most common configuration is a parallel plate capacitor structure. The plasma is electrically excited with an a.c. signal. The excitation frequency is either the standard value of 13.56 MHz, radio frequency, (RF-PECVD) or between 13.56-110 MHz, very high frequency, (VHF-PECVD). In plasma deposition, electrons impacts with SiH_4 molecules and results in a dissociation process and the created SiH_3 radicals are considered to be the most important species for microcrystalline deposition [52].

HW-CVD also called catalytic chemical vapor deposition (Cat-CVD) [53,54] is a relatively new deposition technology and relies on the catalytic decomposition of silane or silane/hydrogen mixture at a resistively heated filament. In the HW-CVD, tungsten or tantalum is usually used as filament. In this system, gases are decomposed to radicals at the surface of the filament that has a temperature higher than 1500 °C. The resulting radicals diffuse to and are deposited on the substrate. The production of radicals in HWCVD is very high compared to PECVD, which leads to a high deposition rate.

The deposition rate, crystalline volume fraction, optical and electrical properties of deposited thin films is strongly dependent on the deposition parameters such as plasma excitation frequency, substrate temperature and hydrogen dilution [7]. The crystalline volume fraction obtained from Raman and XRD measurements depending on silane concentration and schematic diagram showing the microstructure of μc-Si:H is presented in Figure 2.1 and Figure 2.2, respectively.

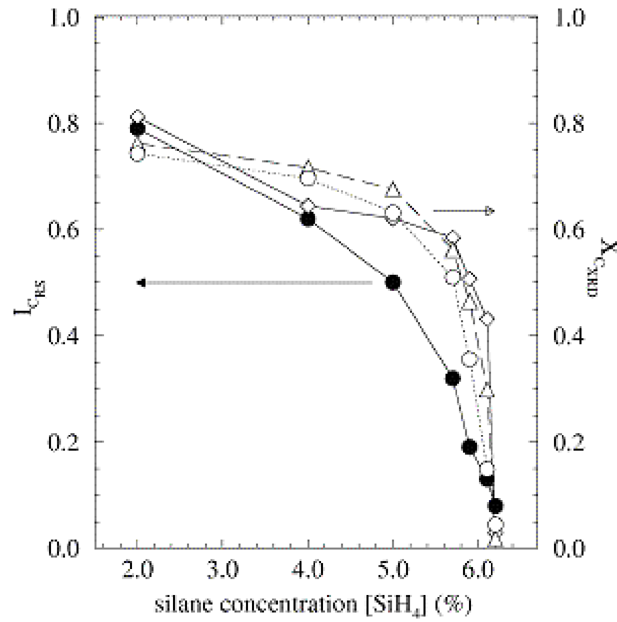

Figure 2.1 Crystalline volume fraction of μc-Si:H films as a function of SC; Raman: • , XRD: ◊ [111], Δ [220], ο [311] After ref [28]

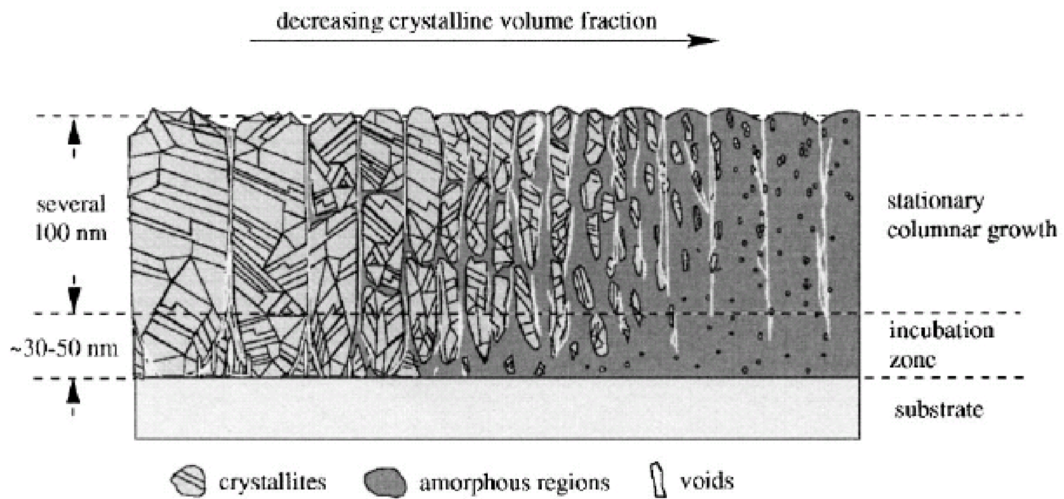

Figure 2.2 Schematic diagram showing the prominent microstructural characteristics of μc-Si:H. After ref [28]

Table 2.1 Deposition parameters and thickness of μc-Si:H thin films used in this study

VHF-PECVD Thin Films			
Sample name	Silane Concentration (SC)	Thickness (T) (μm)	Substrate Temperature (T_S) (^oC)
00c338	4.96	0.70	200
00c341	3.69	0.62	200
00c345	6.25	0.78	200
00c348	4.32	0.60	200
00c354	3.06	0.40	200
HW-CVD Thin Films			
Sample name	Silane Concentration (SC)	Thickness (T) (μm)	Substrate Temperature (T_S) (^oC)
01c320	4	0.68	220
01c328	2.5	0.73	220
01c341	5	0.68	185
02c003	6	0.73	215
02c004	5	0.74	215
02c020	7	0.88	220
02c077	4.5	0.59	220
02c084	2	0.52	210

At lower SC's crystalline volume fraction is very low and amorphous phase dominates the structure. As the silane concentration decreases, crystalline regions increase. Then the structure becomes a mixture of crystalline grains and surrounding amorphous tissues. For the lowest SC's, highly crystalline intrinsic films are grown in a columnar structure. Between the grains, defects are present due to etching effect of the higher hydrogen dilutions.

Intrinsic μc-Si:H samples were deposited using both methods on a borosilicate glass with thickness varying between 0.4 μm to 0.9 μm. Coplanar metal electrodes were then evaporated on the μc-Si:H layer with a length of 0.5 cm and width of 0.5 mm using Silver or Chromium metals. Coplanar sample were used to measure dark and steady state photoconductivity and DBP spectrum. For PDS measurement, μc-Si:H thin film on glass substrate is used without any need for contacts. The intrinsic μc-Si:H sample used in this thesis are listed in Table 2.01

2.2 Characterization Techniques

In this section, experimental techniques that used in this thesis such as steady state photoconductivity, dual beam photoconductivity, and photothermal deflection spectroscopy and transmission spectroscopy will be explained in detail. Finally, the procedure that is used to obtain absolute absorption coefficient spectrum for dual beam photoconductivity method will be given.

2.2.1 Steady State Photoconductivity

Steady state photoconductivity experiments are performed in a homemade steel box as shown in Figure 2.3. An Osram 250 W ENH lamp was used as whit light source. The lamp is cooled by a fan. Interference filters-800, 750, 690 nm- were used to obtain monochromatic light. An RG-610 bandpass filter was also used to obtain higher generation rates. Neutral density filters, which transmit 0.1%, 1%, 10%, and 50% of incoming light beam, were used to adjust intensity of monochromatic light to lower the flux values. Applied voltage was kept in the ohmic regime. A Keitley 6517A electrometer was used to measure dark and photo current. A calibrated silicon p-i-n photodiode having a 14.5 mm^2 active area was used for calibration of incident monochromatic light.

For a sample in coplanar geometry photoconductivity, σ_{ph}, can be derived using Ohm's law.

$$\sigma_{ph} = \frac{I_{ph} d}{Vtl} \quad \left((\Omega cm)^{-1}\right) \tag{2.1}$$

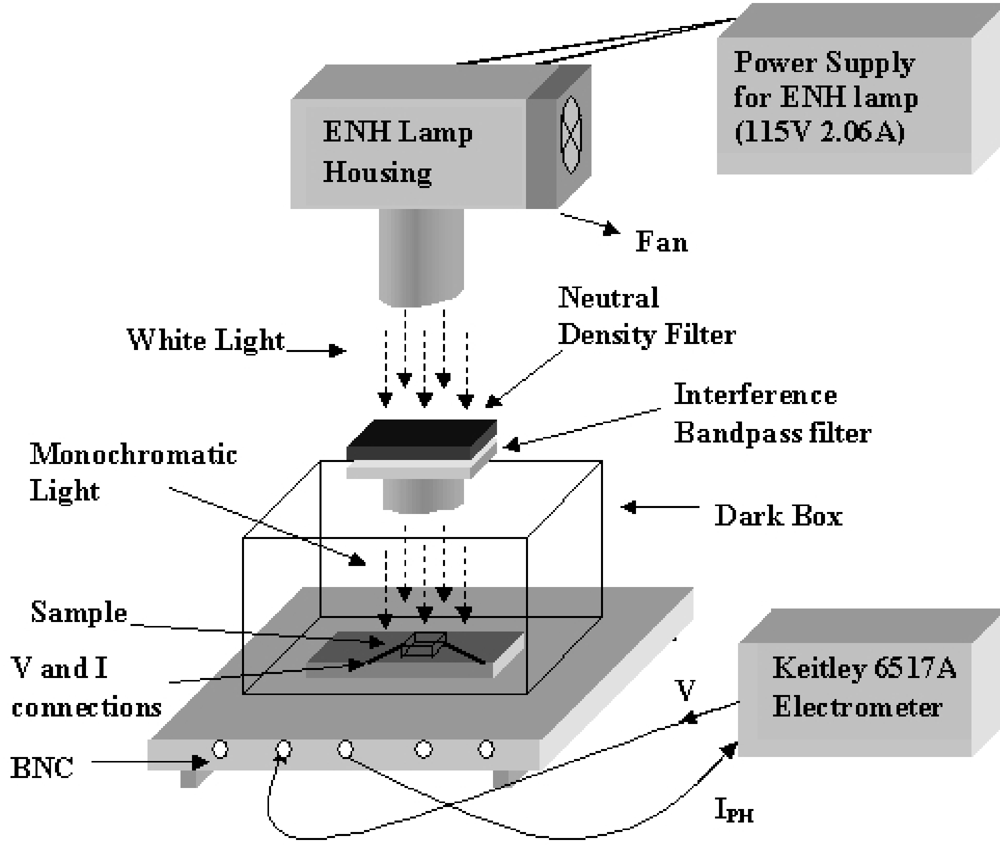

Figure. 2.3. Schematic diagram of experimental setup of steady state photoconductivity system. After ref. [55]

where I_{ph} is photocurrent, d is separation of electrodes, V is applied voltage, t is the thickness of the sample and l is the length of the electrodes. On the other hand, photoconductivity is written as follows,

$$\sigma_{ph} = q\mu_n n + q\mu_p p \qquad (\Omega cm)^{-1} \tag{2.2}$$

where μ_n and μ_p are extended state mobility of free electrons and holes, n and p are the number of free electrons and holes per cm^3 in their respective extended states. Intrinsic μc-Si:H films shows slightly n-type conduction, therefore, only electron dominated conduction is measured in the samples. Using measured photoconductivity, σ_{ph} becomes

$$\sigma_{ph} \cong q\mu_n n \quad (\Omega cm)^{-1} \tag{2.3}$$

Free majority carrier density *n* is created by the generation rate of monochromic light as:

$$n = G\tau_n \quad \left(cm^{-3}\right) \tag{2.4}$$

where G is generation rate and τ_n is lifetime of free electrons. Finally, one of the most important information about the photogenerated electrons, $\mu_n\tau_n$, can be obtained from the measured photoconductivity.

$$\mu\tau = \frac{\sigma_{ph}}{qG} \quad \left(cm^2V^{-1}\right) \tag{2.5}$$

$\mu_n\tau_n$-product is also called "photosensitivity" of the material.

The G of electrons is expressed as follows.

$$G = \frac{F(1-R)[1-\exp(-\alpha t)]}{t} \qquad \left(cm^{-3}s^{-1}\right) \tag{2.7}$$

where R is reflection from film surface, α is the absorption coefficient at given wavelength of monochromatic light, t is the thickness of the film and F is the incident flux calibrated using a p-i-n photodiode, as in Eq. 2.8.

$$F(h\nu) = \frac{I_{ph}(h\nu)}{AQE(h\nu)q} \quad \left(cm^{-2}s^{-1}\right) \tag{2.8}$$

where $I_{ph}(h\nu)$ is corresponding photocurrent measured by p-i-n photodiode at photon energy $h\nu$, *A* is the area of the detector, $QE(h\nu)$ is the quantum efficiency of pin photodiode at energy $h\nu$, and *q* is the electron charge.

Steady state photoconductivity has a non-integer power low dependence on light intensity or on generation rate.

$$\sigma_{ph} \propto G^{\gamma} \quad (\Omega - cm)^{-1} \tag{2.9}$$

and

$$\mu\tau \propto G^{(\gamma-1)} \quad \left(cm^2 V^{-1}\right) \tag{2.10}$$

where γ is the exponent and related to recombination kinetics of light generated electron-hole pairs in the material. Steady state photoconductivity gives information about recombination kinetics of carriers as well. For bimolecular recombination kinetics as in crystalline silicon, γ =0.5 and electrons in the conduction band recombine directly with holes in the valance band. For $0.5< \gamma \leq 1.0$ recombination occur via recombination centers in the bandgap, which is called monomolecular recombination kinetics.

2.2.2 Dual Beam Photoconductivity Spectroscopy

The dual beam photoconductivity (DBP) technique [47-50] is based on measurement of ac photoconductivity as a function of energy of incident monochromatic light. In DBP technique two light beams are used: a uniformly absorbed dc pump beam (bias light) and a monochromatic ac light chopped at a frequency of 13 Hz. Generation rate of ac light, $g(h\nu)$, is small compared to generation rate of dc pump beam, $G(h\nu)$, thus $g(h\nu) << G(h\nu)$. The use of high generation dc bias light is to keep free carrier lifetime constant, thus the electron and hole quasi-Fermi levels are kept constant during the measurements. This means that occupation statistics of the defect states is not changing during the DBP measurements.

Photoconductivity for a sample in coplanar geometry is defined previously as in 2.3. The contribution of hole transport is negligible, since the mobility –lifetime product of holes can be neglected as compared to that of electrons.

$$\sigma_{ph} = q\mu_n n \tag{2.11}$$

Eq. 2.11 can be written in the following form for ac photoconductivity, $\sigma_{ph}(a.c)$, using the relation between free electrons and generation rate of ac light: $\eta(a.c)=\tau_n g(h\nu)$ since the number of electrons can be written in terms of lifetime and generation rate such that $n=\tau_n G$, so

$$\sigma_{ph}(a.c.) = q\mu_n \tau_n g(h\nu) \tag{2.12}$$

Using the expression given in Eq. 2.7 for generation rate and expanding the exponential term in the first order in energy region where the condition of uniform absorption of light is satisfied such that $\alpha t<<1$, photoconductivity can be written as in Eq. 2.13. It must be kept in mind that this equation is valid only if absorption coefficient and thickness product (αt) is smaller than unity.

$$\sigma_{ph}(ac) = q\mu_n \tau_n F_{ac}(h\nu)(1-R(h\nu))\alpha(h\nu) \tag{2.13}$$

Assuming that reflectance, $R(h\nu)$, is constant over the energy region that measurements carried out, together with photoconductivity divided by incident flux gives normalized photoconductivity, which is called DBP yield spectrum, $Y_{DBP}(h\nu)$

$$Y_{DBP}(h\nu) = \frac{\sigma_{ph}(ac)}{F_{ac}(h\nu)} \propto [q\mu\tau(1-R)]\alpha(h\nu) = C\alpha(h\nu) \tag{2.14}$$

where

$$C = \left[q\mu_n \tau_n (1-R)\right]$$

As stated at the beginning of this section, dc bias light is used to keep $\mu_n\tau_n$ product to be constant, so $\alpha(h\nu)$ is proportional to the DBP yield by only a constant, therefore

$$\alpha(h\nu) \propto Y_{DBP} \tag{2.15}$$

or

$$\alpha(h\nu) = CY_{DBP} \tag{2.16}$$

where C is a constant. DBP method does not provide absolute absorption coefficients since it is a relative measurement method. Equation 2.15 implies that DBP yield is proportional to absorption coefficient. In general, DBP spectrum is normalized to absolute absorption coefficient spectrum obtained from transmission and reflection measurement T&R [56] or from photothermal deflection spectroscopy PDS [50] in order to obtain absolute absorption coefficients at lower energies. DBP yield spectrum also exhibits interference fringes due to thickness of the films. These interference fringes are generally removed using fast Fourier transform (FFT) procedure [57]. However, a significant error can be introduced in this procedure for determining fringe free spectrum. At the end of this section, a procedure based on Ritter-Weiser formula will be discussed in order to obtain fringe free absolute absorption coefficients from DBP yield spectrum. The method has already been used for CPM [45] but there have been no attempt to use it for DBP. We will show that the procedure can appropriately be used in the DBP method. Then, the calculated spectrum will be compared to that obtained by PDS method.

The dual beam photoconductivity system is shown in Figure 2.4. A Quartz Tungsten Halogen (QTH) lamp is placed in an Oriel 66182 model lamp housing as a white light source and controlled by a 300 W Radiometric power supply. An Oriel monochromator having 0.2 nm sensitivity was used with a 600-lines/mm grating and was controlled by a Oriel monochromator driver. A set of red light emitting diodes (LED) was used to provide the dc bias light. A chopper blade was mounted near the entrance slit of monochromator to chop white light and controlled by a chopper controller. The chopping frequency was 13 Hz. A filter driver having three long pass filters with wavelength of 500 nm, 700 nm, 900 nm, and a single crystalline silicon with wavelength of 1100 nm was placed at the exit slit of monochromator in order to cut-off second and high order wavelength refraction peaks and controlled by an Oriel filter driver to change filters. Flux is calibrated by means of a pyroelectric detector. A homemade sample holder was used with BNC connections to hold samples and pyroelectric detector. External dc bias voltage

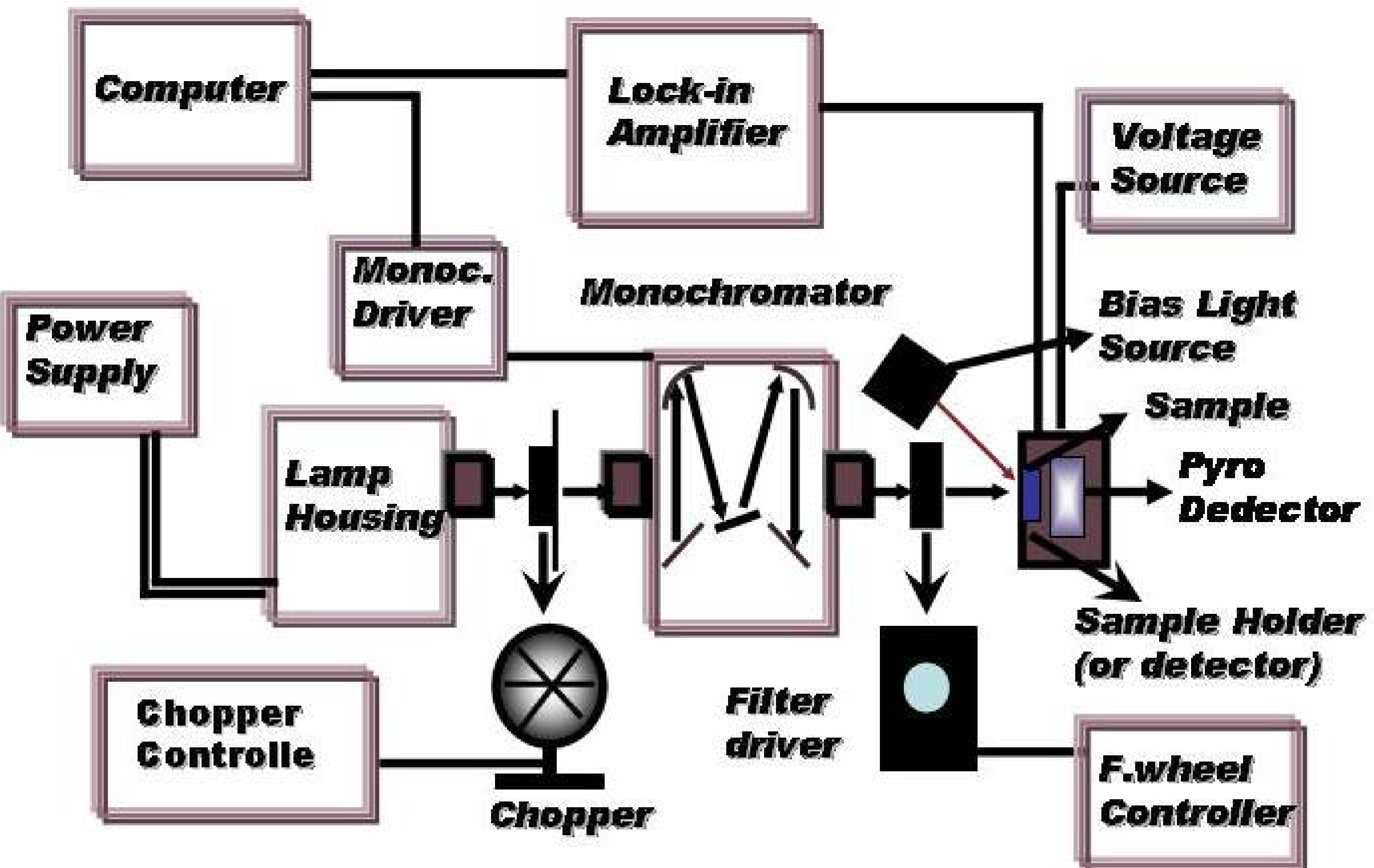

Figure 2.4 Dual beam photoconductivity spectroscopy system used to measure sub-bandgap absorption and transmission in μc-Si:H based materials.

applied using A Keitley 6517A Electrometer and current, both dark and photocurrent, was measured using the same Electrometer. A SR830 lock in amplifier was used to measure a.c. signal. All system was placed on an Oriel optical table in a closed box to provide a dark room.

An improved computer program, written in Objectbench software, is used to control the experimental system and for data acquisition. A Keithley IEEE 488 card was used to provide General Purpose Interface Bus (GPIB) protocol. SR830 lock-in amplifier, monochromator driver and filter driver are connected to IEEE 488 card. Having placed the sample on the sample holder, the computer program was called to start measurements. It starts with initializing lock-in amplifier and monochromator. Program allows adjusting initial energy, energy step and number of measurements for each energy. The bandpass filters are changed at certain energy. In DBP measurement the raw current and phase were measured for each energy value and averaged current values were divided by flux and recorded to data file with the phase of the signal. The computer program used for DBP measurements, flux measurements and transmission measurements is given in Appendix A.

2.2.2.1 Flux Calibration

A Quartz Tungsten Halogen (QTH) lamp is used in DBP system. It does not have a flat flux spectrum. Therefore, flux calibration is necessary. A pyroelectric detector was used for calibration of flux spectrum. Pyroelectric detectors are thermal type infrared detectors. The responsivity of pyroelectric detector is not depending on wavelength of the light. They are sensitive in a range of 0.1 μm-100 μm of the optical spectrum.

The raw flux spectrum of Quartz Tungsten Halogen (QTH) lamp measured using a pyroelectric detector is presented in Figure 2.5. Before performing each measurement, flux calibration was carried out in order to eliminate possible flux change of the lamp with time. Then the flux data were used for normalization of DBP spectrum and transmission spectrum.

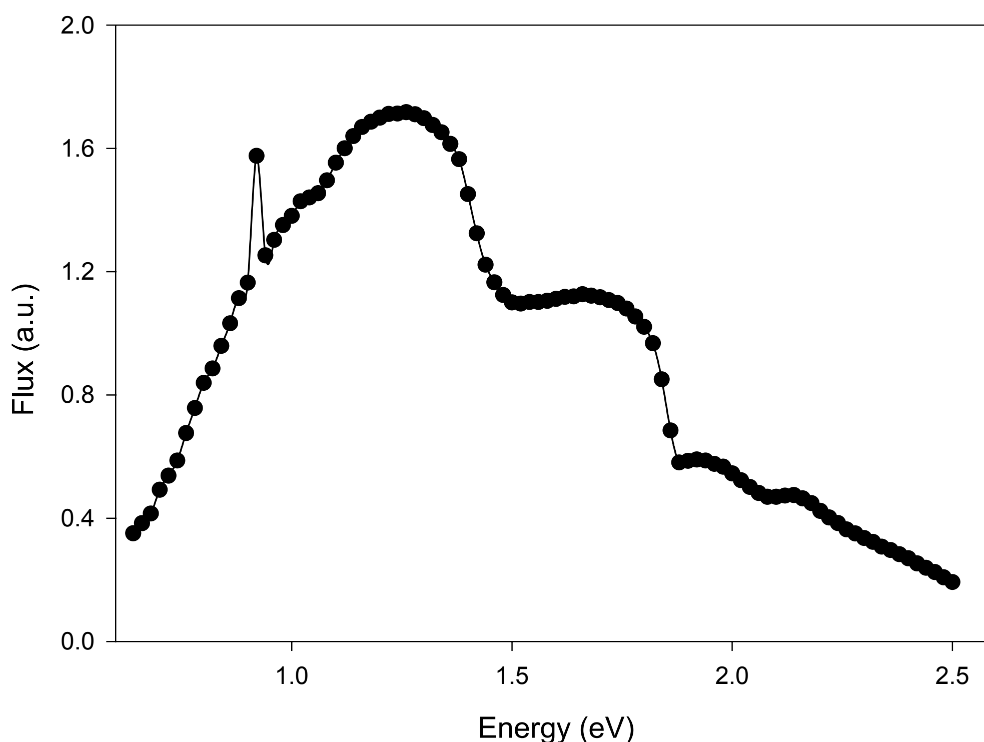

Figure 2.5. Flux spectrum of Quartz Tungsten Halogen (QTH) lamp obtained using pyroelectric detector.

2.2.2.2 Transmission Spectrum

Transmission spectrum was obtained placing the pyroelectric detector just behind the films. A typical transmission spectrum of a μc-Si:H thin film is presented in Figure 2.6. In the high-energy region of the spectrum, absorption is very high so transmission goes to zero at these values. Then it gradually increases with decreasing energy since absorption of investigated films decrease sharply in this energy region. The appearing fringes are due to interference of light in the film resulting from reflection of light in the film-substrate interface. The first interference peak is observed when the wavelength of incident light is comparable to the film thickness. For thicker films, interference fringes appear in the lower energy values. Transmission data were used to calculate the film

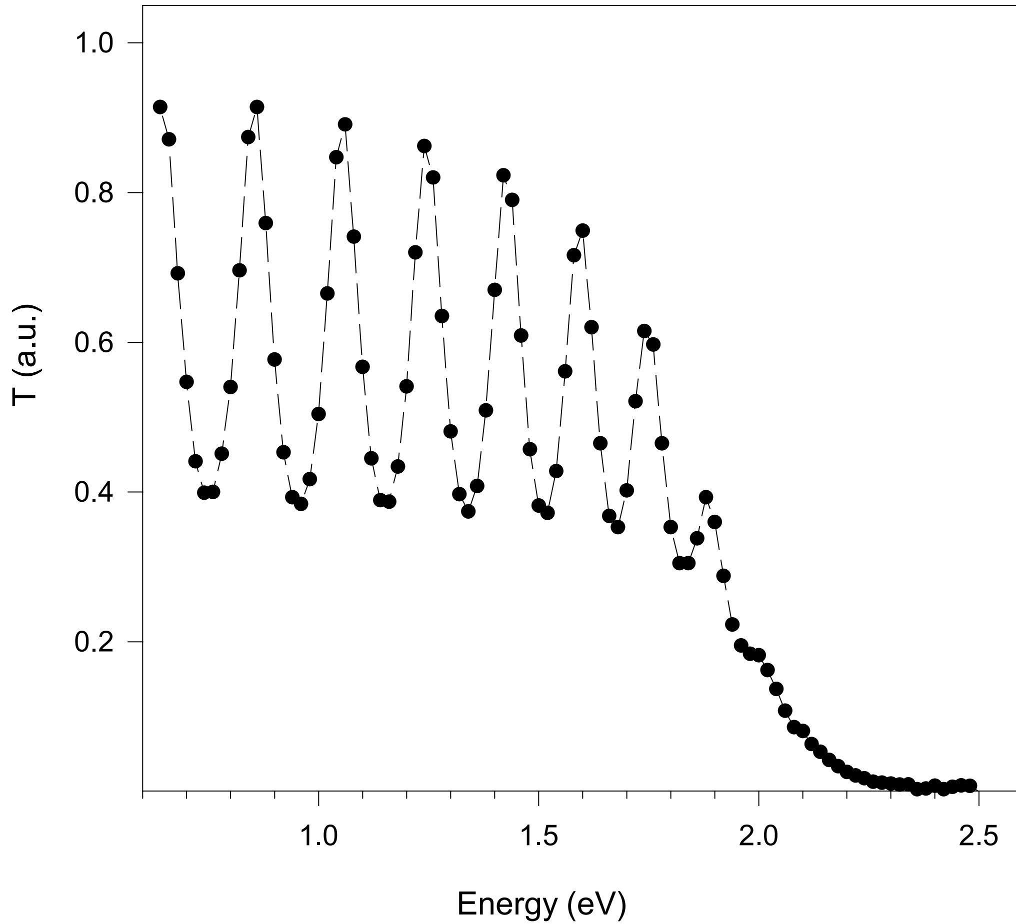

Figure 2.6. Transmission spectrum of a μc-Si:H thin film.

thickness using two energy values corresponding to two peaks in the transmission spectrum in the low energy region and refraction index of silicon. In addition, the transmission spectrum was used to calculate fringe free absolute absorption coefficient spectrum of these films as will be discussed in the last section of this chapter.

2.2.2.3 Dual Beam Photoconductivity Spectrum

The experimental setup and physical principle of dual beam photoconductivity spectrum was discussed at the beginning of this chapter. Dual beam photoconductivity is based on relative measurement of the ac photoconductivity and does not result in absolute

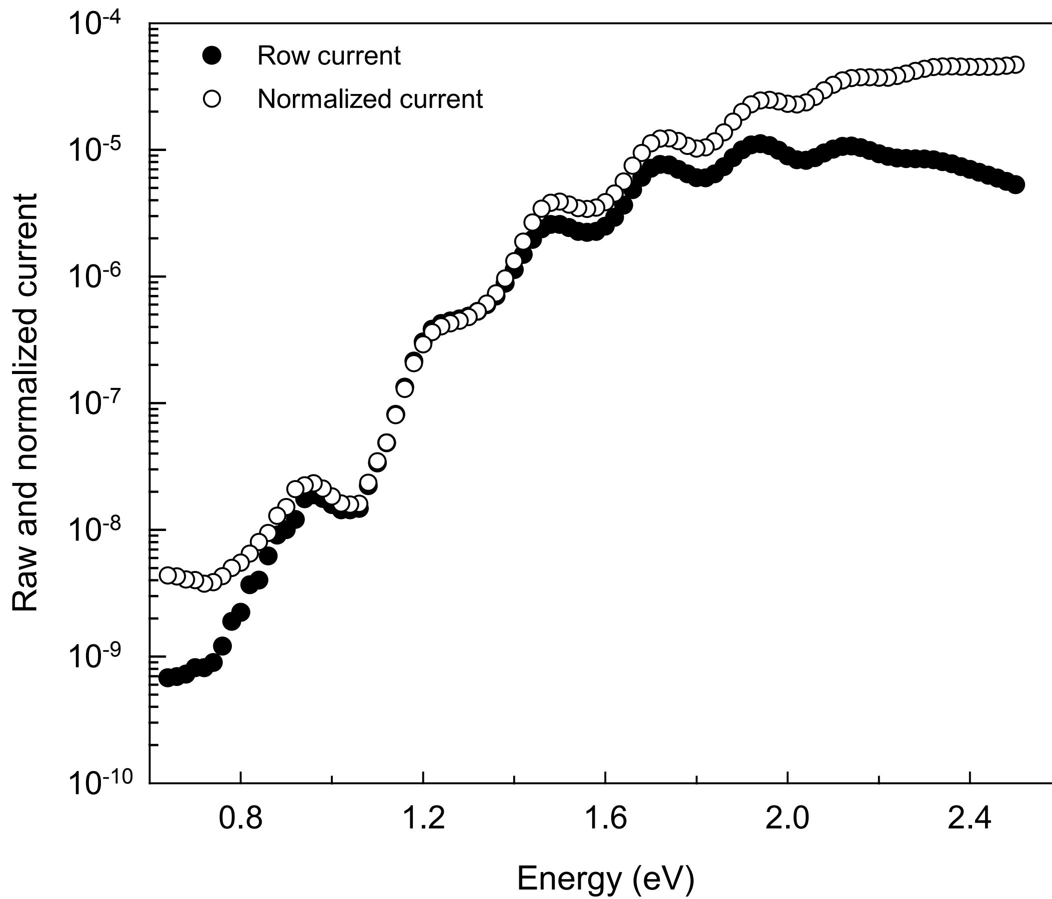

Figure 2.7. A typical raw and normalized photocurrent spectra of a μc-Si:H thin films measured by DBP method.

absorption coefficient spectrum. A typical raw and normalized photocurrent spectra for the μc-Si:H thin films measured by DBP at energies from 0.64 to 2.5 eV are shown in the Figure 2.7. The relative flux data is used to normalize raw photocurrent spectrum. The normalized photocurrent spectrum, DBP yield spectrum ($Y_{DBP}(ac)=\sigma_{ph}(ac)/Flux$), is proportional to the absorption spectrum if only certain assumptions of DBP are satisfied. First, constant μτ product of majority carrier electrons must be satisfied. This condition is controlled by calculating I_{dc} / I_{ac} ratio where I_{dc} is dc photocurrent arising from applied dc bias light and I_{ac} is ac photocurrent is measured by the Lock-in amplifier. For high generation rate of dc bias light, I_{dc} / I_{ac} is much higher than unity which implies that quasi-

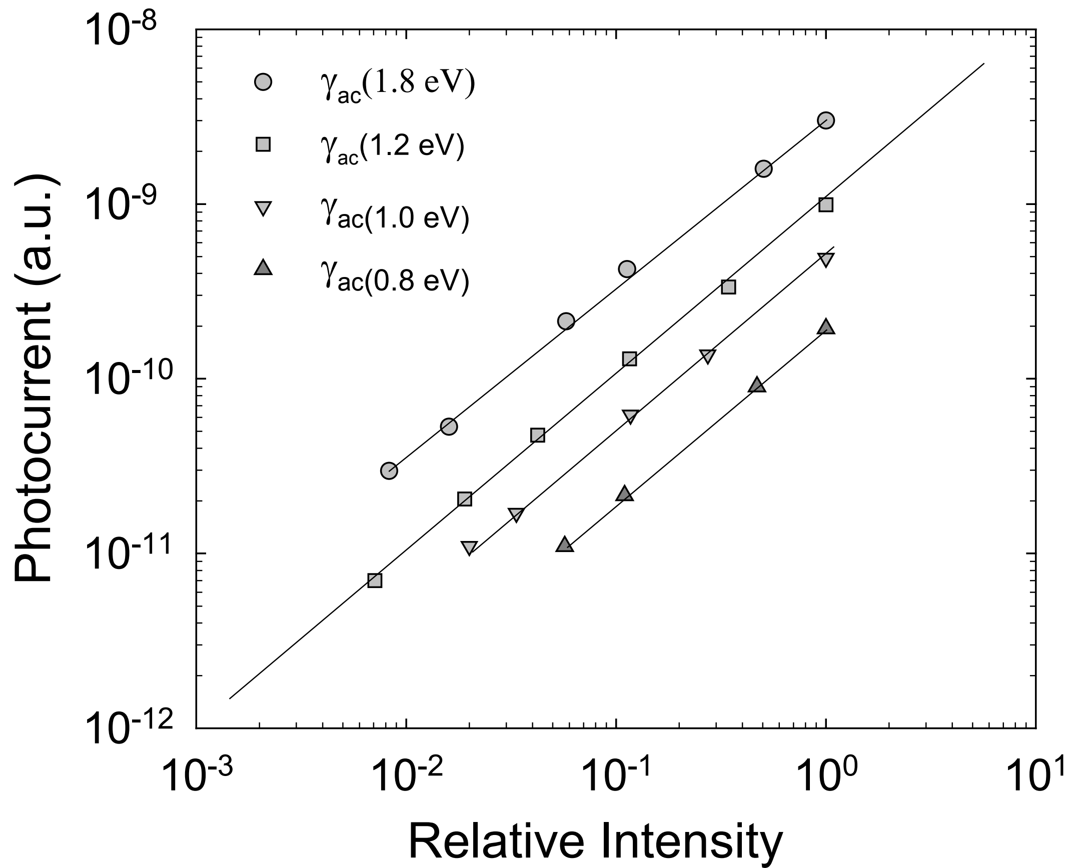

Figure 2.8. Intensity dependence of ac photocurrent on the ac monochromatic light.

Fermi levels of free carriers are fixed by dc bias light and are not altered by ac light. However, this condition is not satisfied for low generation rate of dc bias light especially in the high-energy region of the spectrum. In the case of low generation rate of dc bias light, the section of the photocurrent spectrum that satisfy $I_{dc}/I_{ac}>=10$ were taken as the reliable photocurrent spectrum. The linearity of ac photoconductivity on the intensity of ac light is also double-checked using the neutral density filters. In Figure 2.8, ac photoconductivity versus intensity is shown for different energies. It is seen that the exponent γ of ac photoconductivity is unity at all energies, which indicates that $\mu_n\tau_n$ product of electrons are kept constant during the measurements. That is the most important requirement of DBP method to be satisfied. The second condition is uniform absorption of light. Since absorption coefficient of microcrystalline silicon thin films is

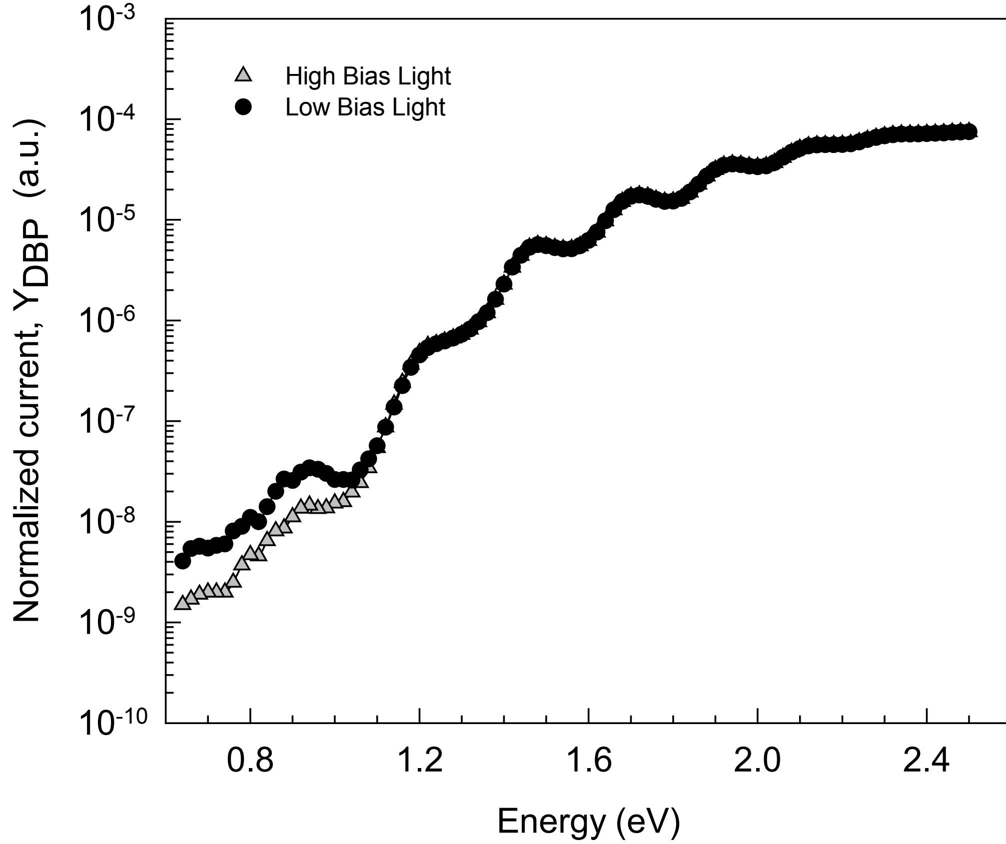

Figure 2.9. Dual beam photoconductivity yield Y_{DBP} of an intrinsic μc-Si:H film for high and low bias light intensities.

typically in the order of 10^3 cm^{-1} in the high-energy region of the spectrum and thickness of the investigated films are in the order of 0.4-0.9 μm, αt ($\alpha t=10^3 x0.9x10^{-4} \ll 1$) is smaller than unity. Therefore, uniform absorption condition is satisfied.

An example of DBP yield spectrum, Y_{DBP}, including interference fringes measured at high and low bias light intensities are shown in Figure 2.9. It is clearly seen that DBP yield spectrum exhibits a dependence on dc bias light intensity in the low energy region.

Since the use of bias light is to control the quasi-Fermi levels and the $\mu_n\tau_n$ product of electrons, the occupation of defect states can be changed by varying bias light intensity. Therefore, by increasing bias light intensity more defect states above the Fermi level are occupied and transition from these occupied states to conduction band can be probed in dual beam photoconductivity spectrum. This is called as the intensity dependence of dual

beam photoconductivity. As it can be seen from the Figure 2.9, the deviation of spectra for different bias light intensities begins at bandgap energy. Therefore, intensity of bias light has no effect on the Y_{DBP} above bandgap energy. However, below the bandgap energy, the Y_{DBP} spectrum is not unique and depends on bias light intensity. The deviation in the spectrum below the bandgap energy is correlated to the occupation of defect states in the midgap. Thus, Y_{DBP} spectrum does not result in absolute absorption coefficient below the bandgap. It rather reflects the effect of electron occupied defect states present in the bandgap of the material. This feature of DBP will be used to understand the defect states present in the bandgap of intrinsic μc-Si:H thin films deposited under different conditions.

2.2.3 Photothermal Deflection Spectroscopy

Photothermal deflection spectroscopy (PDS) [40-42] is based on measurement of generated heat as light absorbed by the material of interest. The physical principal of PDS is straightforward. Sample is illuminated with a chopped monochromatic light. Due to absorption, the temperature of the film changes and results in a temperature gradient in deflection medium (CCl_4), which has a temperature-sensitive refraction index. A laser beam grazing sample surface experience a periodic deflection synchronous with modulated light. The amplitude and phase of the deflected laser beam is measured using a position sensitive detector. The signal is proportional to the absorbed light power, thus absorption coefficient, $\alpha(h\nu)$.

The experimental setup for PDS is presented in Figure 2.10. As a deflection medium CCl_4 is generally used since it has extremely low absorption in the photon energy range of 0.4-2.3 μm [42]. It also does not alter the properties of silicon based thin films. The experimental setup must be well aligned and placed in the optical table in order to avoid effect of vibrations. The probe beam should be as close to the film surface as possible. The deflecting medium should be as clean as possible since particulates in the deflecting medium can results in a significant noise. The optical paths should be enclosed to eliminate effect of air currents. The probe beam should be well focused on the sample.

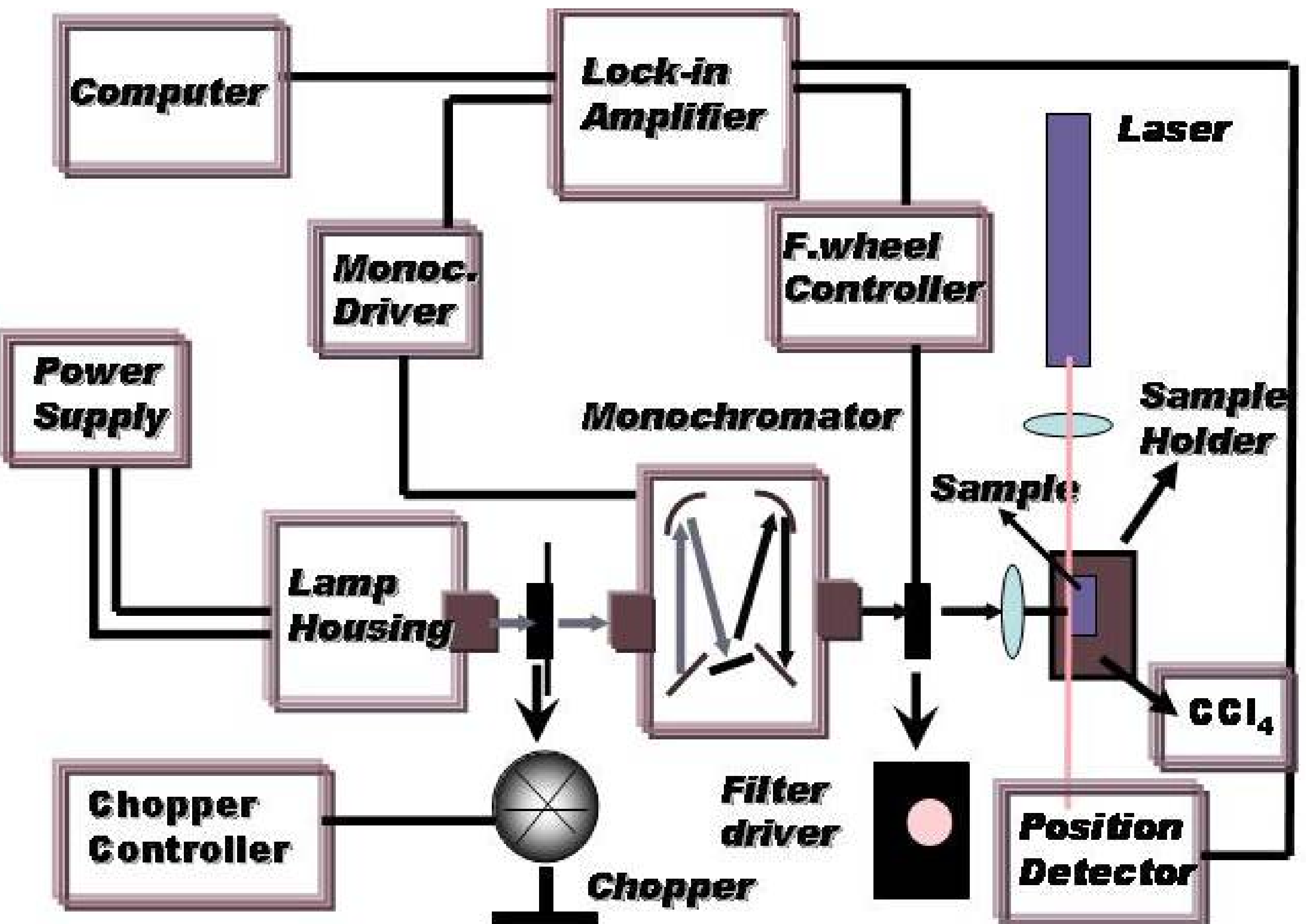

Figure 2.10 Photothermal deflection spectroscopy system used to measure sub-bandgap absorbtion and transmission in μc-Si:H based materials

A PDS setup was established as one goal of this thesis. A 20 mW HeN laser was used as laser probe beam. A 1% neutral density filter is placed in front of laser in order to attenuate laser beam intensity. A position sensitive detector was used to detect deflecting laser beam. The remaining instruments such as Lock-in amplifier, monochromator, white light source, lamp housing, and filters are the same since both systems shares the same setup due to lack of additional instruments. A convex lens having a focal length of 5 cm was placed in front of the monochromatic light beam so as to focus light in the sample. Another convex lens having a focal length of 10 cm is placed in the way of laser beam to focus laser beam just in front of the sample where monochromatic light focused on the sample. The monochromatic light beam, laser beam and sample holder is well aligned. A computer program written in Objectbench was used for data acquisition. A few experiments were done for both optimization of experimental setup and computer program. PDS and DBP setups share the same instruments such as monochromator, lock-in amplifier and lamp housing. In this thesis the focus was mainly on DBP measurements. Therefore, PDS measurements were not performed by us but done in Jülich Research Center, Germany.

2.3 Evaluation of Fringe Free Optical Absorption Coefficients Spectrum from DBP Yield Spectrum.

Interference fringes in the absorption spectrum and transmission spectrum of thin films were usually averaged in order to obtain the real spectrum [58]. In this section, a procedure to obtain fringe free absolute absorption coefficient spectrum will be presented for DBP method. First noted by Ritter and Weiser [51], A/T is free of fringes, since maxima and minima of transmittance and absorptance takes place nearly in the same photon energy of the spectrum for homogeneous samples, and used to calculate absolute absorption coefficient spectrum as carried out for “absolute’ constant photocurrent method (CPM) [45]. Transmittance (T) and reflectance (R) for a film with an absorption coefficient α and refractive index n on a non-absorbing substrate having a refraction index n_s are given as follows [51]

$$T = \frac{(1-R_1)(1-R_2)(1+k_2/n^2)}{\exp(\alpha t)+R_1\ R_2\exp(\alpha t)-2\sqrt{R_1R_2}\cos(2\beta-\delta-\delta_{2\,1})} \tag{2.17}$$

$$R = \frac{R_1\exp(\alpha t)+R_2\exp(-\alpha t)-2\sqrt{R_1R_2}\cos(2\beta+\delta_1-\delta_2)}{\exp(\alpha t)+R_1R_2\cos(2\beta-\delta_1-\delta_2)} \tag{2.18}$$

where 1 and 2 refer to film-air and film-substrate interface respectively and t is the film thickness, $k=\lambda\alpha/4\pi$, $\beta=2\pi nt/\lambda$, λ is the wavelength of light, and δ is the phase of the complex Fresnel coefficient. Interference effect is due to the phase angle β. On the other hand, sum of absorbance, reflectance, and transmittance is equal to unity.

$$A + R + T = 1 \tag{2.19}$$

Using Equations 2.17, 2.18, and 2.19 A/T can be derived as follows

$$\frac{A}{T} = \frac{\exp(\alpha t)-R_2\exp(-\alpha t)-(1-R_2)(1+k^2/n^2)}{(1-R_2)(1+k^2/n^2)} - \frac{4\sqrt{R_1R_2}\sin(\delta_1)\sin(2\beta-\delta_2)}{(1-R_1)(1-R_2)(1+k^2/n^2)} \tag{2.20}$$

The first term is free of interference fringes since it is independent of β. The interference fringes are due to second term. However, for thin films of interest, the second term can be neglected since it is much smaller than first term. The ratio of first term to the second one, as calculated in the original paper of Ritter and Weiser, is 66 for λ=d=1 μm, n=3.5, n_s=1.5 (glass) and $\alpha d \ll 1$. Omitting the second term and neglecting k^2/n^2 in the first term

$$\alpha t = \ln\{0.5\{(1-R_2)(1+A/T)+\{(1-R_2)^2(1+A/T)^2+4R_2\ \}^{1/2}\ \} \tag{2.21}$$

Since t and R_2 are constant in equation 2.21, the only problem remains is setting A/T in absolute scale. To do this, we follow procedure that used for “absolute” CPM method [45]. First step is setting transmission spectrum in absolute scale. The transmittance

maximum T_{max} of a nearly nonabsorbent thin film on a nonabsorbent thick substrate is depend only optical refraction index n_s [59] of the substrate and is given as follows.

$$T_{max} = \frac{2n_s}{n_s^{\,2} + 1} \quad (2.22)$$

Refraction index of Corning glass 7059 is 1.5, so T_{max} is approximately 0.92. Therefore, setting T_{max} of transmission spectrum to 0.92 transmission spectrum is now in absolute scale. The next step is setting A/T in absolute scale. To do this we chose a reference energy E_x in the high photon energy region of the absolute transmission spectrum where transmission spectrum and reflection spectrum is free of interference fringes. In general T_x=0.05 is a good choice since transmission spectra of our films are free of interference fringes at this point, where we take reflectance as R_x=0.41 when sample illuminated from film side and R_x=0.26 when sample illuminated from substrate side. These values are taken for amorphous silicon, however, we will see that using these values our calculated absolute absorption spectra are in agreement with those of PDS. Using the value of T_x and R_x and relation $A_x+T_x+R_x=1$ we have the value of A_x in absolute scale at reference energy E_x. So once we set the value of absorptance to A_x at reference energy E_x, we obtain whole absorptance spectrum in absolute scale. Then the final step is using absolute A/T spectrum in Ritter-Weiser formula as given in equation 2.21. To compare the results of this method on a real absorption spectrum, Y_{DBP} spectrum of a μc-Si:H thin film normalized to that of PDS is shown in Figure 2.11a. It is seen that normalization is done by eye at energies where Y_{DBP} is proportional to absorbance (1.4-1.6 eV). Due to interference fringes, it is difficult to obtain reliable $\alpha(h\nu)$ values at lower energies. To eliminate these fringes, a fast Fourier transform procedure is commonly used in the literature [57], then a better normalization can be done to absolute $\alpha(h\nu)$ spectrum of PDS or T&R. However, fringe removing procedure for thin films less then 1 μm introduces a large error into shape and magnitude of the spectrum. It then results in inaccurate normalization of Y_{DBP}. Furthermore, eliminating fringes completely from the spectrum can also result in loss of some important information that raw Y_{DBP} spectrum carries about the sample.

In this thesis, contrary to the old approach used in the literature [57], we have used the fringe free calculation procedure explained above from the raw Y_{DBP} spectrum and simultaneously measured transmission signal of the same sample. The result of the calculation procedure is shown in Figure 2.11b for the same sample together with the $\alpha(h\nu)$ spectrum of PDS. Here, there is no normalization procedure of fringe free Y_{DBP} spectrum carried out to that of PDS. Both spectra were independently measured by two different methods and the $\alpha(h\nu)$ spectra were calculated using the same procedure. It is clearly seen that the $\alpha(h\nu)$ spectra overlap quite well at higher energies but differences exist at lower energy part. This will be explained in detail through the thesis.

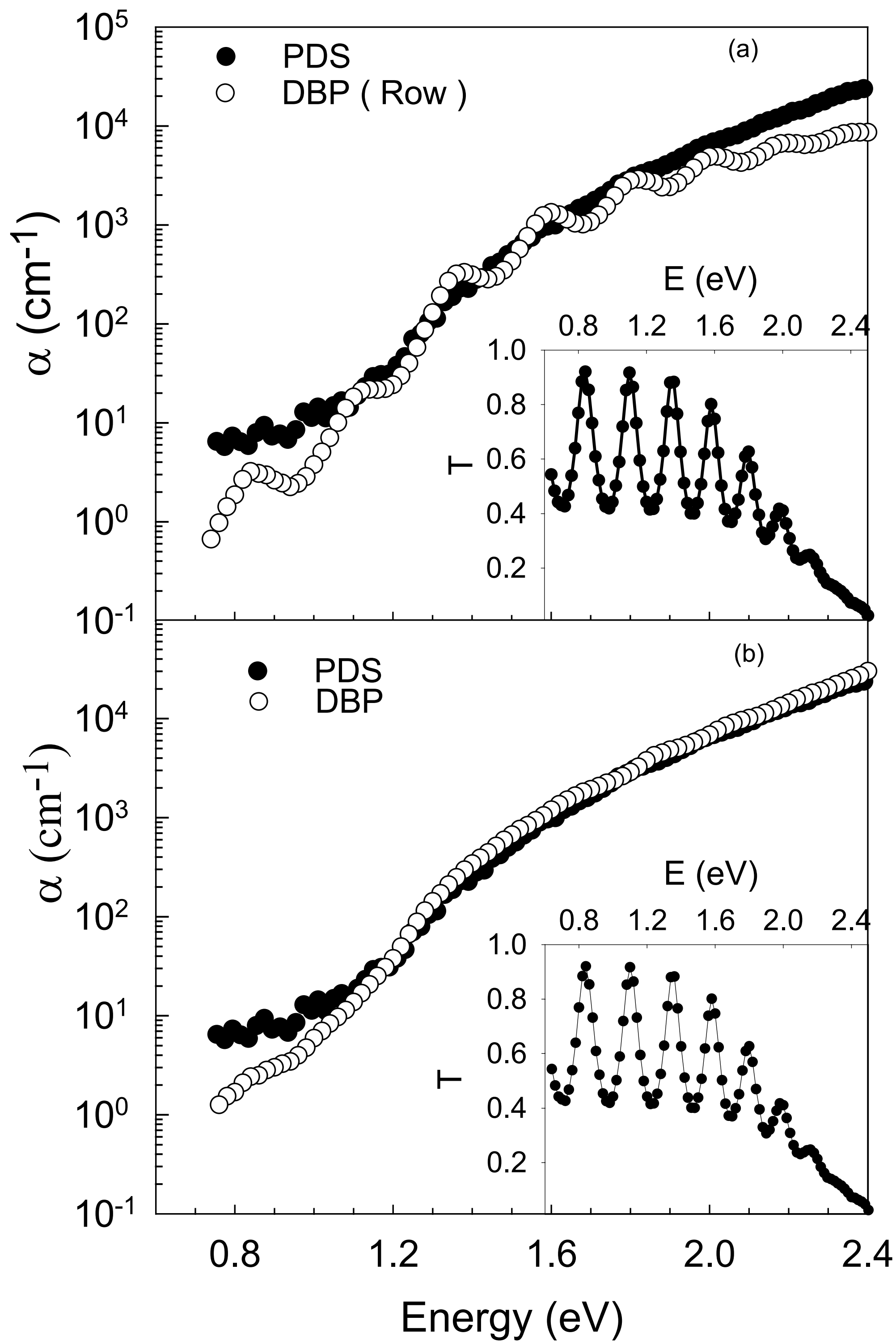

Figure 2.11 a) Y_{DBP} spectrum normalized to PDS directly. In the inset, the transmission of the film is shown. b) Calculated fringe free absolute $\alpha(h\nu)$ spectrum of DBP and PDS measured independently.

CHAPTER 3

EXPERIMENTAL RESULTS IN INTRINSIC HYDROGENATED MICROCRYSTALLINE SILICON THIN FILMS

3.1 Introduction

Intrinsic hydrogenated microcrystalline silicon thin films are important candidate for large area photovoltaic and solar cells applications. Therefore, its optical and electronic properties must be appropriately characterized in order to understand the physics involved in this material. In this thesis, intrinsic μc-Si:H thin films prepared by VHF-PECVD and HW-CVD methods were characterized using the methods of steady state photoconductivity (SSPC), photothermal deflection spectroscopy (PDS), and dual beam photoconductivity method. In SSPC measurements, mobility-lifetime product ($\mu_n\tau_n$) of majority carriers, electrons, was obtained. The $\mu_n\tau_n$ –product is one of the major properties of photoactive materials and it must be appropriately measured. In PDS measurements, absolute absorption coefficient spectrum from 2.5 eV down to 0.6 eV was obtained. The $\alpha(h\nu)$ spectrum must be known to use the material as absorber layer in solar cells, which must fit the solar spectrum. In DBP measurements, photoconductivity yield spectrum was measured. Then the resulting DBP yield spectrum and transmission spectrum was used to calculate absolute $\alpha(h\nu)$ spectrum for the first time in this thesis.

3.2. Steady State Photoconductivity Results of Intrinsic μc-Si:H Thin Films

Steady state photoconductivity is a complex process of free carrier generation across the bandgap, recombination of free carriers through the defect states and transport of free carriers at the mobility edge. Therefore, it involves the absorption coefficient of material, density and nature of recombination centers and mobility of free carriers at the extended states. The well-known non-integer power-law dependence on generation rate of steady state photoconductivity is an important physical feature. It provides information about recombination kinetics between electrons and holes. The mobility-lifetime product, $\mu\tau$, of electrons can also be derived

from steady state photoconductivity. The mobility-lifetime product of electrons is an important parameter for device applications.

The measured photoconductivity and calculated $\mu\tau$ product versus generation rate are shown in Figure 3.1 and Figure 3.2 for intrinsic μc-Si:H thin films deposited by VHF-PECVD and HW-CVD methods, respectively. The photoconductivity versus generation rate obeys the well-known non-integer power-law dependence rule, $\sigma_{ph} \propto G^{\gamma}$. The exponent γ is in the same order for both type of films. It is between 0.8 - 1.0, indicating a continuous distribution of recombination centers present in the material. The steady state photoconductivity is dominated by the majority carriers, electrons, transport for these intrinsic hydrogenated microcrystalline silicon thin films. Since the $\mu_n\tau_n$- product of electrons is much higher than that of holes ($\mu_n\tau_n \gg \mu_p\tau_p$). Therefore the investigated thin films exhibit slightly n-type character. The $\mu_n\tau_n$- products decreases as generation rate increase, with its characteristic power law $\mu\tau \propto G^{\gamma-1}$, implying that more defect states act as recombination centers with increasing generation rate. In Figure 3.3 photoconductivity and $\mu\tau$-product of PECVD and HW-CVD deposited μc-Si:H thin films are presented together. The $\mu_n\tau_n$- products of VHF-PECVD grown thin films have almost factor of ten higher values than those of HW-CVD grown thin films for the samples deposited with SC's from 3.7% to 7.0%. For both type of investigated μc-Si:H thin films, there is no functional dependency found on silane concentration. However, the film deposited for the lowest SC has the lowest $\mu_n\tau_n$- product indicating an increased defect density present in the material, which mainly decreases the lifetime τ_n of electrons.

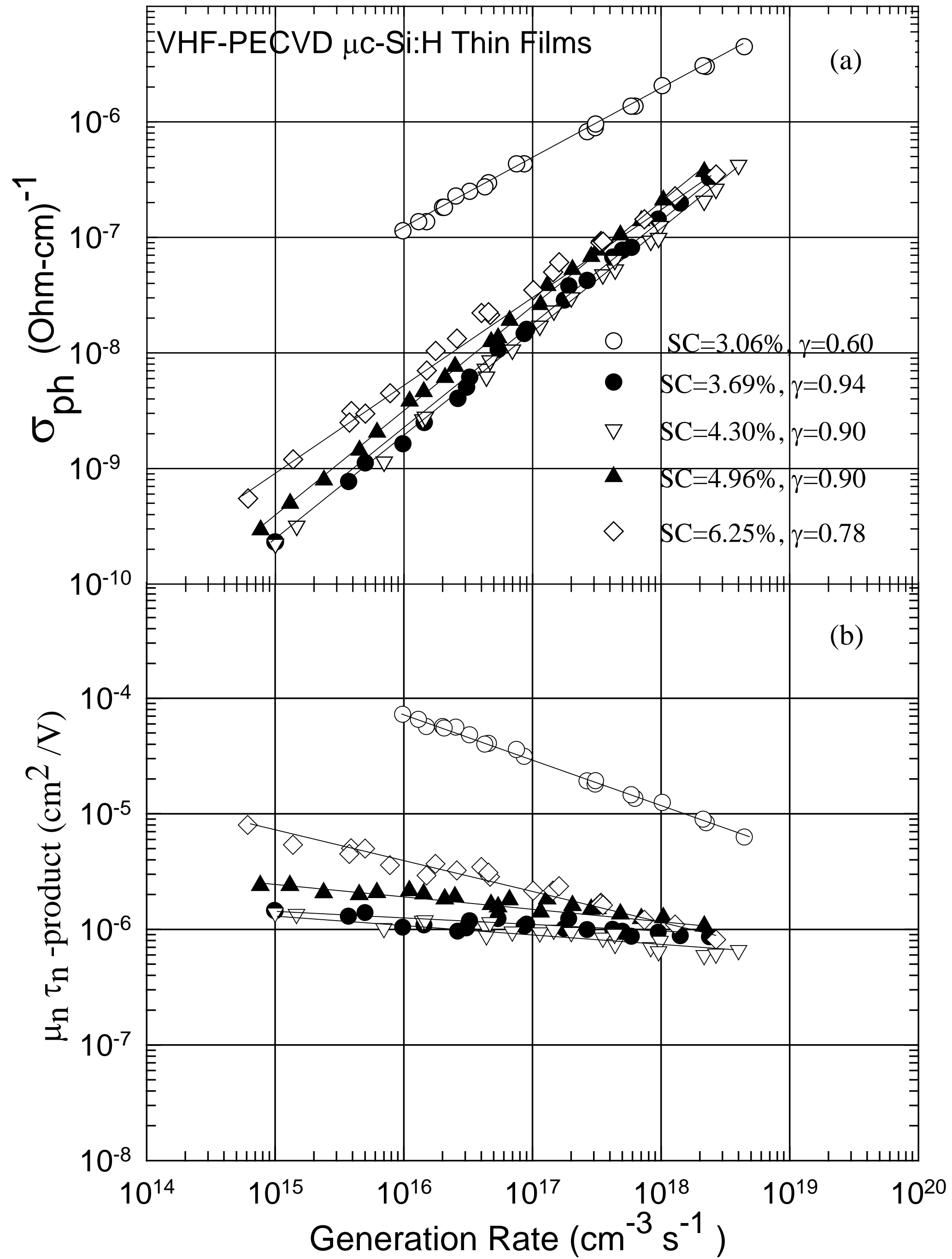

Figure 3.1 (a) σ_{ph} versus generation rate for intrinsic μc-Si:H films prepared using VHF-PECVD method. b) $\mu_n\tau_n$-product versus generation rate of the same intrinsic μc-Si:H thin films

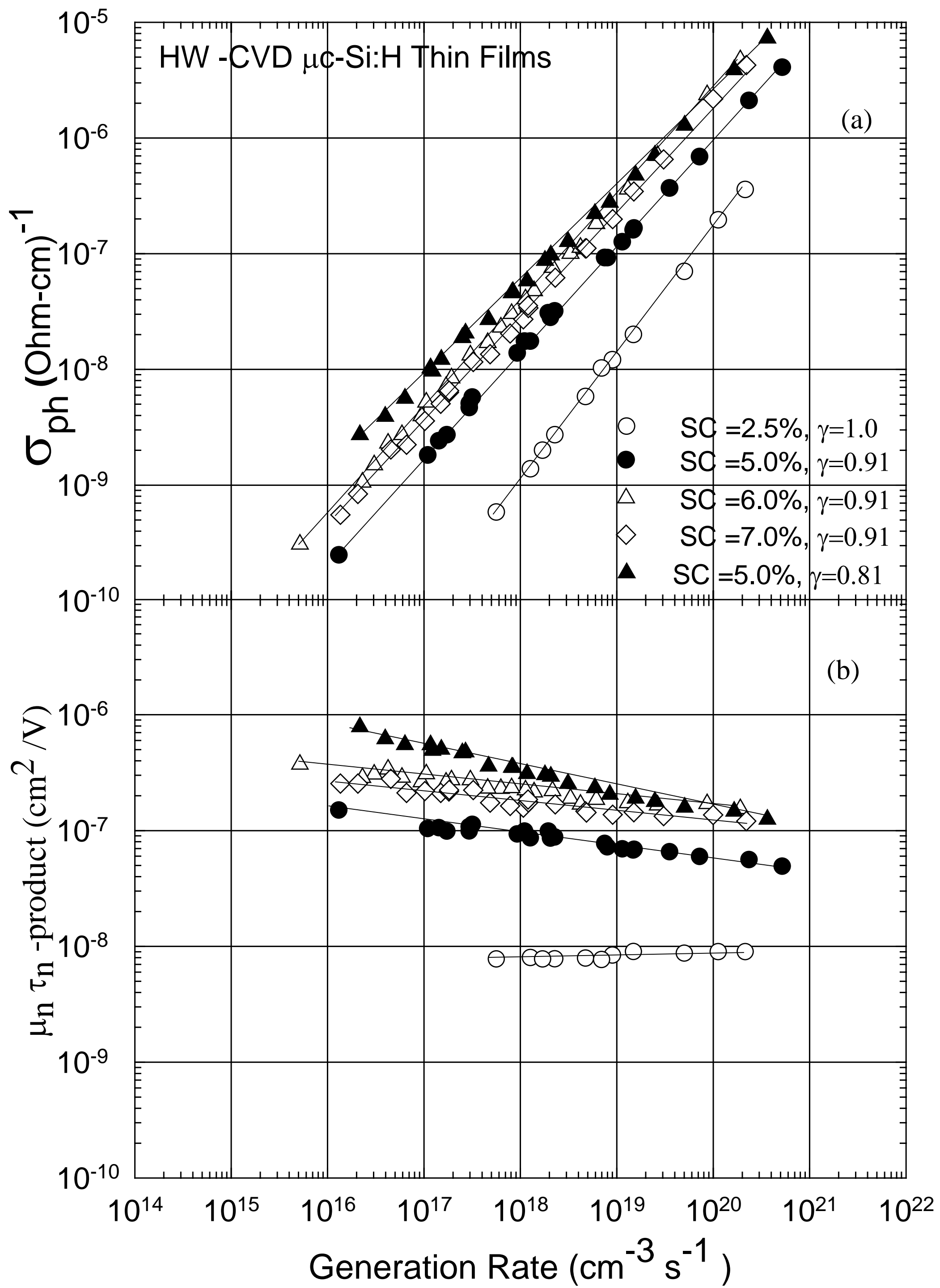

Figure 3.2 (a) σ_{ph} versus generation rate for intrinsic μc-Si:H films prepared using HW-CVD method. b) $\mu_n\tau_n$-product versus generation rate of the same intrinsic μc-Si:H thin films

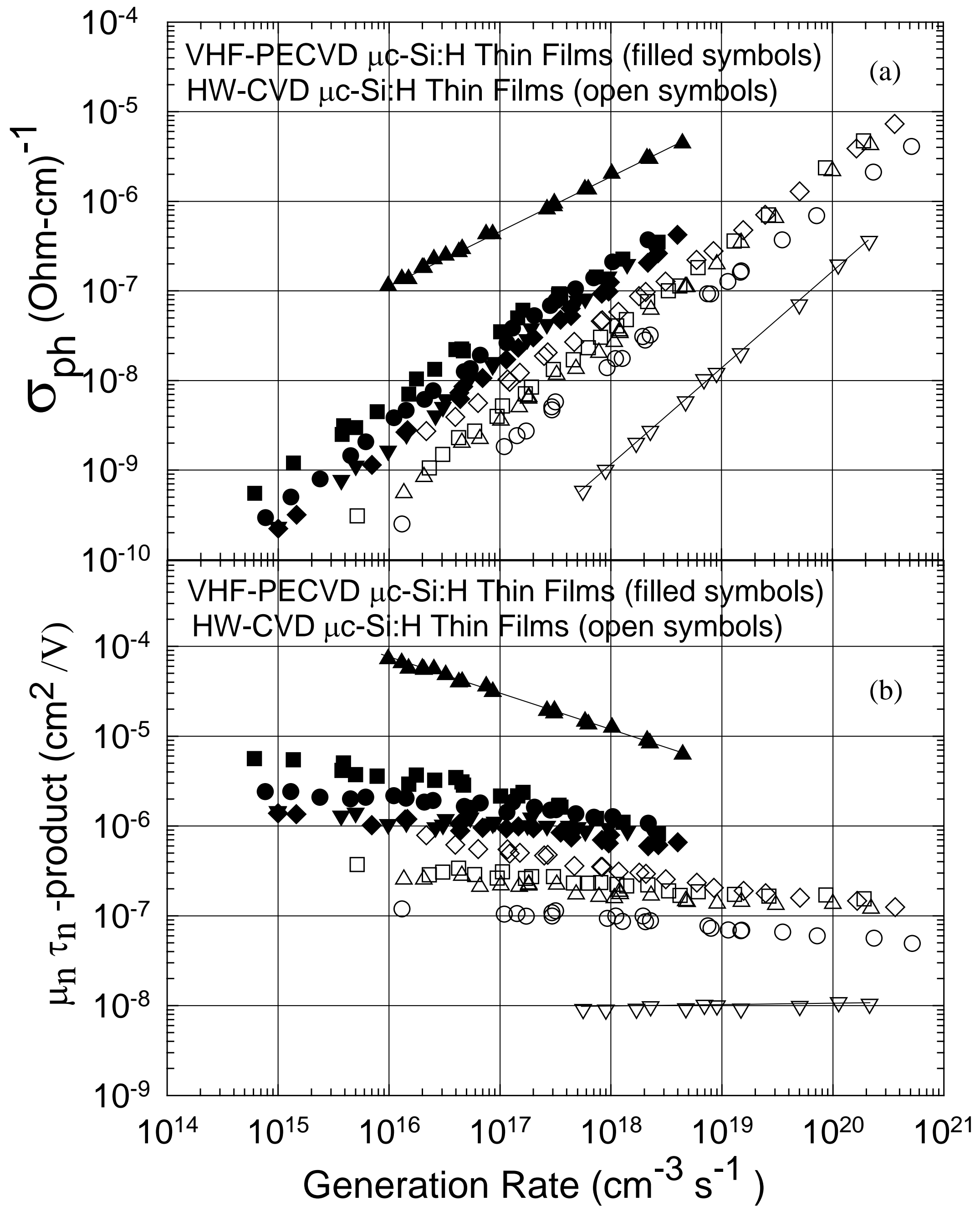

Figure 3.3 Summary of σ_{ph} (a) and $\mu_n\tau_n$ –product (b) versus generation rate of μc-Si:H thin films deposited by VHF-PECVD and HWCVD techniques.

3.3 Sub-Bandgap Absorption Spectra of intrinsic μc-Si:H thin films

Optical absorption spectrum of thin films is an important parameter to characterize optical and electronic properties of the materials. The measurements of optical absorption especially in the sub-bandgap region is very important since absorption in that region is related to defect states present in the materials. As the deposition condition changes, the microstructure of the μc-Si:H thin films changes substantially. This affects the resulting optical and electronic properties of deposited thin films. In order to obtain reliable $\alpha(h\nu)$ spectrum of intrinsic μc-Si:H thin films, especially in the sub-bandgap region, is one of the crucial subject of ongoing research. In this section, experimental optical absorption spectra of intrinsic microcrystalline silicon thin films measured using PDS and DBP methods will be given separately for VHF-PECVD and HW-CVD grown thin films. PDS measurements were performed in Jülich Research Center, Germany.

3.3.1 VHF-PECVD Grown Thin Films

An example of DBP yield spectrum for high bias and low bias light intensities together with transmission spectrum is presented in Figure 3.4a and Figure 3.4b, respectively, for a intrinsic microcrystalline silicon thin film deposited using VHF-PECVD with SC=4.3%. As seen from Figure 3.4, the maxima and minima of transmission and DBP yield spectra occur at the same photon energies. For low bias light, DBP spectrum results in lower values than high bias DBP spectrum only at sub-bandgap energies as seen in Figure 3.4a. The deviation is related to occupation of defect states in the bandgap as explained in Chapter 2. At the low bias light condition, DBP probes the distribution of defect states, which is very close to that in the dark condition below the Fermi level. When intensity of bias light is increased, more defect states above the Fermi level are occupied. This will result in an increase in the number of transition from these occupied states into the conduction band, therefore the Y_{DBP} values in the lower energy region increase as seen in Figure 3.4a. Y_{DBP} at high bias light contains more information since the occupation of defect states determines this increase at

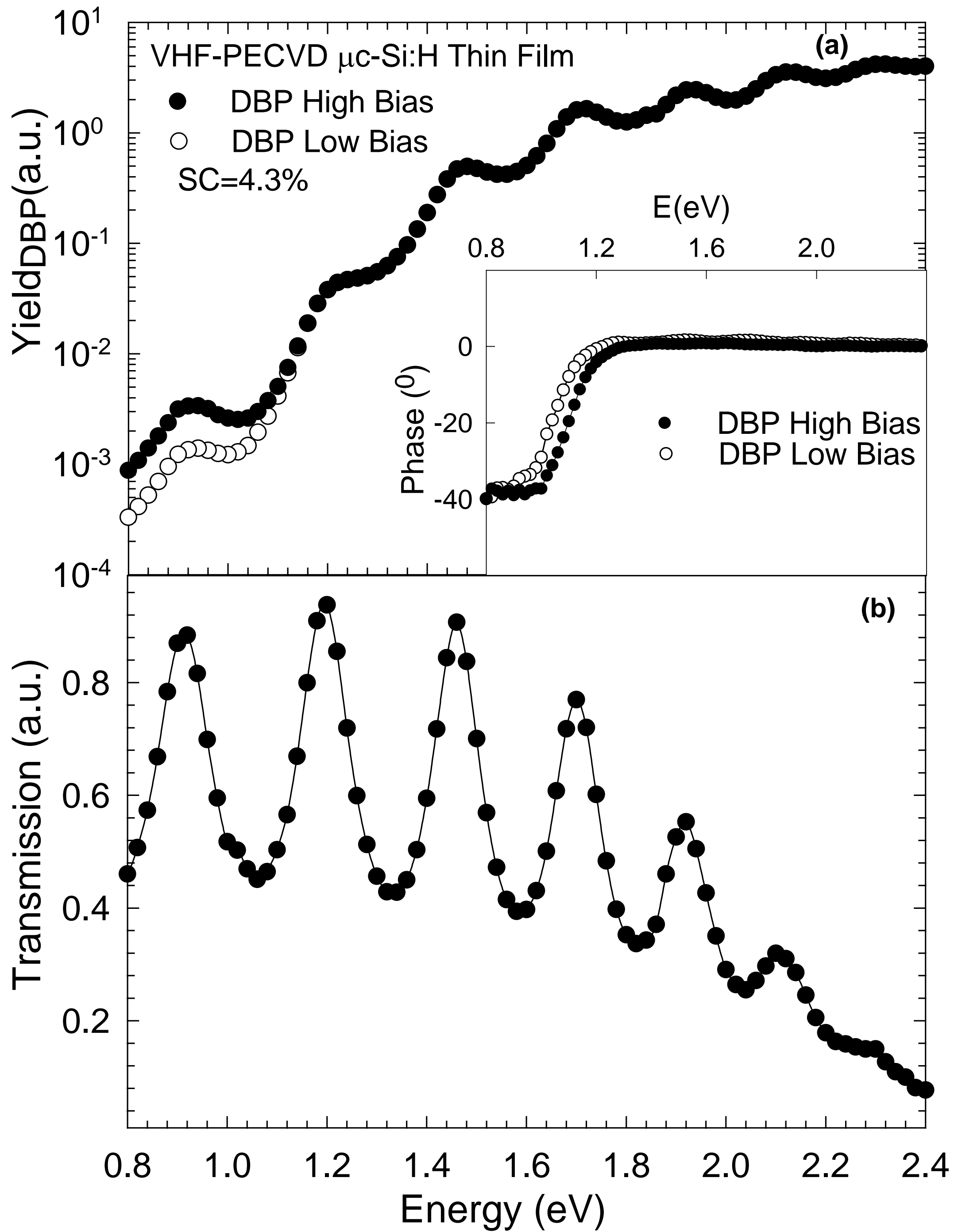

Figure 3.4 a) DBP Yield spectrum measured with high and low bias light intensities for a μc-Si:H thin film deposited SC=4.3%. In the inset, phase of both measurements are shown. b) Transmission spectrum of the same sample.

lower energies. For both cases, DBP yield spectrum is directly proportional to the absorptance and thus absorption coefficient. There are also interference fringes on the spectrum due to multiple reflections of the incoming light. The aim is to obtain absorption coefficient spectrum from the Y_{DBP} spectrum without interference fringes. Generally, the fringes have been removed using fast Fourier transform method [57] and resulting fringe free Y_{DBP} spectrum is normalized to absolute $\alpha(h\nu)$ values obtained from T&R or from PDS measurements [47,49]. Then, the $\alpha(h\nu)$ values at lower energies, obtained by setting Y_{DBP} to absolute scale, are used to compare the level of defect states present in the material. It is frequently discussed in the literature that fast Fourier transforms process introduces artificial errors in the spectrum for films less than 1 μm and absolute $\alpha(h\nu)$ obtained from T&R measurement is not reliable for such thin films (< 1 μm). Therefore fringe free normalization of Y_{DBP} always introduces a significant degree of errors and accuracy is questioned. In this thesis, for the first time, the fringe free absolute $\alpha(h\nu)$ spectrum is directly calculated from DBP yield spectrum and transmission spectrum shown in Fig. 3.4b measured on the same sample using a procedure based on the Ritter-Weiser formula as explained in the Chapter 2.

In the Figure 3.5a, DBP yield spectrum for high and low bias light intensity and raw spectrum of PDS signal are shown. As clearly seen from the figure, the maxima and minima of both spectra are at the same energy points. However, for some samples a shift in maxima and minima of both methods are observed since sometimes the thickness of investigated films can show a variation on the substrate. In the inset of the Figure 5a, transmission spectra obtain for both methods are also presented. It is seen that transmission spectra obtained for both methods are also identical. In the Figure 3.5b, absolute $\alpha(h\nu)$ spectrum calculated from PDS and DBP measurements and simultaneously measured transmission signals for the same sample are presented. In the inset of the figure, the phase of PDS and DBP signal are also shown. For the PDS spectrum, a deviation begins below the bandgap energy since in that region absorption arising from substrate dominates the PDS spectrum. The absorption due to substrate can be monitored in the phase of PDS signal and a correction process is carried out to get rid of the substrate contribution in the absorption spectrum. But in general, phase of PDS signal is noisy in the lower energy region. Therefore, the accuracy of this

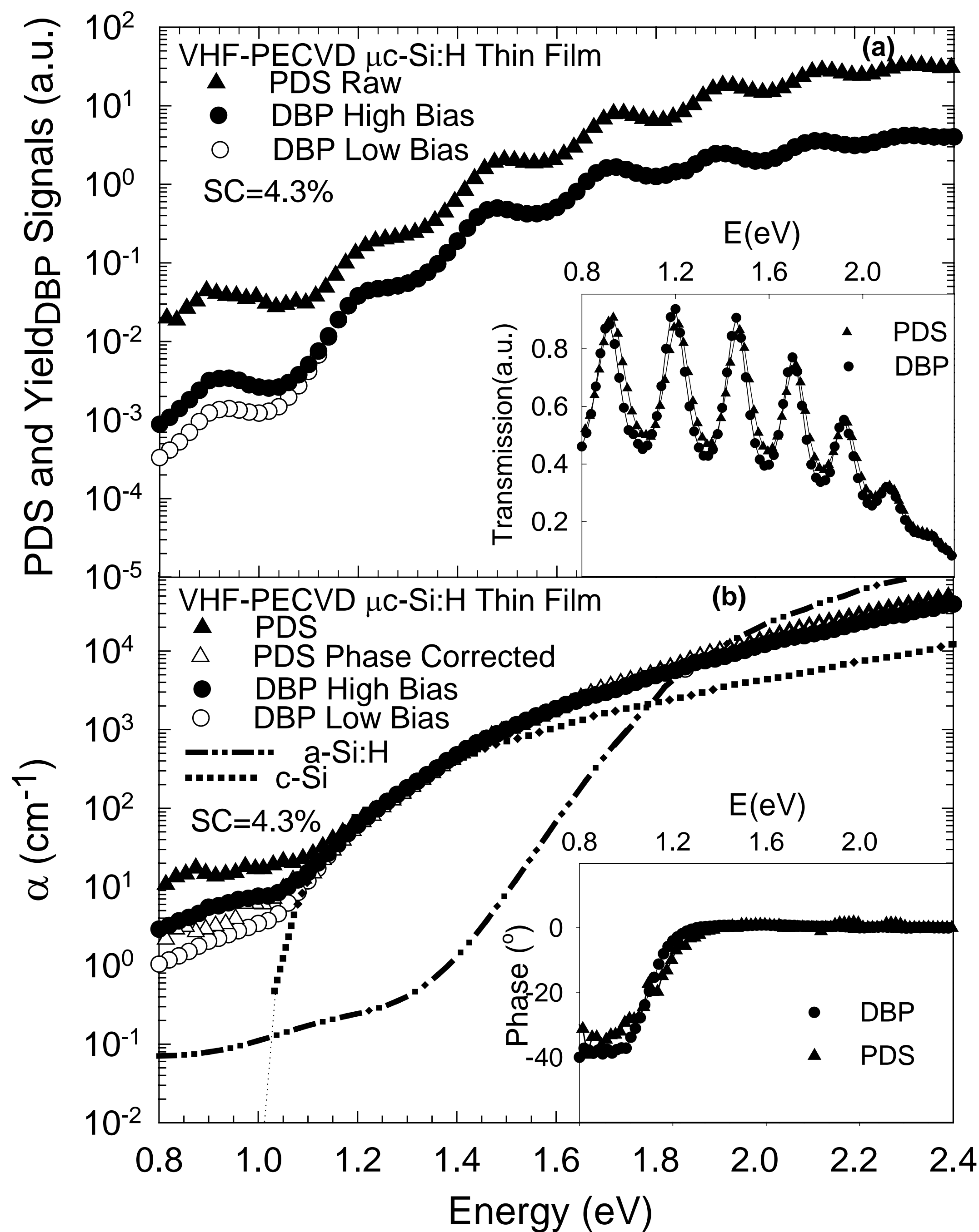

Figure 3.5 a) Raw PDS and Y_{DBP} signals of a μc-Si:H thin film. In the inset transmission spectra of both methods are shown. b) Absolute α(hν) spectra of PDS and DBP measurements and that of c-Si and s-Si:H for comparison. In the inset, the phase of PDS and DBP are illustrated.

correction is not very well especially below 1.0 eV. The phase corrected absolute absorption spectrum of PDS for the same sample is also presented in the same figure.

Similarly, the fringe free $\alpha(h\nu)$ spectrum calculated from Y_{DBP} spectrum for high and low intensities of bias light are also shown in the Figure 3.5b using the same procedure explained in chapter 2. As seen from figure3.5b, the absorption spectra obtained from both methods are in agreement above bandgap energy. At lower energies, PDS spectrum deviates because of substrate effect. Phase corrected spectrum of PDS reflects the noise of phase in that region. On the other hand, DBP spectrum in that region is a smooth curve and is relatively noise free when compared to PDS spectrum. However, as discussed in chapter 2, the DBP spectrum below the bandgap energy does not reflect true absorption coefficient of investigated thin films; rather it has an intensity dependence on bias light and reflects the occupation of defect states in the bulk of the material In addition, absolute $\alpha(h\nu)$ spectrum of μc-Si:H obtained in this study is also compared with those of a-Si:H and c-Si. It is seen that the $\alpha(h\nu)$spectrum of μc-Si:H is consistent with data reported in the literature as compared to its amorphous and crystalline counterpart.

Another important feature of these methods is the phase of the signal. Phase of DBP and PDS signal is presented in the inset of Figure 3.5b. As seen from the figure, phase of PDS and DBP signals begin to change at about 1.2 eV. The shift in the phase of PDS signal is due to substrate absorption. On the other hand, the shift in the DBP signal can be attributed to recombination kinetics of defect states present in the band gap since DBP method is insensitive to substrate absorption. In addition, the use of bias light results in a change in the occupation of defect sates from that in the dark condition. This additional defect kinetics is different from the defects in the extended states, which dominates at the high photon energy region of $\alpha(h\nu)$ spectrum. Small modulations in the phase of DBP signal as well as PDS signal are also important as seen in the inset of Fig. 3.5b. The degree of modulations in the phase varies. For some sample the modulation in the phase become significantly large. These modulations can be considered as indication of an inhomogeneous absorption of light due to inhomogeneity present in the material.

To investigate inhomogeneity of the material in growth direction, DBP measurements were also performed for ac monochromatic light incident form substrate side for the same sample while keeping the remaining condition to be the same as for

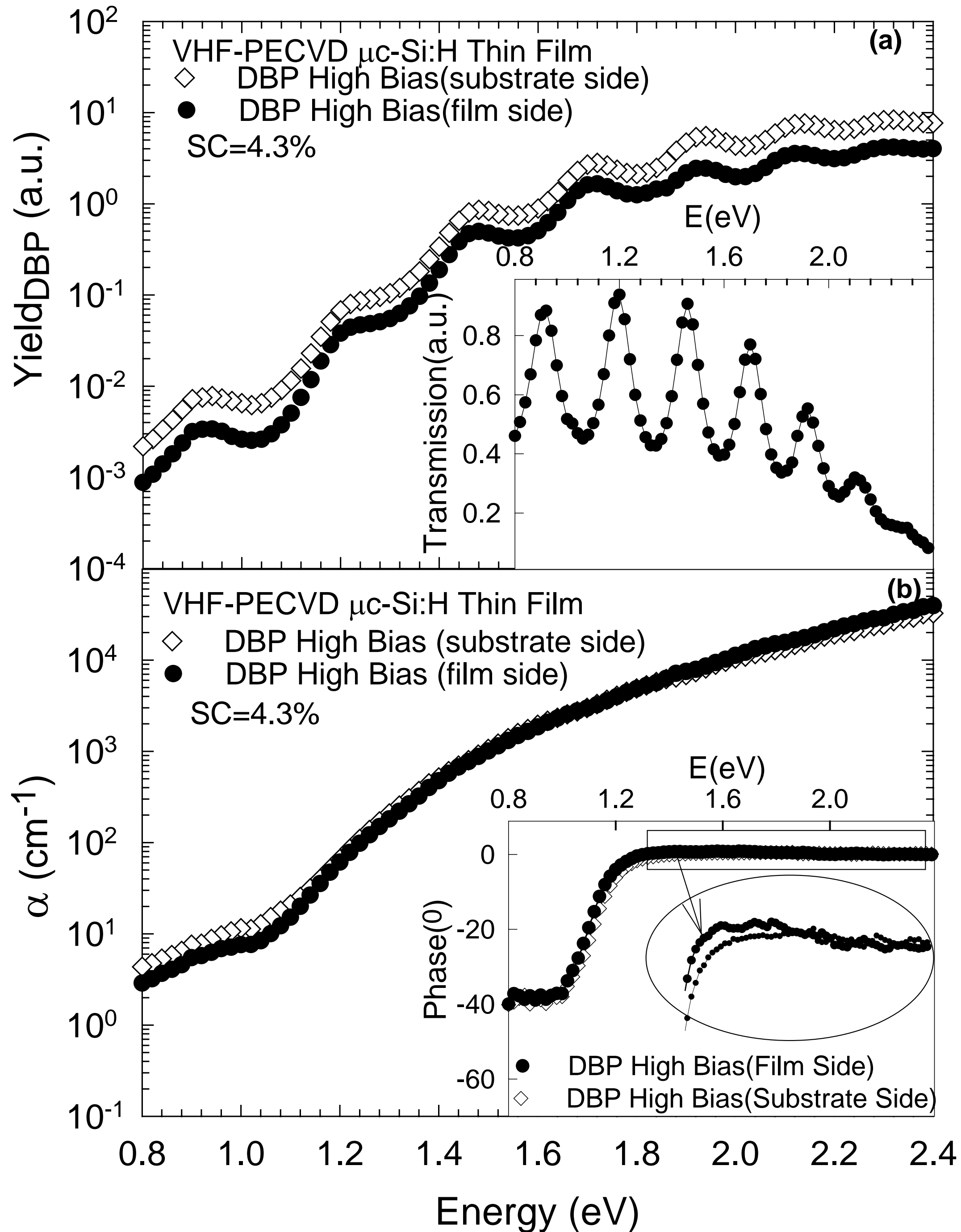

Figure 3.6 a) Y_{DBP} spectra measured for ac light incident from film side and substrate side for intrinsic μc-Si:H film deposited by VHF-PECVD method with SC=4.3%. In the inset, transmission spectrum of the same sample is shown. b) Calculated α(hν) spectra of the same sample for both front and back ac illumination cases. In the inset, phase of both measurement signals are shown.

conventional measurement geometry (ac light incident to film side). The transmission spectrum was also measured for both front and back ac illumination and was found to be identical for both cases. The results are shown in Figure 3.6a and Figure 3.6b for raw Y_{DBP} and calculated $\alpha(h\nu)$ spectra, respectively. In the insets, corresponding transmission signals and phase of DBP measurements are illustrated. As clearly seen from Figure 3.6a, no difference between the raw Y_{DBP} spectra of front and back ac illumination DBP measurements can be distinguished. There are no significant differences either in the modulation depth of fringes of DBP yield spectra or in the phase of both measurements. This is an indication of homogeneous absorption. This can also be confirmed after fringe free calculation of absorption spectrum. There is no fringes remain on absolute absorption spectrum of this sample as seen in Figure 3.6b. This indicates that light is uniformly absorbed throughout the material. However, this is not observed in all the samples. In addition, there is also important difference in the $\alpha(h\nu)$ spectra at low energies, where DBP back ac illumination gives slightly higher $\alpha(h\nu)$ values. This indicates that DBP back ac illumination probes slightly higher defective layer, which cause high $\alpha(h\nu)$ values at low energies even though high-energy part of $\alpha(h\nu)$ spectrum is almost identical.

Some films exhibit remnant fringes on the $\alpha(h\nu)$ spectrum. As an example of this situation, the results of DBP of a VHF-PECVD grown thin film deposited with SC=6.25% is shown in the Figure3.7. The raw Y_{DBP} spectra and corresponding $\alpha(h\nu)$ spectra measured for ac light coming from film side and substrate side is presented in the Figure 7a and Figure 7b, respectively. The depth of fringes in the raw spectrum measured for ac light incident from film side is slightly higher than that of measured for ac light incident from substrate side. Both measurements were performed for the same intensity of dc bias light to provide the same volume generation rate. The only difference between both measurements is direction of light. There remain fringes after calculation of fringe free absorption spectra in the both spectrum as shown in Fig. 3.7b. For a uniformly absorbing sample, no fringe remains after fringe free calculation as reported by Ritter-Weiser [51]. The remaining fringes can be considered as a indication of inhomogeneous absorption in the material as discussed elsewhere for a-Si:H [60, 61]. The phase of DBP signal for both measurements is also shown in the inset of the Figure 3.7b. An indication of inhomogeneous light absorption can also be

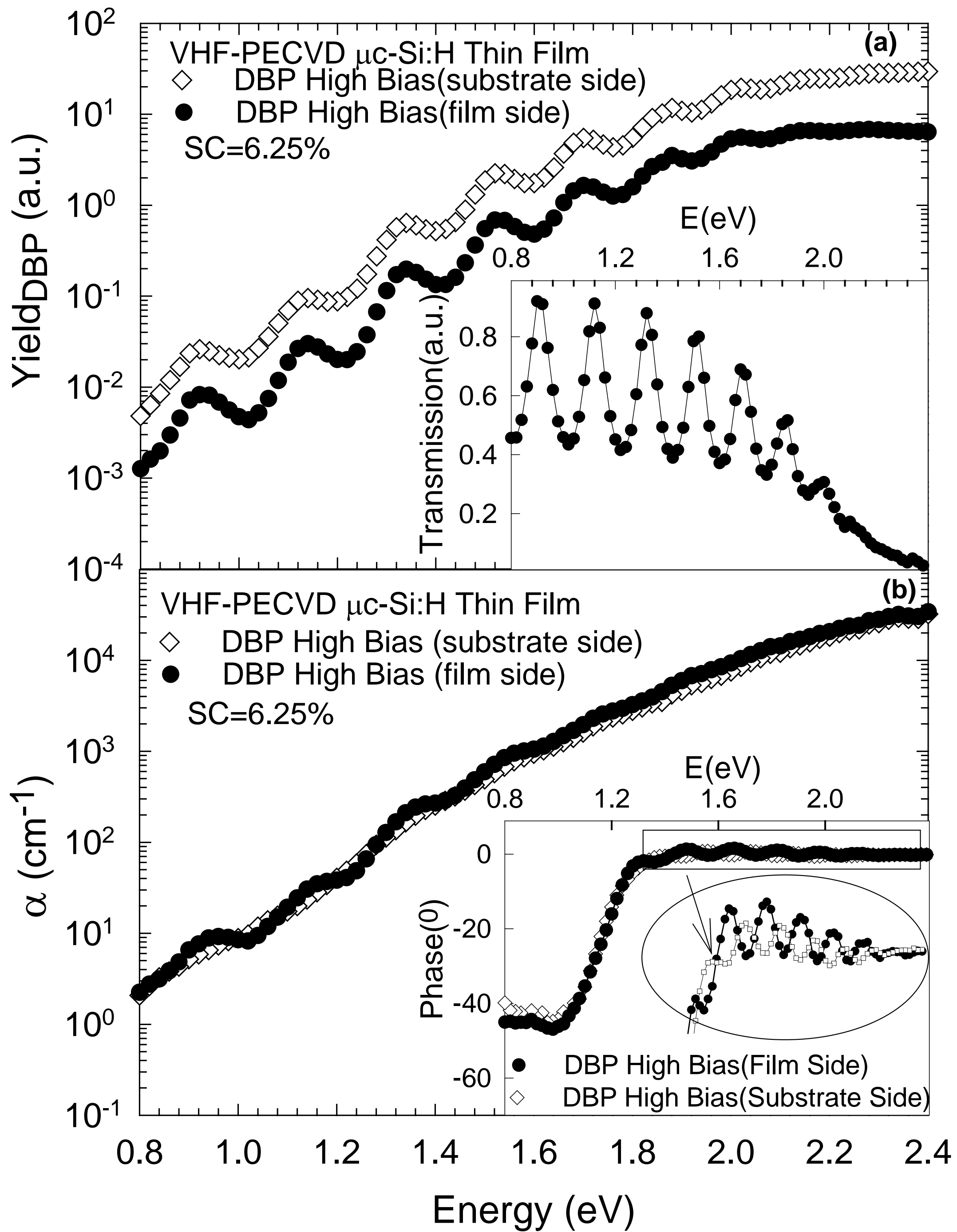

Figure 3.7 a) Y_{DBP} spectra of a intrinsic μc-Si:H thin film deposited using VHF-PECVD with SC=6.25% for ac light incident from substrate side and film side. In the inset, transmission spectrum of the sample is shown. b) Calculated absolute α(hν) spectra of both DBP front and back ac illumination measurements. In the inset, phase of DBP signal are shown

monitored in the phase of signal of both measurements. The phase signal of both measurements exhibits small modulations. However, the modulation depth of phase signal for front ac illumination measurement is much higher. A defective layer closer to the surface of the material could results in such effect in the absorption spectrum of the material. Such kind of fringe patter left on the fringe free calculated $\alpha(h\nu)$ spectrum and modulation in the phase of signal is an indication of the inhomogeneity present in the material. This could be on the surface, at the interface or throughout the bulk of the film or combination of all which can be understood from the calculated $\alpha(h\nu)$ spectrum.

The results of other intrinsic μc-S:H thin films prepared using VHF-PECVD have been obtained using a similar procedure and the $\alpha(h\nu)$ spectrum calculation were carried out. These results are shown in the Figure 3.8, Fig 3.9, Fig 3.10, and Fig 3.11 for the intrinsic μc-Si:H thin films deposited with SC's 3.06%, 3.7 %, 4.3%, 4.9% and 6.25% respectively. For each sample, first part of figure (a) shows raw data of PDS and DBP methods and the corresponding transmission spectra are shown in the inset. In the second part of the figure (b), calculated absorption spectra of both methods are given and their phase are shown in the inset of the figure.

As a summary of the results of PDS and DBP indecently measured on the same sample, it can be said that the $\alpha(h\nu)$ spectra obtained using the both methods at high photon energy part agree very well. However, there exist differences between PDS and DBP at sub-bandgap energies. PDS data is very high due to dominating substrate absorption. After phase correction process to eliminate the substrate absorption, the $\alpha(h\nu)$ values decrease substantially. The PDS phase corrected spectrum and DBP low bias light spectrum can be compared for different μc-Si:H thin films to understand the effect of the microstructure.

In Figure 3.12, the $\alpha(0.80\ eV)$ values obtained from the phase corrected PDS and low bias light DBP spectra are shown as a function of the silane concentration (SC). It is seen that more scatter exist in PDS data due to the noise in the phase of PDS at lower energies, which affects the phase corrected PDS spectrum. However, DBP data show a clear dependence on the SC's. At the lowest SC's, the $\alpha(0.80\ eV)$ values are high due to increased defects in the material. This is also observed in ESR experiments [1,24,62,63]. Similarly, high $\alpha(0.80\ eV)$ values observed in PDS and DBP

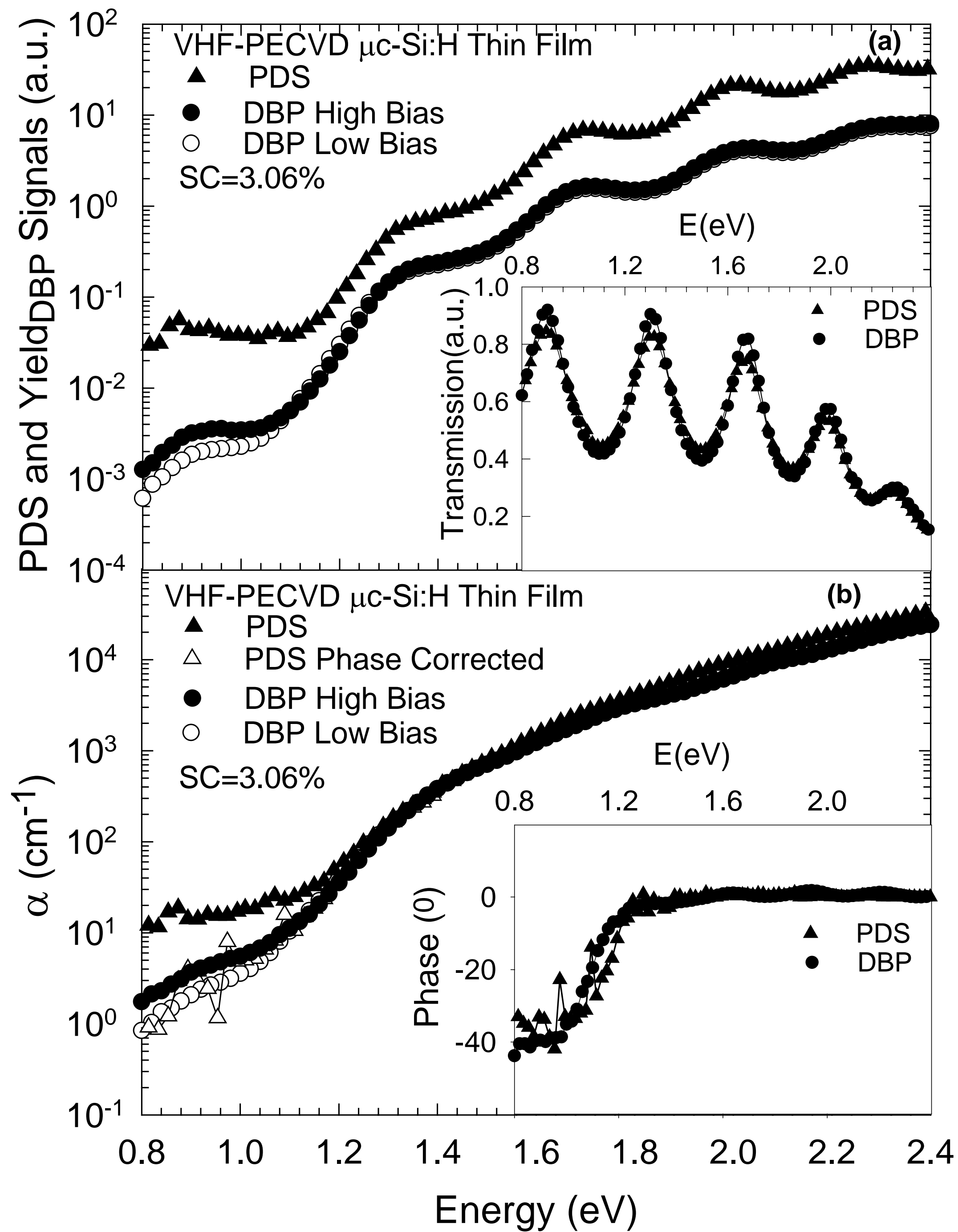

Figure 3.8 a) Raw PDS and Y_{DBP} spectra measured at high and low bias light intensities. In the inset, corresponding transmission spectra are given for a μc-Si:H sample deposited with SC=3.06 %. b) The calculated α(hν) spectra of PDS, phase corrected PDS, and those of DBP measurements. In the inset, the phase of PDS and DBP are given.

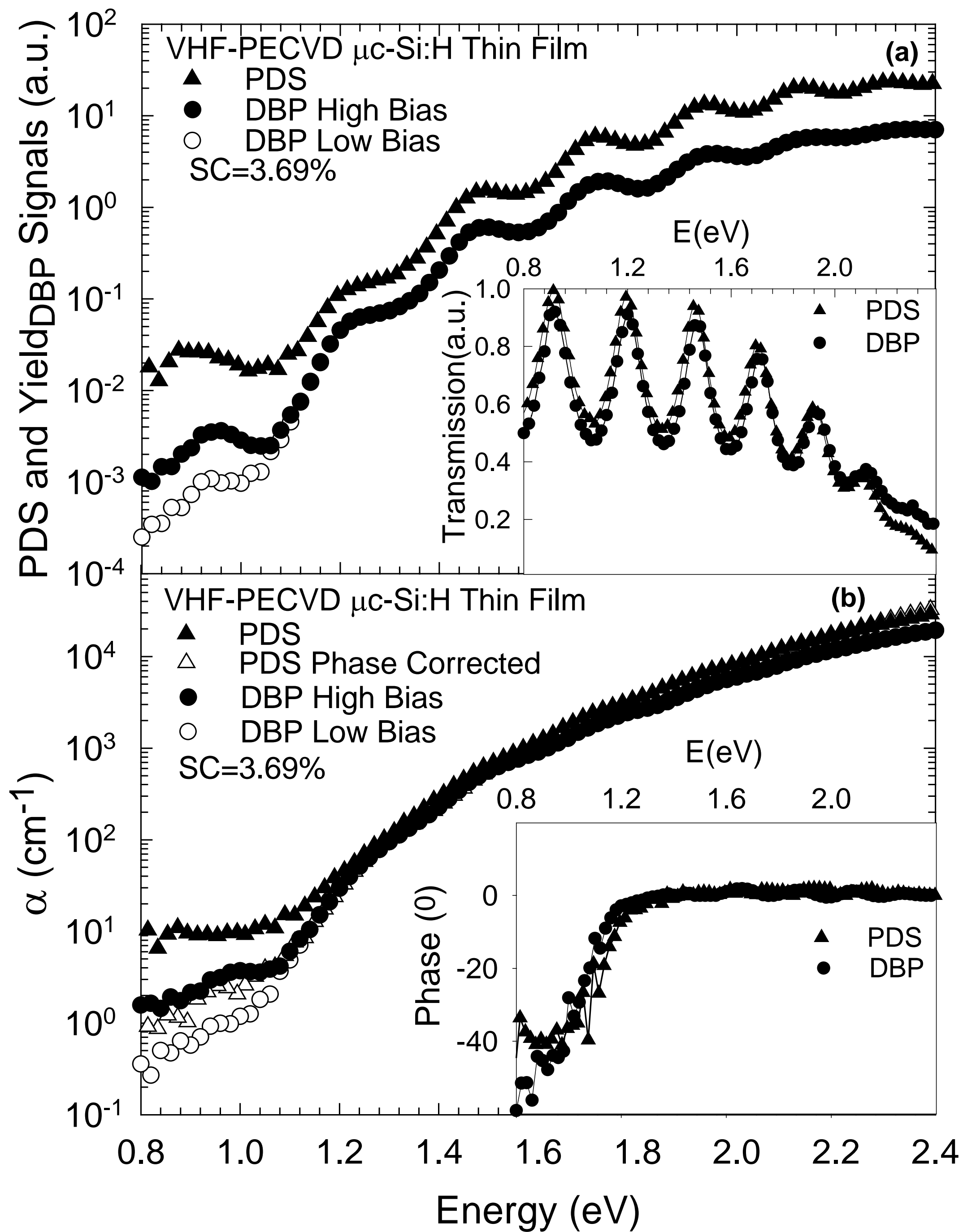

Figure 3.9 a) Raw PDS and Y_{DBP} spectra measured at high and low bias light intensities. In the inset, corresponding transmission spectra are given for a μc-Si:H sample deposited with SC=3.69 %. b) The calculated α(hν) spectra of PDS, phase corrected PDS, and those of DBP measurements. In the inset, the phase of PDS and DBP are given.

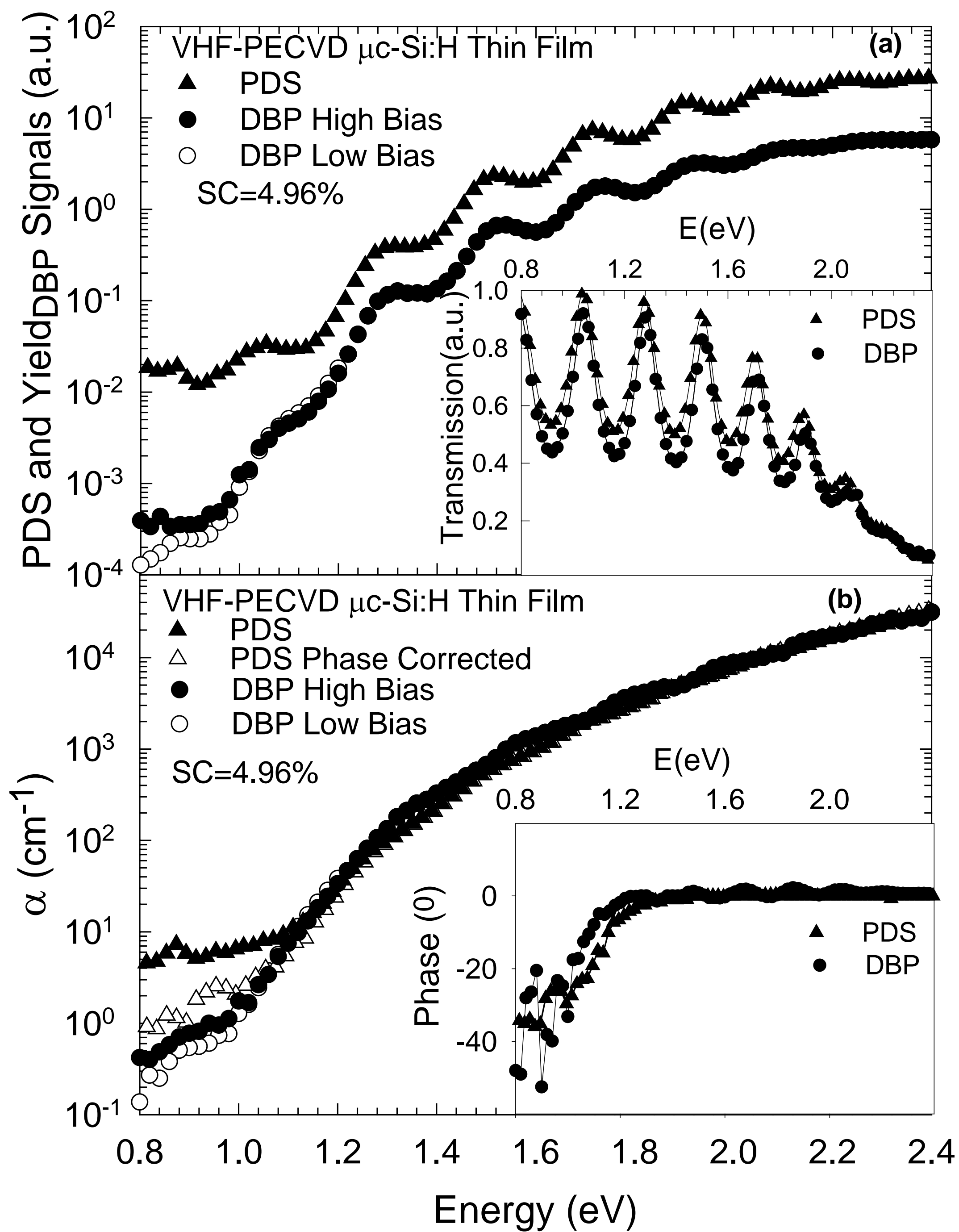

Figure 3.10 a) Raw PDS and Y_{DBP} spectra measured at high and low bias light intensities. In the inset, corresponding transmission spectra are given for a μc-Si:H sample deposited with SC=4.96%. b) The calculated α(hν) spectra of PDS, phase corrected PDS, and those of DBP measurements. In the inset, the phase of PDS and DBP are given.

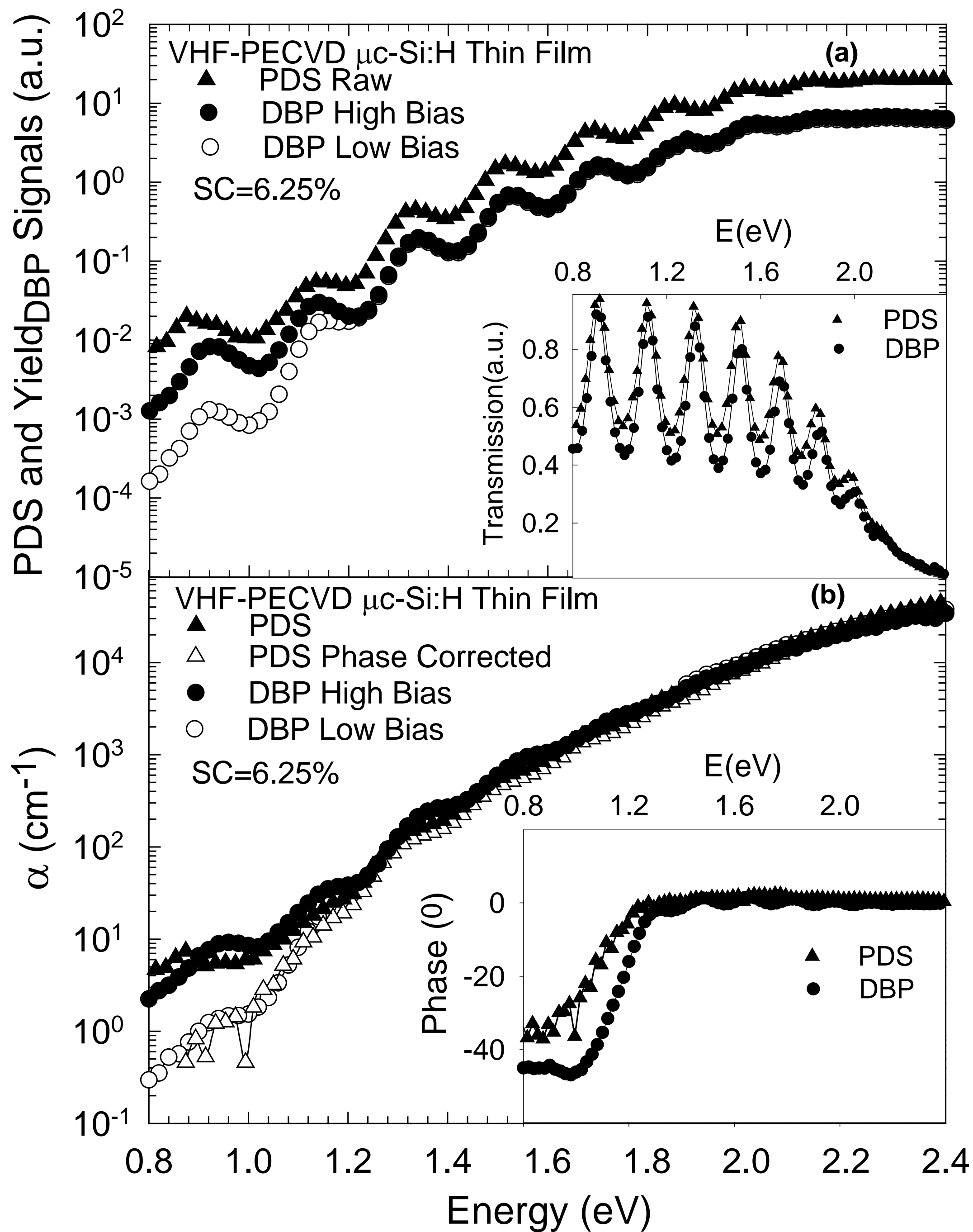

Figure 3.11 a) Raw PDS and Y_{DBP} spectra measured at high and low bias light intensities. In the inset, corresponding transmission spectra are given for a μc-Si:H sample deposited with SC=6.25 %. b) The calculated α(hν) spectra of PDS, phase corrected PDS, and those of DBP measurements. In the inset, the phase of PDS and DBP are given.

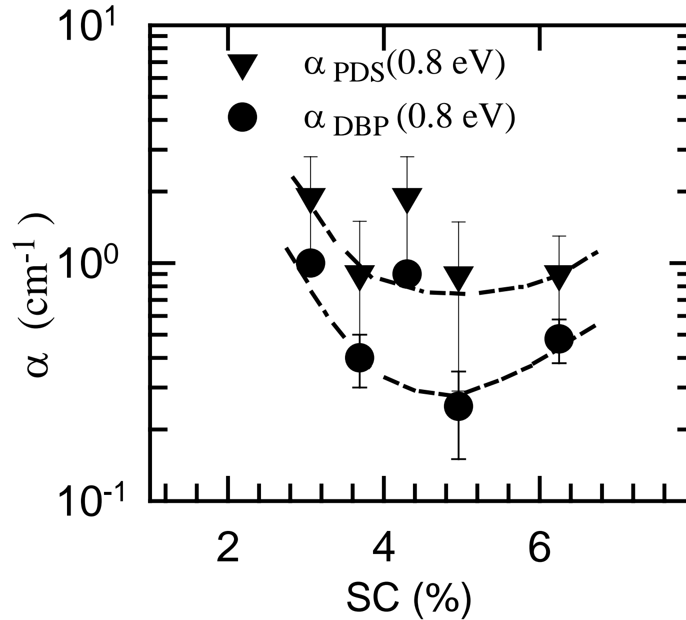

Figure 3.12 Comparison of the α(hν) values at sub-bandgap energy 0.8 eV independently measured by PDS and DBP front ac illumination for intrinsic μc-Si:H thin films deposited by VHF-PECVD. Lines are guide to eye.

indicate that material has higher defect density for lower SC's. As SC increases, the α(0.80 eV) decreases and gives a minimum around SC=5%. This value of SC corresponds to a transition from a microcrystalline to fully amorphous growth. As SC increases further, α(0.80 eV) values tends to increase again due to increased ratio of defective amorphous phase. The results in Figure 3.12 indicates that the μc-Si:H thin films deposited in the transition region have the lowest defect density.

The differences between PDS and DBP curves are also consistent as the nature of both techniques is taken into account. PDS is an absolute absorption measurement technique. As light is absorbed, a transition occurs from the occupied states into empty states above the dark Fermi level. These transitions result in a periodic heat in the material, which cause a modulated temperature gradient in the ambient thus a modulated change in the refraction index of ambient. The change in the refraction index is detected as a deflection in the probe beam, which is used to calculate the α(hν) spectrum of the material of interest. After phase correction of PDS spectrum, PDS give absolute α(hν) spectrum of the material in a wide energy region. However,

in DBP low bias light condition, only distribution of occupied defect states close to that in the dark condition is probed. Only transition of electrons from these occupied defect states into conduction band is measured by DBP photocurrent spectrum, transition into empty states between conduction band and the dark Fermi level are not probed since these transitions do not result in free electrons, neither in photocurrent, but trapped electrons. For this reason, a significant amount of the transition is not probed in DBP method. Therefore, DBP values, for low bias light condition, are approximately two times lower than the corresponding values in the PDS spectrum.

3.3.2 HW-CVD Grown Thin Films

Similar quality intrinsic μc-Si:H films were also prepared using the Hot-wire CVD method for similar range of SC's. The resulting microstructure is altered accordingly, which leads to a change in the electronic and optical properties of the materials. The investigation of the effect of SC on the optical absorption spectrum is extended to HW-CVD grown thin films. PDS and DBP methods were used to obtain reliable $\alpha(h\nu)$ spectrum of HW-CVD grown thin films.

An example of DBP yield spectrum for high and low intensities of dc bias light together with the PDS raw spectrum are shown in the Figure 3.13a for an intrinsic microcrystalline silicon thin film deposited with SC=2.5%. The phase of PDS and DBP signal are shown in the inset of Figure 3.13b. The corresponding transmission spectrum is shown in the inset of in Fig 3.13a. As seen from the figure, there exist a shift between the peak of PDS spectrum and Y_{DBP} spectrum. The same shift is observed in the transmission peaks of both methods as well. This is due to nonidentical samples taken from different part of substrate. However, for each method, measured signal and its corresponding transmission signal have peak points at the same energies as seen from the given figures.

The calculated fringe free absolute $\alpha(h\nu)$ spectrum of the same sample measured by PDS and DBP are shown in the Figure 3.13b. However, for this sample, the spectra of DBP for low and high bias light condition overlap over the entire energy region and difference between two spectra is indistinguishable at lower energies since $\alpha(h\nu)$ values at lower energies are very high. As seen from Figure 3.13b, the PDS and DBP spectra shows a good overlap down to bandgap energy. The deviation in the PDS

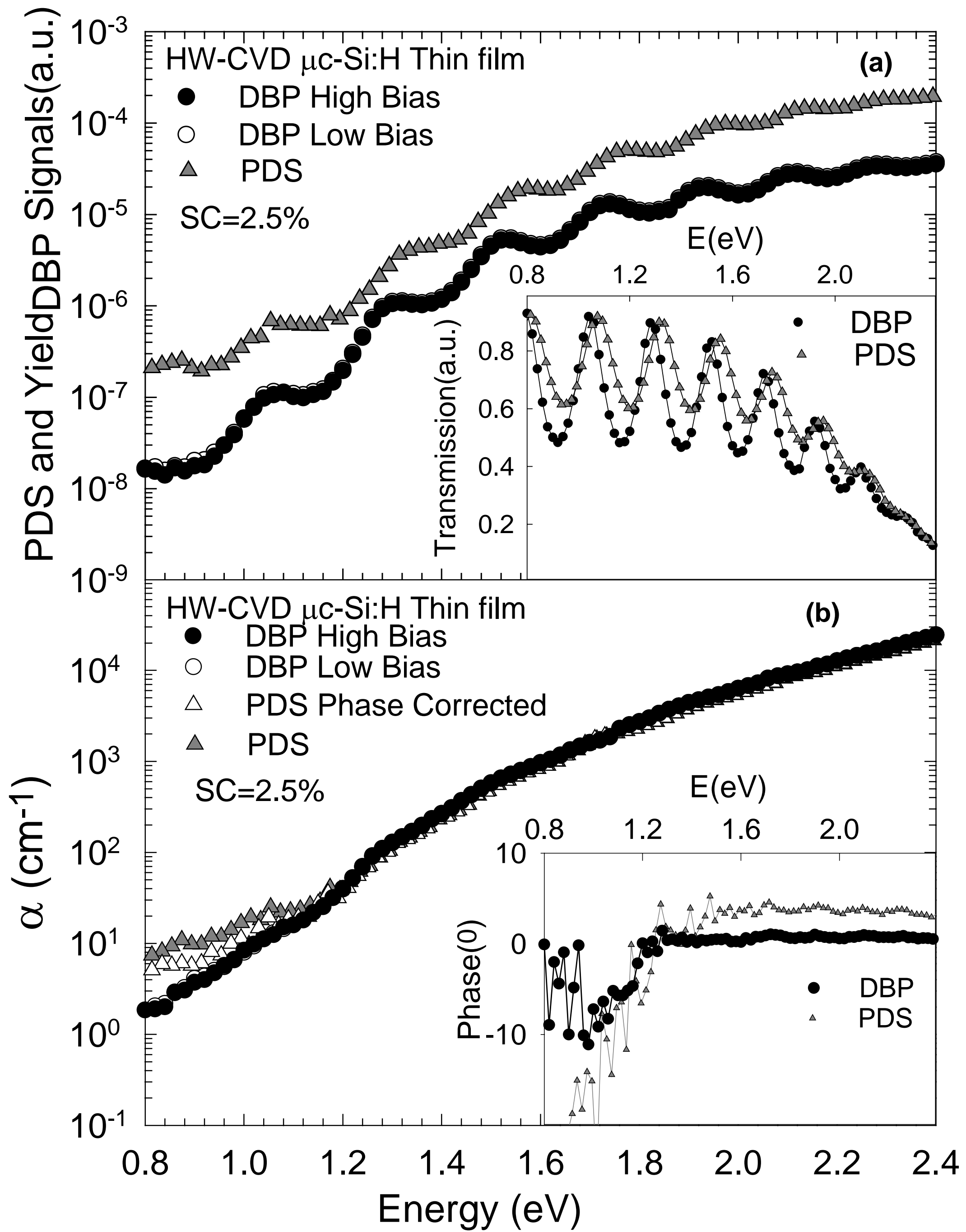

Figure 3.13 a) Raw PDS and DBP Yield spectra of a μc-Si:H thin film deposited by HW-CVD method with SC=2.5%. In the inset, simultaneously measured corresponding transmission signal of PDS and DBP methods are shown. b) Corresponding absolute α(hν) spectra independently obtained from PDS and DBP measurements. In the inset the phase of PDS and DBP measurements are shown.

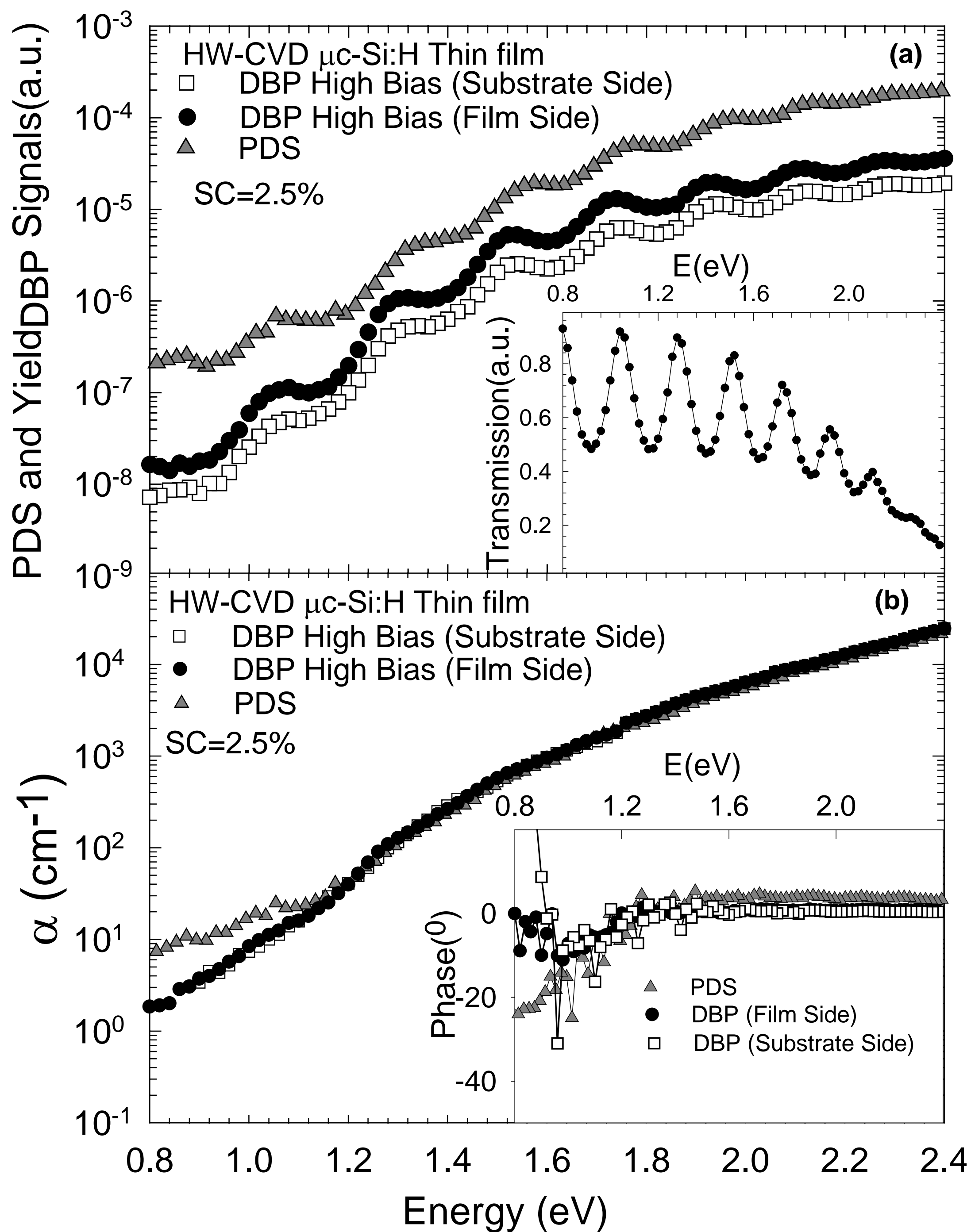

Figure 3.14 a) Raw PDS and DBP Yield spectra of a μc-Si:H thin film deposited by HW-CVD method with SC=2.5%. In the inset, simultaneously measured corresponding transmission signal of PDS and DBP methods are shown. b) Corresponding absolute α(hν) spectra independently obtained from PDS and DBP measurements. In the inset the phase of PDS and DBP measurements are shown.

spectrum below this energy is due to substrate effect as discussed before for VHF-PECVD grown thin films and a phase correction has been carried out.

To investigate the effects of inhomogeneity present in the material, DBP measurements were also performed for ac light incident from substrate side. The intensity of bias light was the same for both measurements to provide the same volume generation rate. The only difference between two experiments is direction of the ac illumination. Y_{DBP} measured for front and back ac illumination are shown in Figure 3.14a together with that of uncorrected PDS measurement. The corresponding transmission and phase data are shown in the inset of Figure 3.14a and Figure 3.14b, respectively. The data measured for light incident from substrate side is labeled as substrate side. As seen from the Figure 3.14a, there is no difference between front and back ac illumination DBP measurements. The corresponding transmission spectra are also identical. The calculated absolute $\alpha(h\nu)$ spectra of these measurements are shown in the Figure 3.14b. It is clearly seen that there remain no fringes in both spectra. The DBP spectra measured for film side and substrate side agree very well and overlap with that measured on the PDS method. This indicates that light is uniformly absorbed throughout the material. However, as discussed for the PECVD grown thin films, this is not always the case for μc-Si:H thin films deposited by HW-CVD method.

To illustrate an example of inhomogeneous absorption of light, sub-bandgap absorption result of PDS and DBP is given in Figure 3.15a, for a HW-CVD grown sample deposited for SC=4%. In the inset transmission of both methods are shown. The peaks of both spectra are located at same energy points and they are identical. The calculated fringe free absolute $\alpha(h\nu)$ spectrum derived from Y_{DBP} for low and high bias light condition together with that of PDS are shown in the Figure 3.16b. In the inset of the figure, the phase of PDS and DBP are shown. As seen from the figure, the PDS and DBP data show a good overlap over the entire photon energy region except below the bandgap. The deviation in the PDS spectrum in that region is due to substrate effect as discussed before. The phase corrected PDS spectrum exhibits a significant scattering since the phase of PDS signal is very noisy in the low energy region. However, the DBP spectrum at low photon energies is a smooth curve and relatively noise free. The DBP spectrum obtained for low bias light condition has lower values below the bandgap energy as expected.

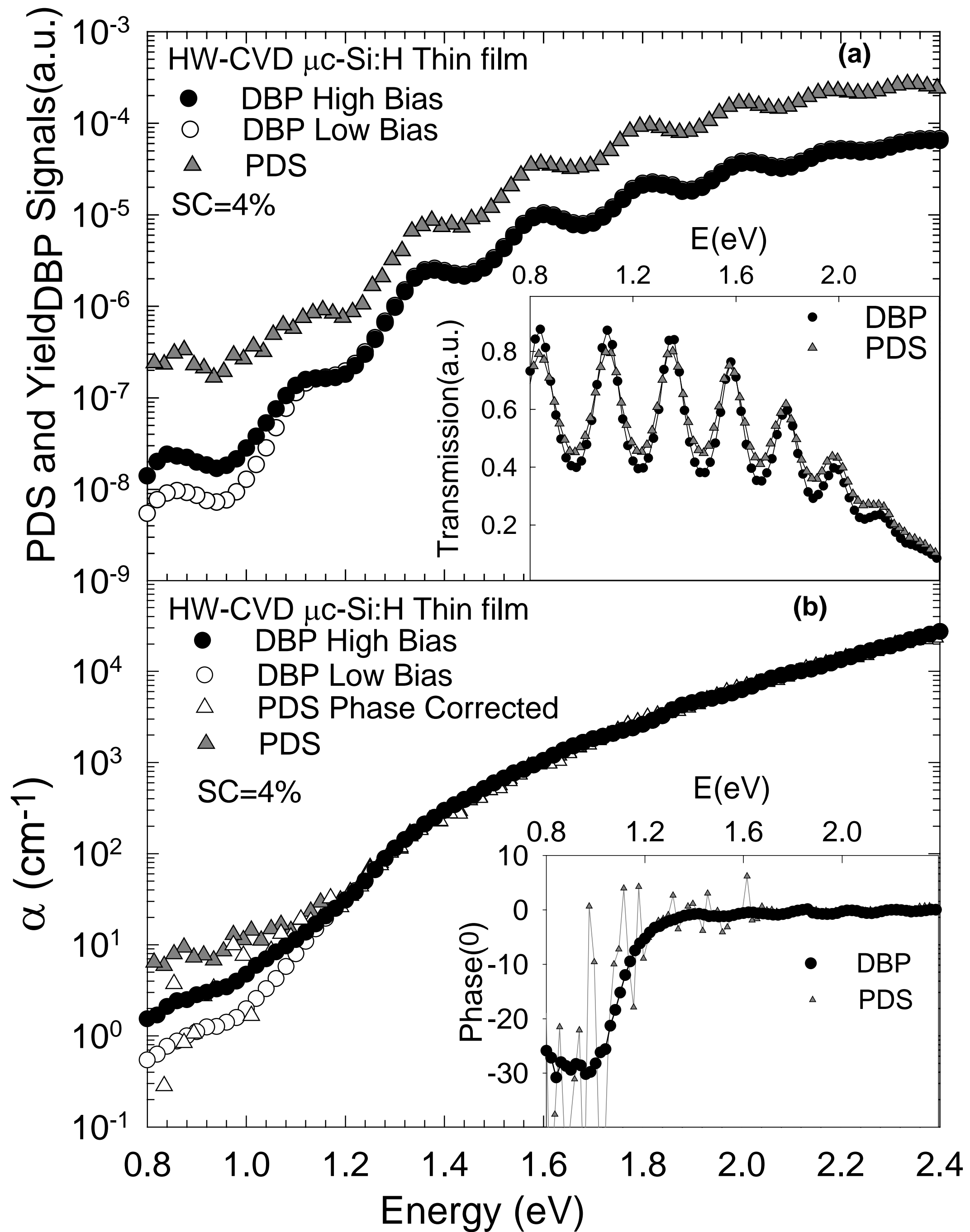

Figure 3.15 a) Raw PDS and DBP Yield spectra of a μc-Si:H thin film deposited by HW-CVD method with SC=2.5%. In the inset, simultaneously measured corresponding transmission signal of PDS and DBP methods are shown. b) Corresponding absolute α(hν) spectra independently obtained from PDS and DBP measurements. In the inset, the phase of PDS and DBP measurements are shown.

At the low bias light condition, DBP probes the distribution of occupied defect states, which is very close to that present in the dark condition. This reflects the effect of occupied defect states bellow the dark Fermi level, which is controlled by the deposition conditions and microstructure. An increase in the $\alpha(h\nu)$ spectrum at lower energies is obtained for HW-CVD grown films as intensity of bias light increase as observed in VHF-PECVD grown thin films. Furthermore, there is a small fringe pattern left on the calculated fringe free $\alpha(h\nu)$ spectrum as seen in Figure 3.15b. Again, this is an indication of inhomogeneous microstructure of sample detected by front ac illumination DBP method. In order to see the effect of the inhomogeneity, DBP with back ac illumination is also carried out. The Y_{DBP} spectra of the same sample for front and back ac light illumination are shown in the Figure 3.16a. There is a significant difference between spectra measured for ac light coming from substrate side and film side, whereas transmission spectra for both cases are almost identical as shown in the inset of Figure 3.16a. The depths of fringes are comparable while the location of maxima and minima of fringes are shifted with respect to each other. The peaks of interference fringes for front ac DBP measurement are in agreement with the peaks of transmission spectrum and located at the same energy points as expected. However, there is a significant shift in the DBP back ac illumination spectrum with respect to that of transmission spectrum. This is a strong indication of inhomogeneous layer at film-substrate interface. The small modulation in the phase for both cases is clearly seen in the inset of Figure 3.16b. The corresponding absolute $\alpha(h\nu)$ spectra calculated for both front and back ac illumination DBP measurements are shown in the Figure 3.16b together with that of PDS. As seen in the figure, the PDS and DBP front ac illumination spectra are in agreement and free of interference fringes. However, DBP spectrum measured for back ac illumination exhibits fringes in it. The remaining fringes are a strong indication of highly inhomogeneous layer at the film-substrate interface. This causes high recombination of photogenerated carriers and decrease photoresponse. However, this is not the case for all the HW-CVD deposited samples investigated in this study. Some of other investigated samples also have differences for spectra of film side and substrate side measurements but no one has such an enormous distinction.

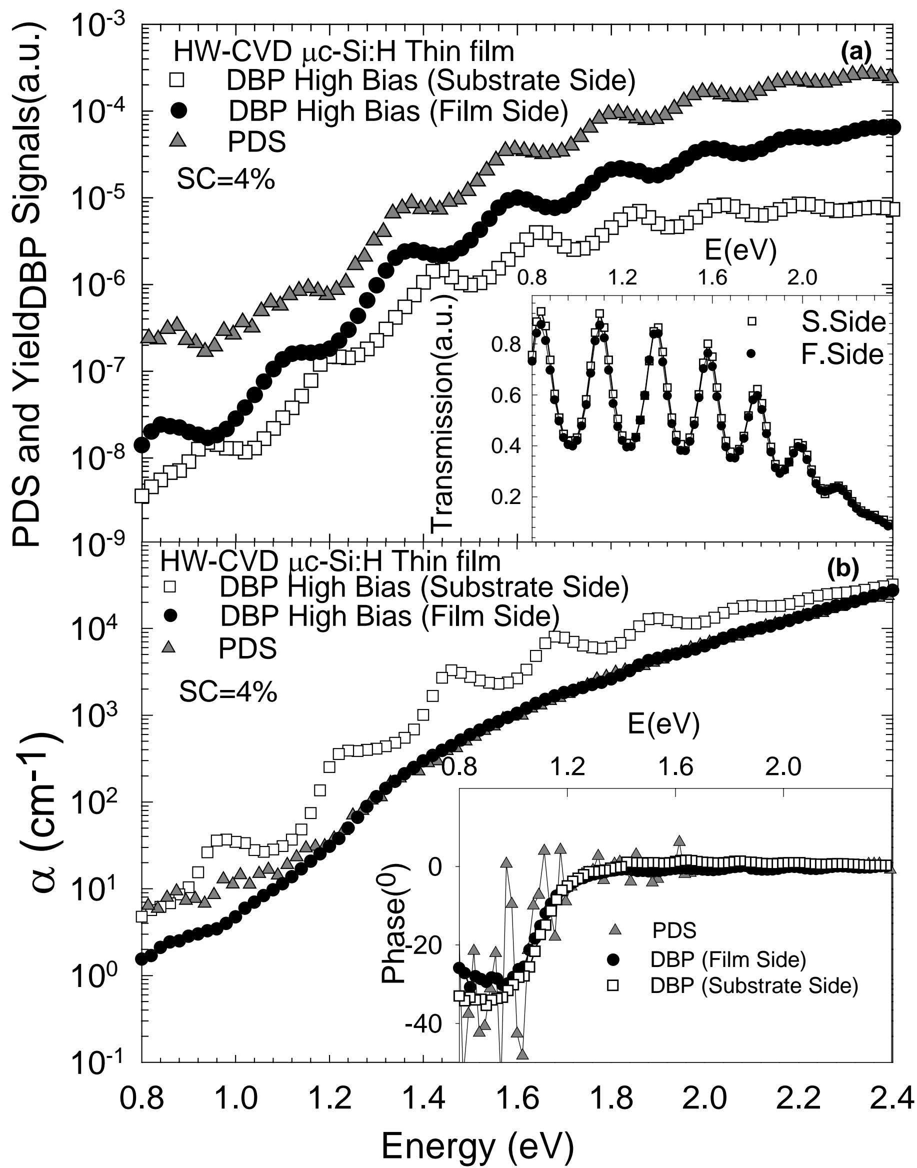

Figure 3.16 a) DBP yield spectra of a a μc-Si:H thin film deposited by HW-CVD method with SC=4% for front and back ac illumination, which is shifted vertically for clarity together with raw PDS spectrum. In the inset, corresponding transmission signals of DBP front and back ac illuminations are shown. b) Calculated α(hν) spectra of DBP measurements for both front and back ac illuminations and that of PDS independently measured on the same sample. In the inset, phase of DBP and PDS are shown

The results for other HW-CVD deposited intrinsic μc-Si:H thin films are given in the Figure 3.17, Figure 3.18, Figure 3.19, Figure 3.20, Figure 3.21 and Figure 3.22 for films deposited with SC's 2%, 4.5%, 5% (for substrate temperature of 185), 5% (for substrate temperature of 215), 6%, 7%, respectively. Each figure is consisting of four parts and is labeled as a, b, c, d and will be presented in two pages. In the (a) part of the each figure Y_{DBP} for low and high bias light condition is shown together with raw signal of PDS. The corresponding transmission measurements of both methods are shown in the inset. The part (b) of the each figure is presented at lower part on the same page and shows the absolute $\alpha(h\nu)$ spectrum of PDS with and without phase correction together with DBP spectrum for low and high bias light. In the second page the (c) and (d) part of each figure is presented. In the (c) part, Y_{DBP} spectra for ac light incident from film side and from substrate side are shown. The corresponding absolute $\alpha(h\nu)$ spectra are shown in the (d) part of each figure.

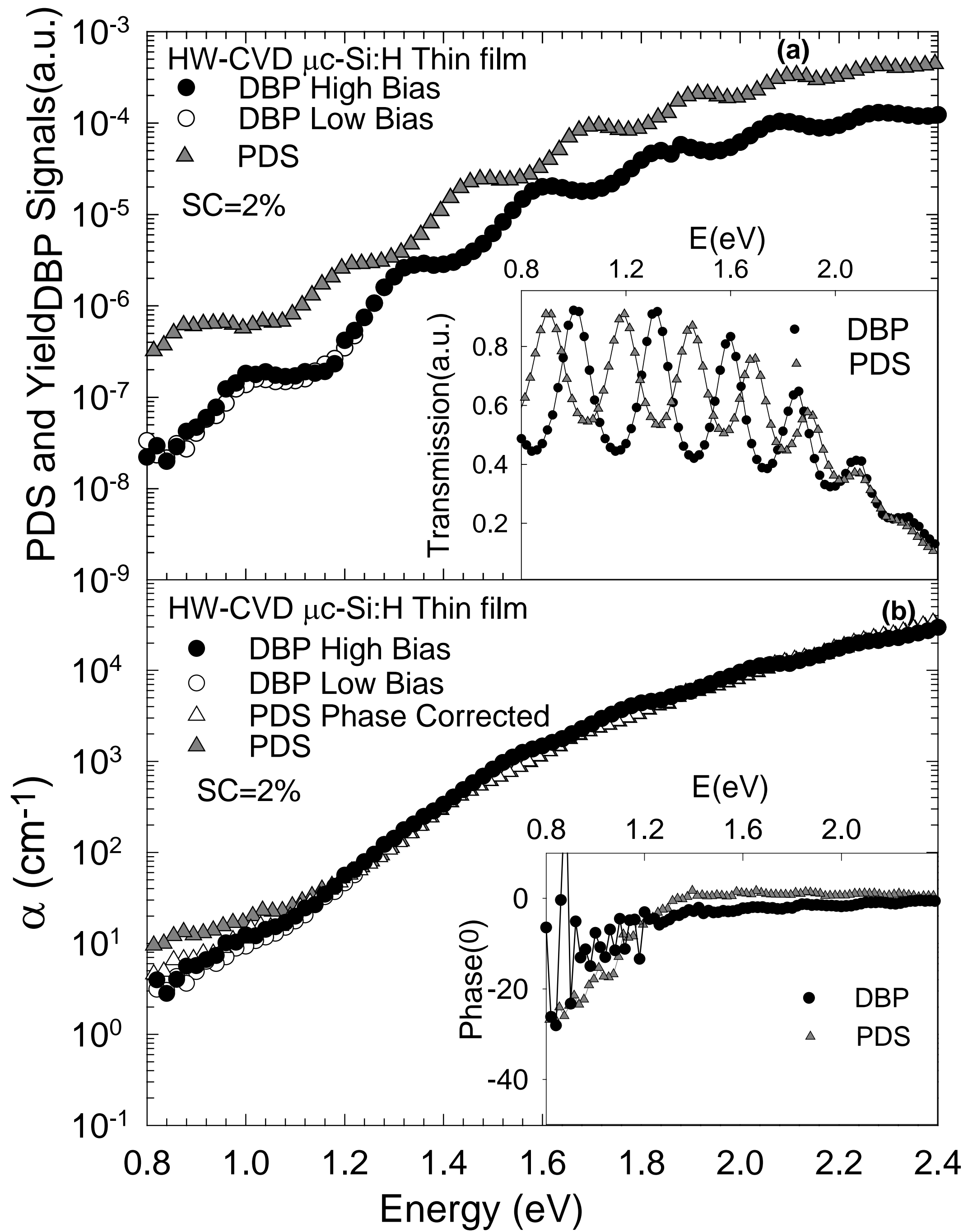

Figure 3.17 . a) Raw PDS and DBP Yield spectra of a μc-Si:H thin film deposited by HW-CVD method with SC=2%. In the inset, simultaneously measured corresponding transmission signal of PDS and DBP methods. b) Corresponding absolute α(hν) spectra independently obtained from PDS and DBP measurements. In the inset the phase of PDS and DBP measurements are shown.

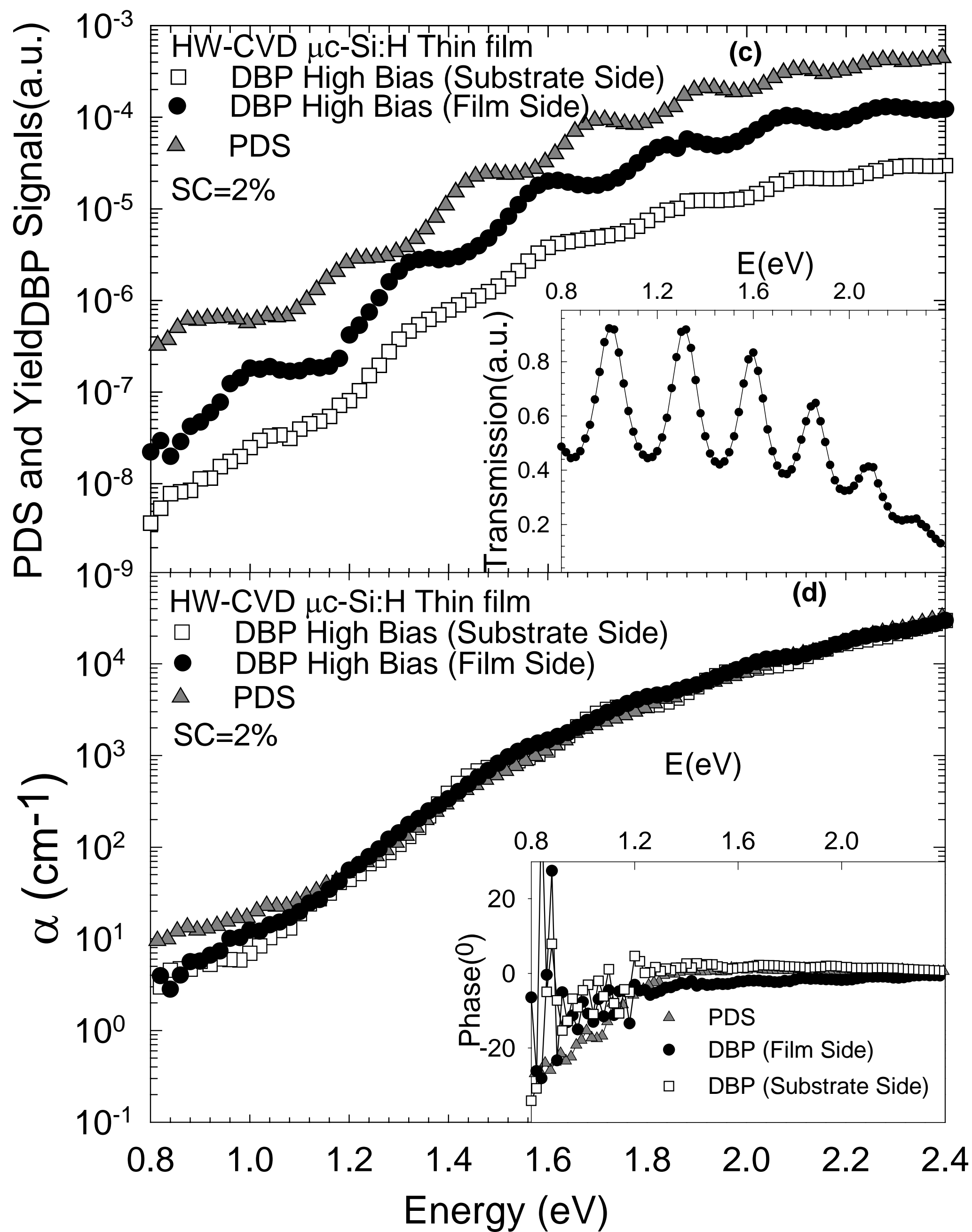

Figure 3.17 c) DBP yield spectra of a a μc-Si:H thin film deposited by HW-CVD method with SC=4% for front and back ac illumination, which is shifted vertically for clarity together with raw PDS spectrum. In the inset the transmission of the sample is shown. d) Calculated α(hν) spectra of DBP measurements for both front and back ac illuminations and that of PDS independently measured on the same sample. In the inset phase of DBP and PDS are shown.

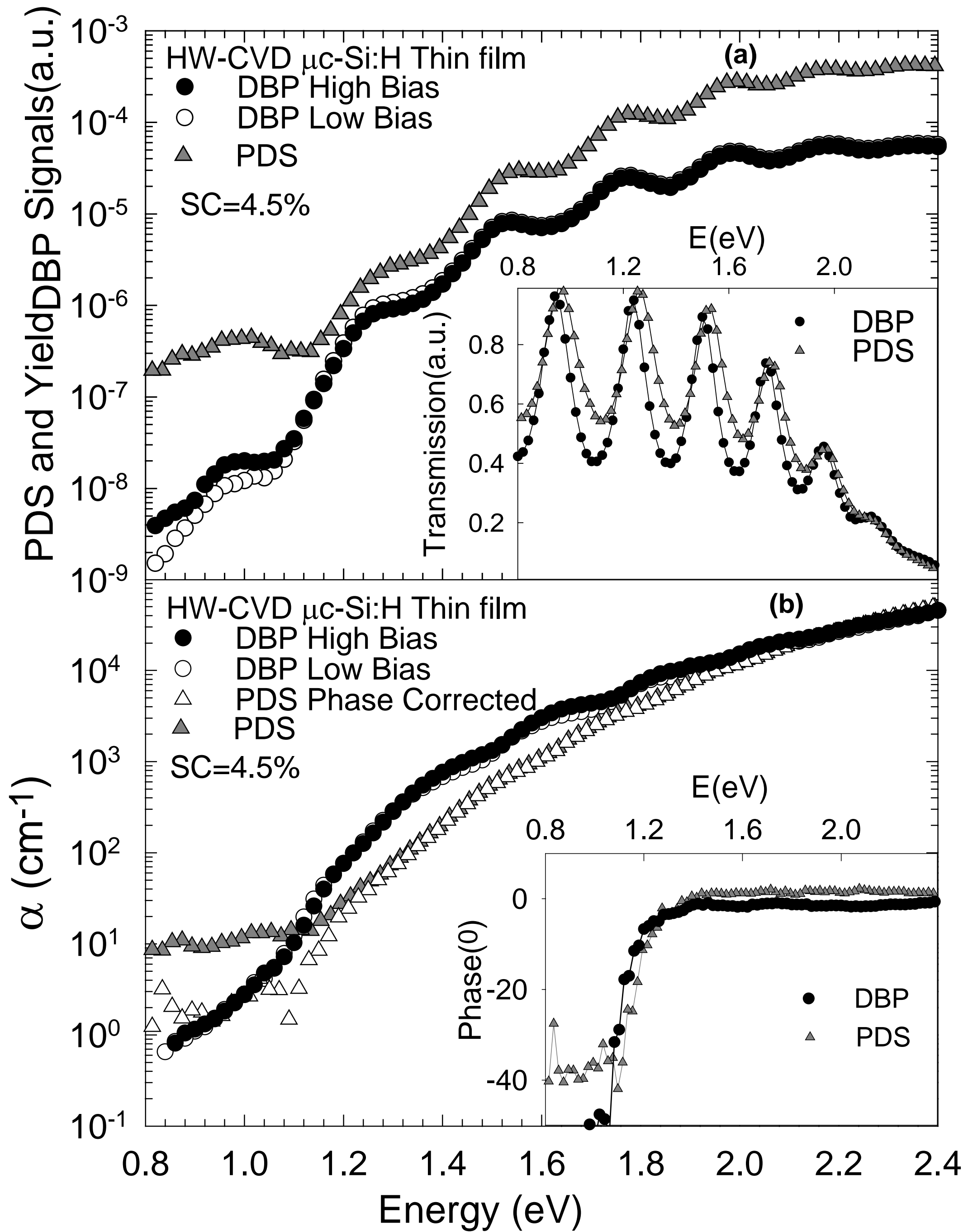

Figure 3.18 a) Raw PDS and DBP Yield spectra of a μc-Si:H thin film deposited by HW-CVD method with SC=4.5%. In the inset, simultaneously measured corresponding transmission signal of PDS and DBP methods. b) Corresponding absolute α(hν) spectra independently obtained from PDS and DBP measurements. In the inset, the phase of PDS and DBP measurements are shown.

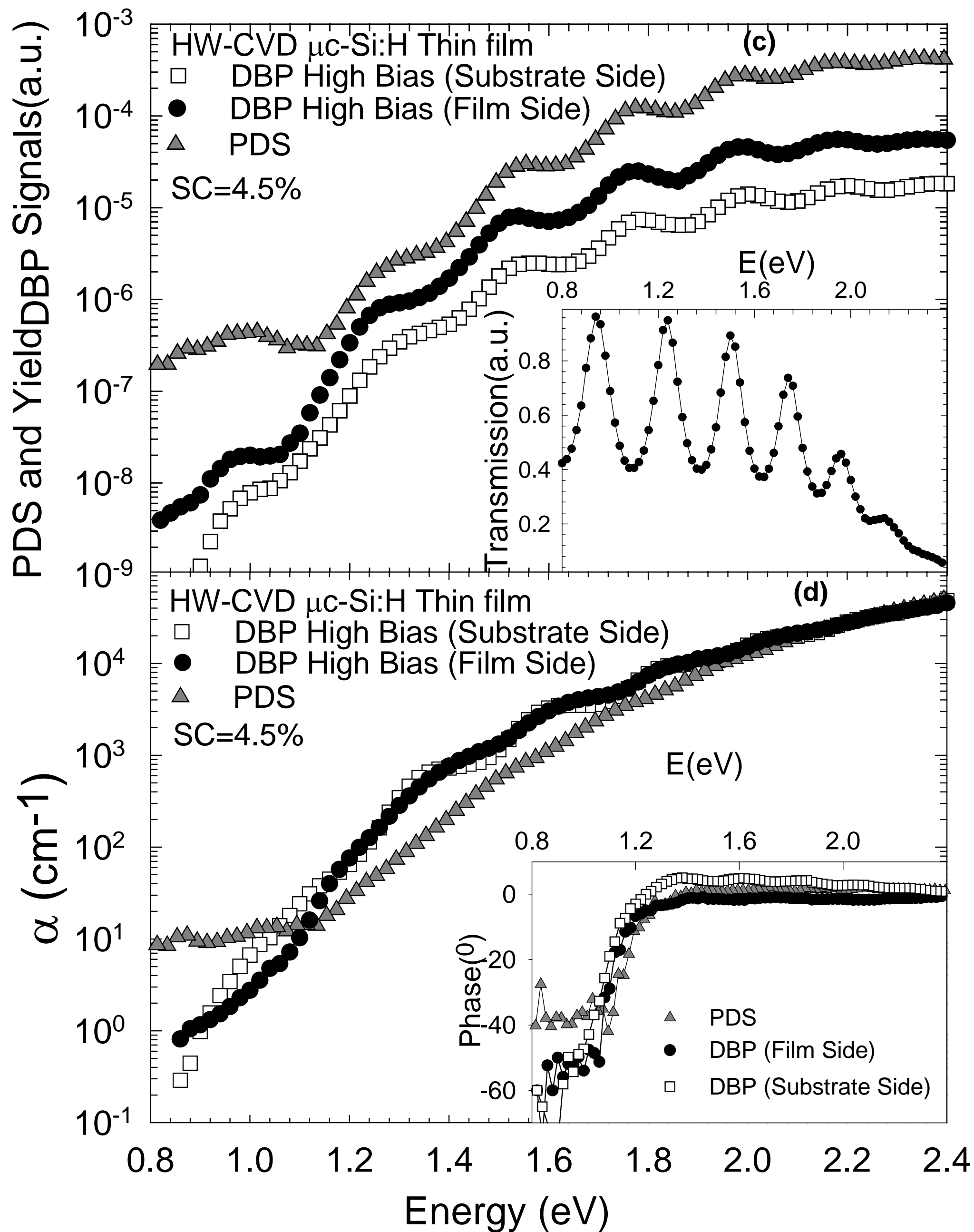

Figure 3.18 c) DBP yield spectra of a a μc-Si:H thin film deposited by HW-CVD method with SC=4.5% for front and back ac illumination, which is shifted vertically for clarity together with raw PDS spectrum. In the inset the transmission of the sample is shown. d) Calculated α(hν) spectra of DBP measurements for both front and back ac illuminations and that of PDS independently measured on the same sample. In the inset, phase of DBP and PDS are shown.

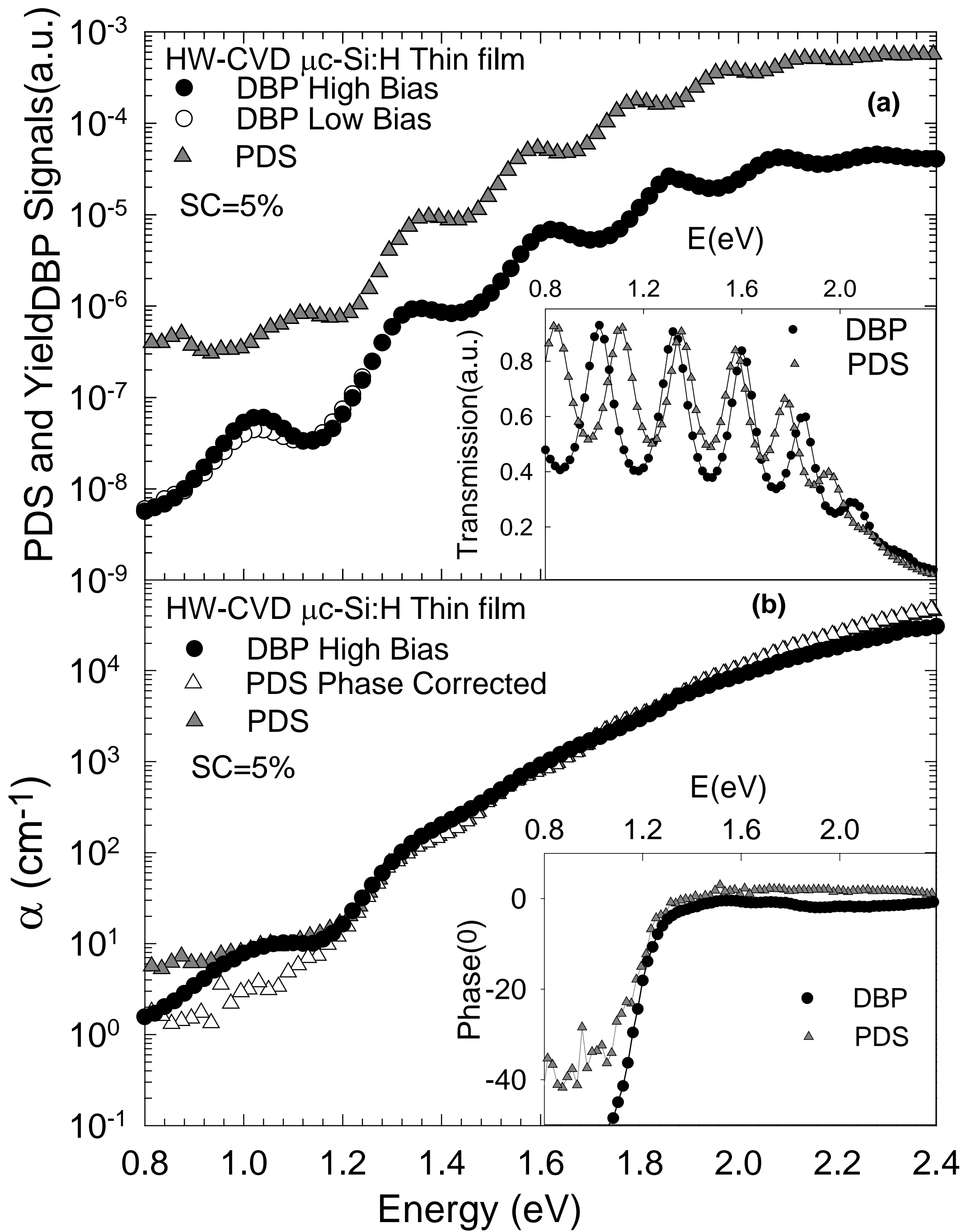

Figure 3.19 a) Raw PDS and DBP Yield spectra of a μc-Si:H thin film deposited by HW-CVD method with SC=5% for substrate temperature of 185 ^{o}C . In the inset, simultaneously measured corresponding transmission signal of PDS and DBP methods. b) Corresponding absolute α(hν) spectra independently obtained from PDS and DBP measurements. In the inset, the phase of PDS and DBP measurements are shown.

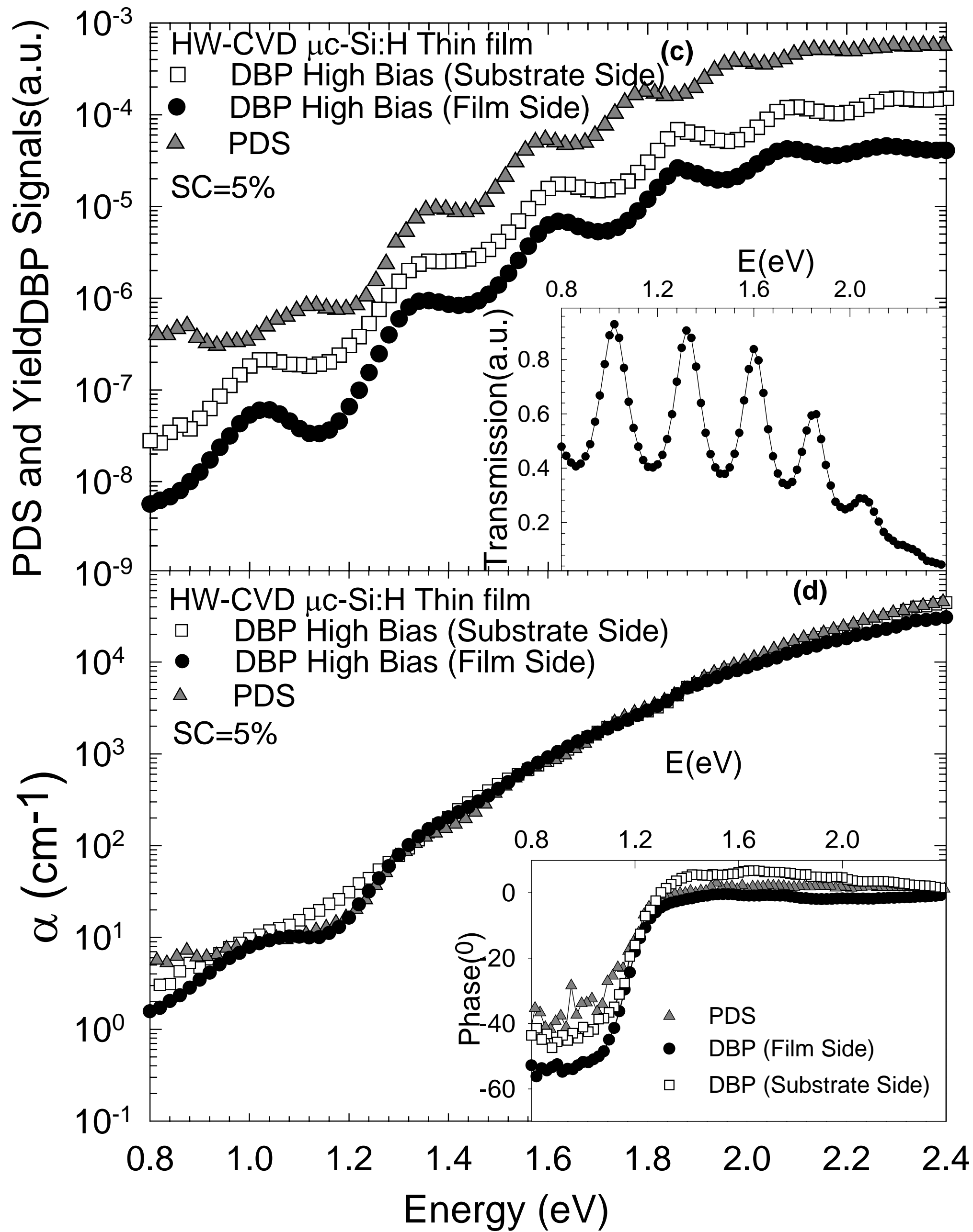

Figure 3.19 c) DBP yield spectra of a a μc-Si:H thin film deposited by HW-CVD method with SC=5% (Substrate temperature is 185 ^{o}C) for front and back ac illumination, which is shifted vertically for clarity, together with raw PDS spectrum. In the inset, the transmission of the sample is shown. d) Calculated α(hν) spectra of DBP measurements for both front and back ac illuminations and that of PDS independently measured on the same sample. In the inset, phase of DBP and PDS are shown.

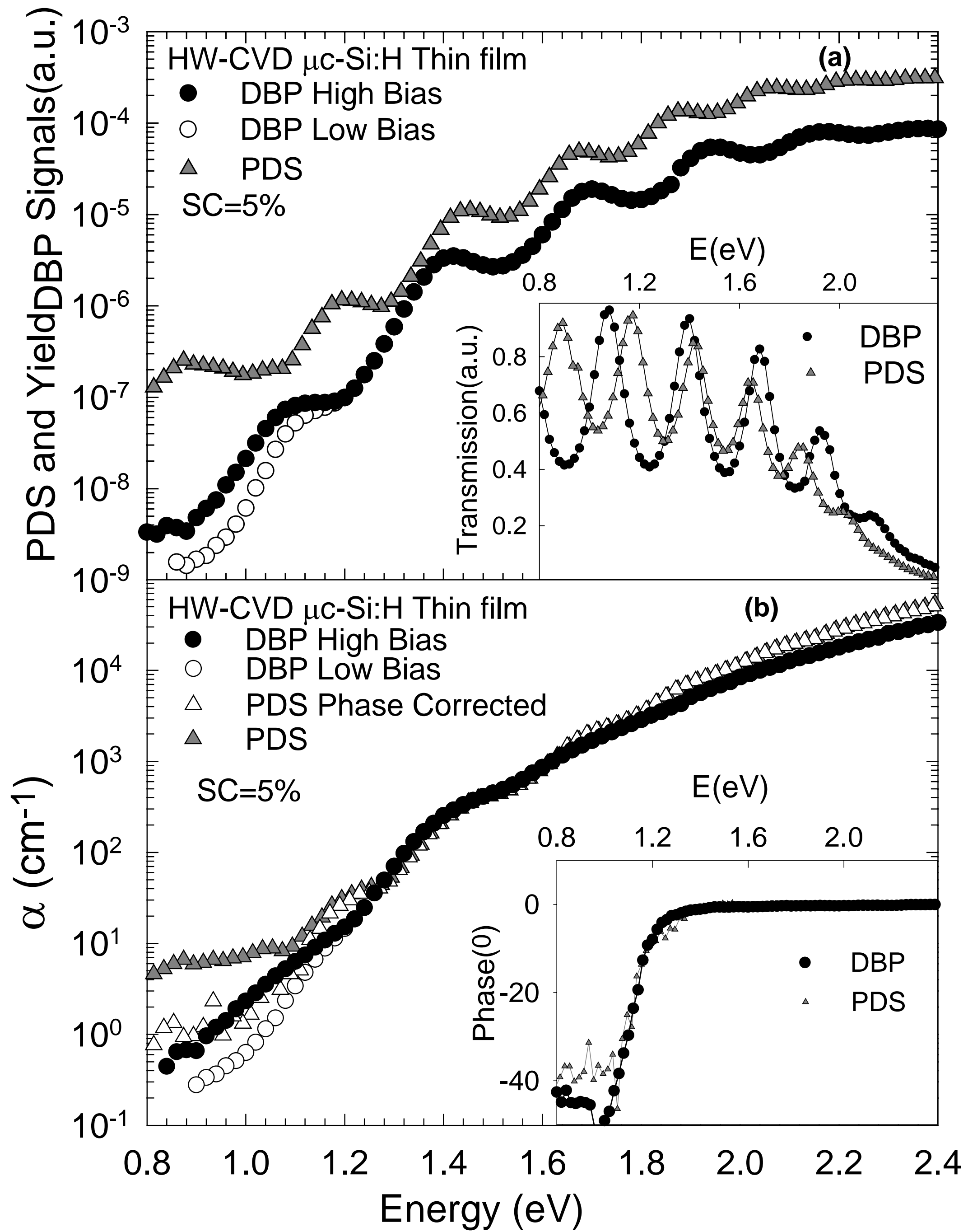

Figure 3.20 a) Raw PDS and DBP Yield spectra of a μc-Si:H thin film deposited by HW-CVD method with SC=5% for substrate temperature of 215 °C . In the inset, simultaneously measured corresponding transmission signal of PDS and DBP methods. b) Corresponding absolute α(hν) spectra independently obtained from PDS and DBP measurements. In the inset, the phase of PDS and DBP measurements are shown.

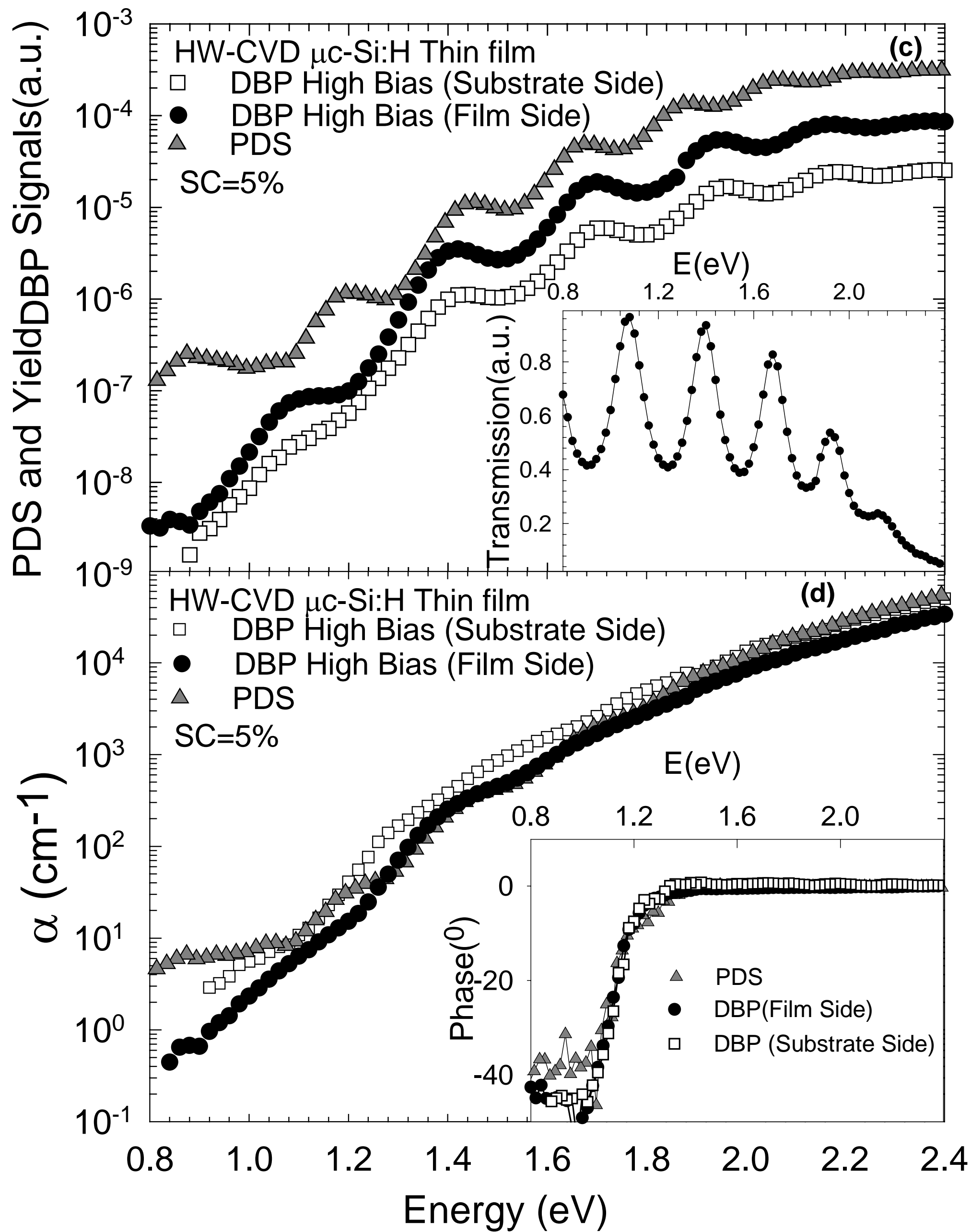

Figure 3.20 c) DBP yield spectra of a a μc-Si:H thin film deposited by HW-CVD method with SC=5% (Substrate temperature is 215 ^{o}C) for front and back ac illumination, which is shifted vertically for clarity together with raw PDS spectrum. In the inset, the transmission of the sample is shown. d) Calculated α(hν) spectra of DBP measurements for both front and back ac illuminations and that of PDS independently measured on the same sample. In the inset, phase of DBP and PDS are shown.

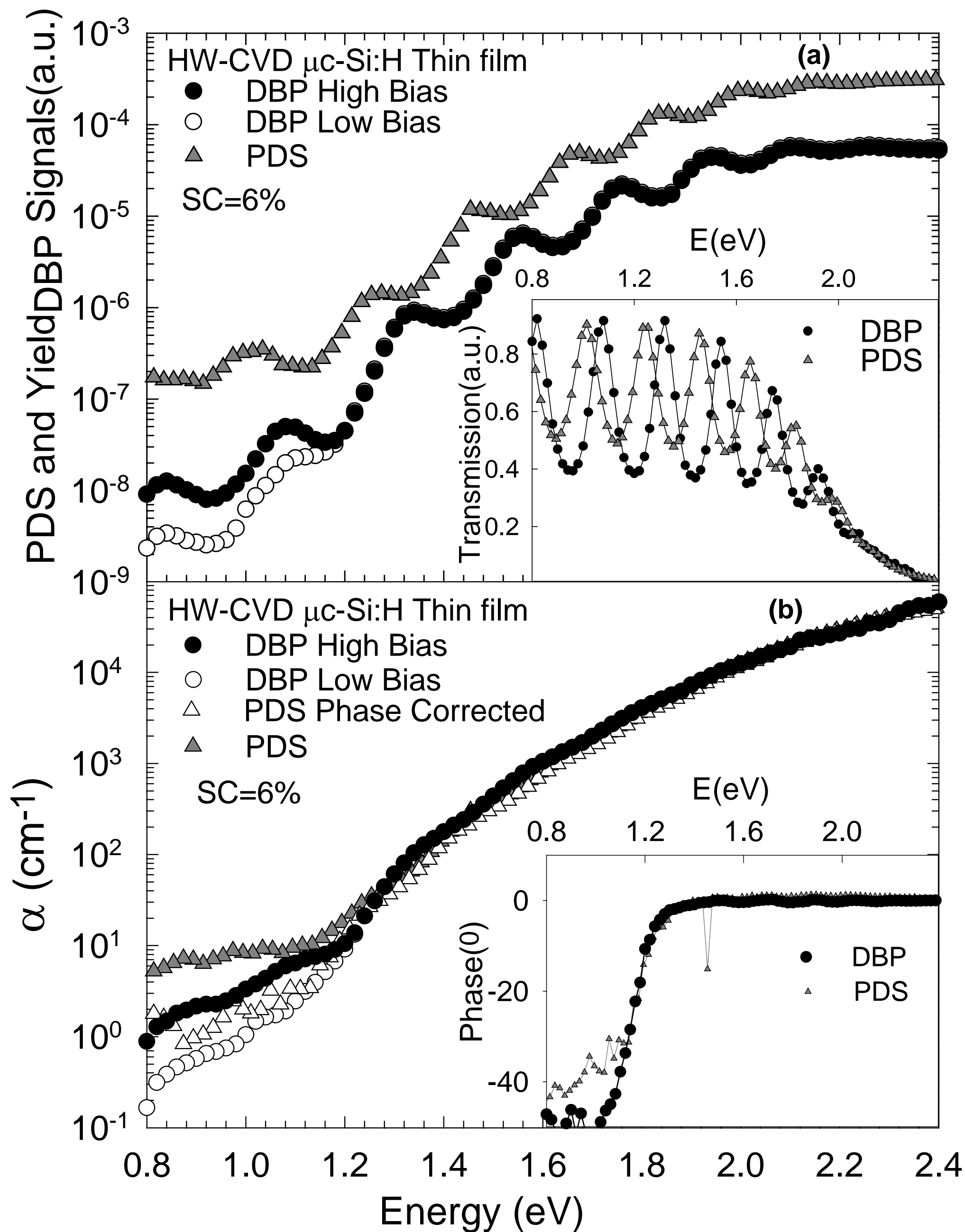

Figure 3.21 a) Raw PDS and DBP Yield spectra of a μc-Si:H thin film deposited by HW-CVD method with SC=6%. In the inset, simultaneously measured corresponding transmission signal of PDS and DBP methods. b) Corresponding absolute α(hν) spectra independently obtained from PDS and DBP measurements. In the inset, the phase of PDS and DBP measurements are shown.

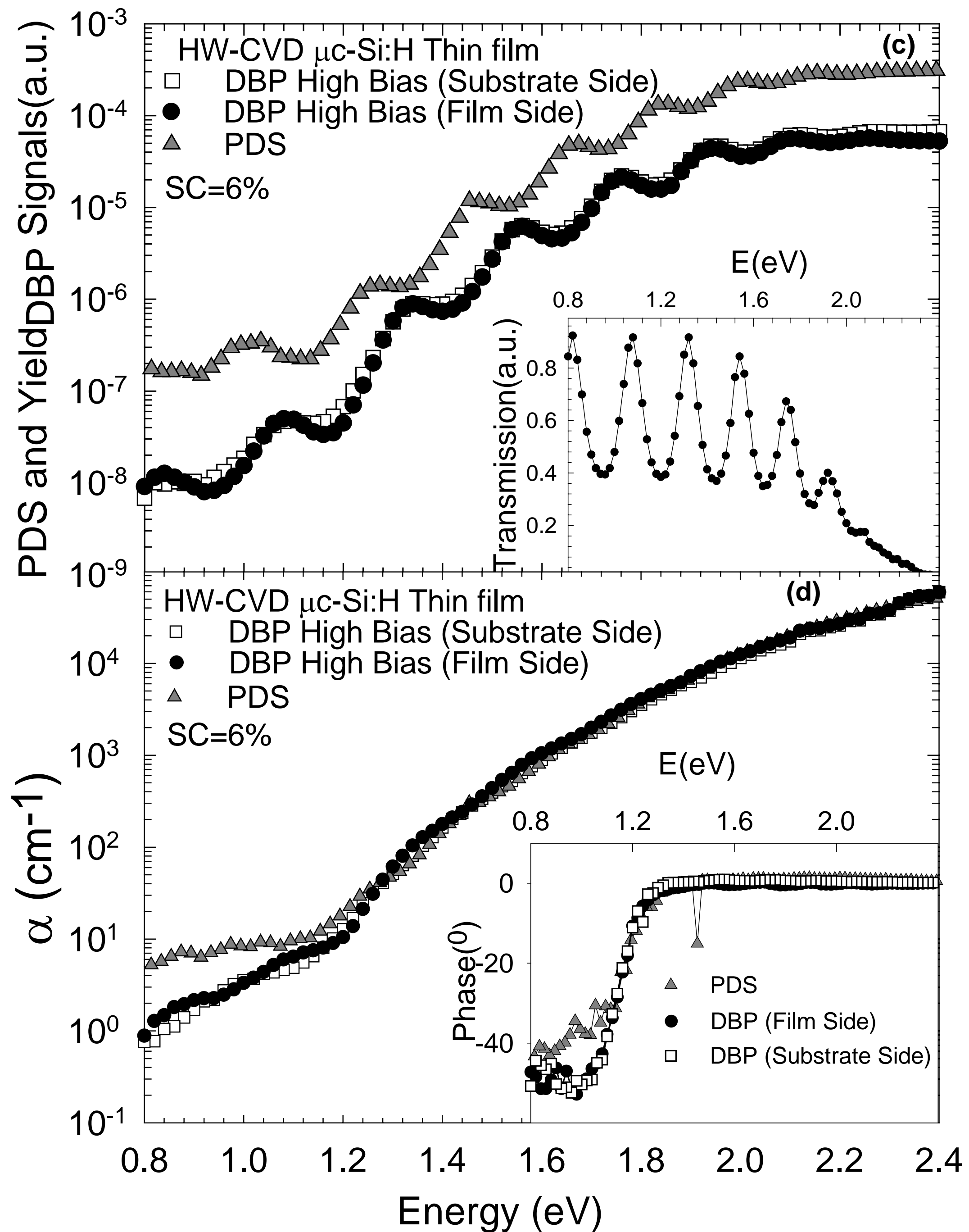

Figure 3.21 c) DBP yield spectra of a a μc-Si:H thin film deposited by HW-CVD method with SC=4.5% for front and back ac illumination, which is shifted vertically for clarity, together with raw PDS spectrum. In the inset the transmission of the sample is shown. d) Calculated α(hν) spectra of DBP measurements for both front and back ac illuminations and that of PDS independently measured on the same sample. In the inset, phase of DBP and PDS are shown.

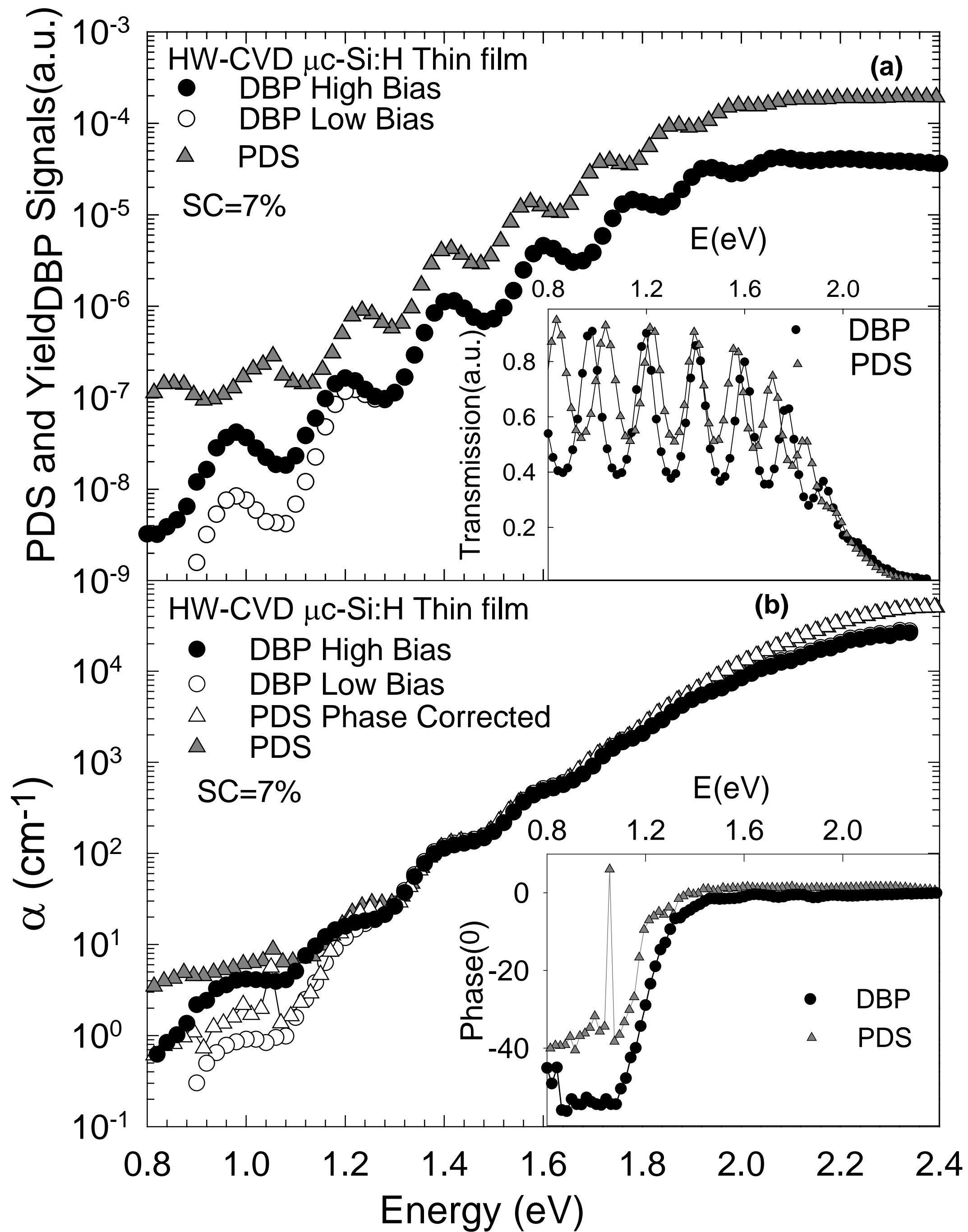

Figure 3.22 a) Raw PDS and DBP Yield spectra of a μc-Si:H thin film deposited by HW-CVD method with SC=7%. In the inset, simultaneously measured corresponding transmission signal of PDS and DBP methods. b) Corresponding absolute α(hν) spectra independently obtained from PDS and DBP measurements. In the inset, the phase of PDS and DBP measurements are shown

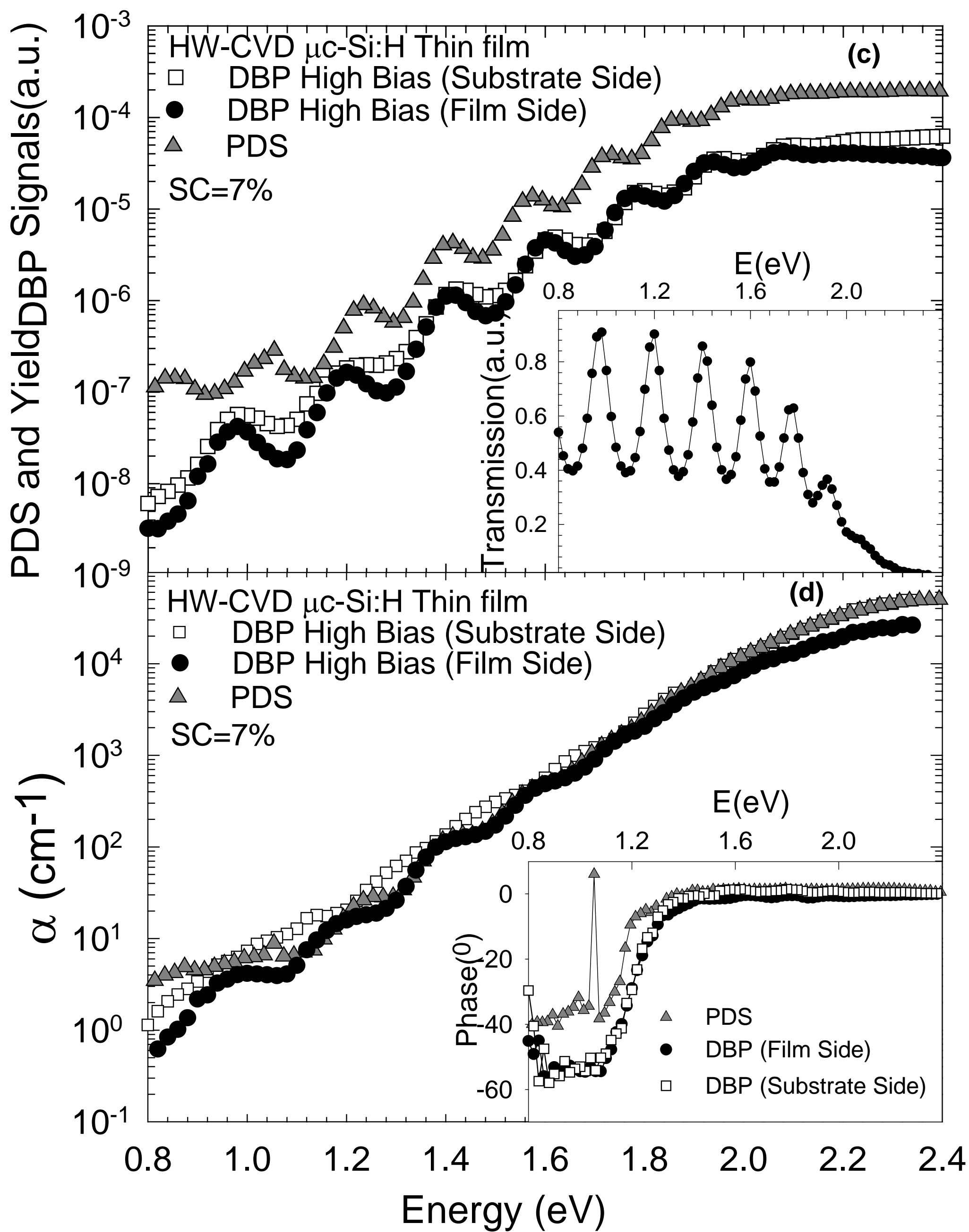

Figure 3.22 c) DBP yield spectra of a a μc-Si:H thin film deposited by HW-CVD method with SC=7% for front and back ac illumination, which is shifted vertically for clarity, together with raw PDS spectrum. In the inset, the transmission of the sample is shown. d) Calculated α(hν) spectra of DBP measurements for both front and back ac illuminations and that of PDS independently measured on the same sample. In the inset, phase of DBP and PDS are shown.

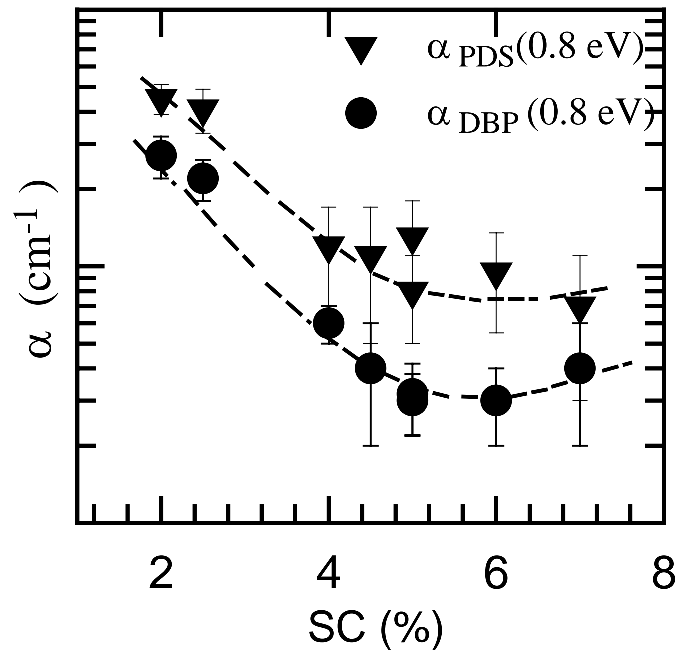

Fig 3.23 Comparison of the α(hν) values at sub-bandgap energy 0.8 eV independently measured by PDS and DBP front ac illumination for intrinsic μc-Si:H thin films deposited by HW-CVD. Lines are guide to eye.

As a summary of sub-bandgap absorption spectroscopy on intrinsic hydrogenated microcrystalline silicon thin films deposited using HW-CVD, it can be concluded that PDS and DBP spectra are in agreement in the high photon energy region when DBP measurements are carried out for front ac illumination. The existing differences between the results of both methods in the lower energy region is either due to substrate effect in the PDS method or intensity dependence of DBP spectrum on the bias light, as discussed in the previous section for VHF-PECVD deposited thin films. The phase corrected PDS spectrum and the DBP spectrum measured for the low bias light condition reflects the defects states present in the bulk of the material. Therefore, α(hν) values at 0.8 eV can be taken as a measure of defect states present in the material, as previously done for PECVD deposited thin films.

The α(0.80 eV) values measured using PDS and DBP low bias light as a function of silane concentration (SC) is presented in the Figure 3.23. For PDS, data was taken from the phase corrected spectrum to eliminate substrate contribution. Similar to PECVD deposited thin films, there exists a systematic difference between PDS and DBP curves. The α(0.80 eV) values measured using DBP for low intensity of

dc bias light is a factor of two lower than that of PDS. The reason of this fact, as previously discussed, is that PDS probes all the transition, whereas DBP only probes the transitions to conduction band. Similar characteristic dependence on SC is observed for both techniques. α(0.8 eV) decreases with increasing silane concentration. It takes its lowest value at around 5-6%, and then exhibits a tendency to increase with increasing silane concentration. The minima occur at about so-called transition region were a transition from the microcrystalline to fully amorphous phase takes place. The results of sub-bandgap absorption spectroscopy manifest that the intrinsic hydrogenated microcrystalline silicon thin films deposited in the transition region have lowest defect density. Therefore, it can be expected that thin films deposited with a silane concentration in that region will results in better device performance. This fact has already been confirmed in the literature both for μc-Si:H based solar cells prepared using the HW-CVD and PECVD deposited thin films [1,4, 62-64].

3.4 Conclusion

In this chapter, the steady state photoconductivity, dual beam photoconductivity (DBP) and photothermal deflection spectroscopy (PDS) methods were used to investigate electronic and optical properties of μc-Si:H thin films prepared using VHF-PECVD and HW-CVD method. From steady state photoconductivity measurements, it is found that for the investigated thin films σ_{ph} versus generation rate obeys the well-known non-integer power-law. The exponent γ was found to be similar for both PECVD and HW-CVD deposited thin films and changes between 0.6 and 1.0, and shows no dependence on the silane concentration. The value of exponent γ indicates that a continuous distribution of defect states present in these structurally inhomogeneous materials. The calculated $\mu_n\tau_n$- product of electrons for PECVD deposited thin films was found to be about a factor of ten higher than that of HW-CVD deposited thin films, which indicates that better device quality thin films were prepared in the VHF-PECVD process. Since the photoconductivity measurements give limited information about the nature of the defect states present in these materials, sub-bandgap absorption of thin films were also measured independently using two different experimental methods, in order to obtain deeper information about these

defect states present in these materials. By using PDS and DBP, optical absorption of the investigated thin films was obtained in a wide energy region. The calculation of fringe free absolute $\alpha(h\nu)$ spectrum from DBP yield spectrum was done for the first time in this study. It is found that for almost all sample the results are in agreement with the absolute $\alpha(h\nu)$ spectrum obtained from PDS. The results of both methods show a good agreement in the high-energy region down to bandgap energy. However, there exist differences between two methods below the bandgap energy. PDS suffers from the substrate effect since absorption in the substrate becomes significant at lower energies and dominates the spectrum, while DBP is insensitive to substrate absorption and is relatively noise free in the sub-bandgap region. However, DBP does not result in the absolute $\alpha(h\nu)$ spectrum below the bandgap energy, since it has a dependence on the bias light intensity. DBP only probes the transition from the empty states into the conduction band whereas PDS probes all the transitions. So in the sub-bandgap region DBP results in lower $\alpha(h\nu)$ values than those measured by PDS, but both values reflect the defects present in the bulk of material. The $\alpha(0.80\ eV)$ values of phase corrected PDS spectra and those of DBP low bias light was used to obtain information about defect states present in the material. It is found that the thin films deposited for silane concentration in the so-called transition region has the lowest defect density.

Since μc-Si:H is structurally inhomogeneous, the DBP measurements, in addition to conventional measurement geometry, were also carried out for ac monochromatic light incident form substrate side. It is found that, for some samples, light is not uniformly absorbed due to the inhomogeneity of the material in the growth direction. The degree of inhomogeneity depends on the deposition condition. The investigations showed that the degree of inhomogeneity is not systematic and variations exist. More investigation is necessary on this important issue present for μc-Si:H thin films.

CHAPTER 4

DISCUSSION AND CONCLUSION

Intrinsic μc-Si:H has recently becomes a very attractive material for electronic applications, especially photovoltaics due to its unique properties. It has extended spectral response of a-Si:H in the high energy region and that of crystalline silicon in the low energy region of solar spectrum. In addition, it is cost-effective, compatible with existing thin film technology presently used for a-Si:H based solar cells and does not suffers from light induced metastability (Staebler-Wronski effect), which is an obstacle for a-Si:H in photovoltaics applications. One of the most interesting properties of intrinsic μc-Si:H is its complicated microstructure which strongly depends on the deposition conditions. Electronic and optical properties of intrinsic μc-Si:H strongly depend on its microstructure, which is mainly controlled by silane concentration. Much effort has been paid for electronic and optical characterization of this material. However, it is still less understood that what leads the best device performance. In this thesis, intrinsic μc-Si:H thin films prepared by VHF-PECVD and HW-CVD techniques have been investigated in detail to understand the electronic and optical properties as a function of changes in microstructure . Steady state photoconductivity (SSPC), Photothermal deflection spectroscopy (PDS),dual beam photoconductivity (DBP), and transmission spectroscopy were used to investigate electronic and optical properties of these materials.

Steady state photoconductivity measurements were performed to understand transport and recombination kinetics of photogenerated carriers in the material. The photoconductivity versus generation rate obeys the well-known non-integer power-low ($\sigma_{ph} \propto G^{\gamma}$). The value of exponent γ was found to be between 0.6-1.0 and similar for both types of films. The obtained values of exponent γ indicate that the material has a continuous distribution of defect states present in its bandgap and photogenerated electrons and holes recombine through these defect states. The calculated $\mu_n \tau_n$- product of electrons for PECVD deposited thin films was found to be almost a factor of ten higher than that of HW-CVD deposited thin films, which implies that better device quality thin films were prepared in the VHF-PECVD process. There is no functional dependence

found on silane concentration for both type of investigated μc-Si:H thin films However, the film deposited for the lowest SC has the lowest $\mu_n\tau_n$- product, which indicates the increased defect density present in the material, which mainly decreases the lifetime τ_n of electrons.

Since steady state photoconductivity provides limited information about defect states present in the material, sub-bandgap absorption spectra of these materials are also measured to get deeper insight about the defects present in the material. Optical absorption of μc-Si:H thin films were measured in a wide photon energy range using PDS and DBP independently. The transmission spectrum of the films was also measured in the both systems. Transmission spectrum is used to obtain thickness of the samples and also to calculate fringe free $\alpha(h\nu)$ spectra of the samples. From PDS measurements, absolute optical absorption of thin films can be obtained. However, for DBP, this was not the case. DBP is based on relative measurement of ac photoconductivity and does not result in the absolute absorption spectrum. Up to this study, DBP yield spectrum has been normalized to PDS spectrum or T&R data in order to set relative spectrum of DBP in absolute scales. This is a difficult task since it necessitates another measurement method to be used to obtain $\alpha(h\nu)$ spectrum in absolute scale. Furthermore, DBP raw spectrum has fringes due to multiple reflections in the sample. These interference fringes are generally averaged. However, this procedure will introduce a significant amount of error in the $\alpha(h\nu)$ spectrum. In addition, this averaging procedure cause a loss of information since appearing fringes in the raw spectrum of the DBP is not only due to interference of light but also due to inhomogeneity of materials [60, 61]. For the first time, in this thesis, we used a procedure, based on Ritter-Weiser formula [51], to get rid of interference fringes on the raw spectra of DBP as explained in Chapter 2. Using this procedure only those fringes arising form interference of light removed and those arising from inhomogeneity of material remains in the spectrum and gives information about the material. In addition, absolute $\alpha(h\nu)$ spectrum is calculated using the DBP yields spectrum and simultaneously measured transmission spectrum. The obtained results were found to be in agreement, with those of PDS in high-energy region for all investigated samples. For VHF-PECVD thin films, the absolute $\alpha(h\nu)$ spectra of both methods shows a good overlap above the 1.2 eV, whereas there are differences for some of HW-CVD films, which can be attributed to

the nonidentical structure of films. In the low photon energy region, PDS spectra deviate due to dominating substrate absorption. The phase corrected $\alpha(h\nu)$ spectrum of PDS is used to eliminate substrate contribution. The accuracy of this procedure, however, is not very high since phase of PDS signal is also noisy in the low energy region of the spectrum. DBP spectrum, on the other hand, is relatively noise free since it is insensitive to substrate absorption. However it does not result in absolute absorption coefficient below the bandgap energy since it has a dependence on the bias light intensity. It rather reflects the occupation of defect states present in the bandgap of the material. DBP low bias light measurement probes the occupation of defect states very close to that in the dark condition. By increasing bias light intensity more defect states in the bandgap are occupied therefore more transition occurs, which results in an increase in the photocurrent and in the $\alpha(h\nu)$ spectrum at lower energies only.

At lower energies, the $\alpha(h\nu)$ values of DBP low bias condition and phase corrected PDS can be used to obtain information about defect states present in the material. It is found that the $\alpha(h\nu)$ values of DBP is smaller then those of PDS. This is consistent with the nature of both methods. PDS probes all transition to conduction band or to the empty states in the bandgap. However, DBP probes only transition to conduction band since transition to empty states above Fermi level does not result in photocurrent. Therefore, apparent absorption measured by DBP below the bandgap energy is smaller than that measured by PDS. However, $\alpha(h\nu)$ values measured by both methods reflect the defect states present in the bulk of the materials. Therefore, absorption in the sub-bandgap region can be used to compare different materials or the materials for different deposition condition.

The measured $\alpha(0.8\ eV)$ values were used to investigate the effect microstructure, which is mainly controlled by silane concentration, on the defect density present in the materials. Form the $\alpha(0.8\ eV)$ values versus silane concentration, Figures given in chapter 3, it is found that the curves has the same characteristics both for VHF-PECVD and HW-CVD deposited thin films .The films deposited for lowest silane concentration have the higher $\alpha(0.8\ eV)$ since those films are highly crystalline and contains high defect density as also measured by ESR. With increasing silane concentration, $\alpha(0.8\ eV)$ values decrease and give minima at about 5%. This value of SC corresponds to so-called

transition region, which means a transition from microcrystalline to fully amorphous growth. As silane concentration further increases, α(0.8 eV) tends to increase for both VHF-PECVD and HWCVD film. As a result, it can be concluded that the films deposited in the transition region have the lowest defect density and will results in the best device performance. This finding is consistent with ESR studies and confirmed by many groups [64,1,65,4,62,63]. However, SC is not directly reflect the microstructure of μc-Si:H since the composition of microstructure is also depends on the other deposition conditions such as substrate temperature and pressure. Therefore, the crystalline volume fraction I_C^{RS}, derived from Raman spectra, is a representation of the changing microstructure to compare different films. In the Figure 4.1 the α(0.8 eV) values of PDS and DBP for both HWCVD and PECVD films are shown as a function of I_{CRS} .At the highest I_{CRS}, α(0.8 eV) values are higher, indicating that high crystalline films are more defective as also confirmed by ESR measurements [24]. As I_C^{RS} decreases, α(0.8 eV) decreases and gives a minimum around 0.5 for HWCVD films, and around 0.6 for VHF-PECVD films. This region is the transition region to amorphous growth region for both type films. As I_C^{RS} decreases further, the α(0.8 eV) values tend to increase due to the effects of defective amorphous phase in the material. The results in Figure 4.1 indicate that lowest defect density films are prepared at the transition region to amorphous growth. Therefore, solar cells fabricated using these materials, as an absorber layer, should result in the highest solar cell efficiencies. These findings have recently been confirmed by the reported results on the solar cells prepared by VHF-PECVD [1] and HWCVD [4] methods.

Furthermore, the discussion about the defect states inferred from the α(0.8 eV) values measured by PDS and DBP requires more explanation. Even though at highly crystalline growth region sub-bandgap absorption coefficient at 0.8 eV indicates that thin films are more defective and ESR measurements also confirms this findings. However, in ESR measurements mainly three different paramagnetic defects are detected with g=2.0052, g=1.996-1.998, and g=2.0043. The first one is attributed to Si dangling bonds, the second one is attributed to conduction electrons and the last one is not identified yet. In DBP, defects probed are not only the defect states detected by ESR but also those are non-paramagnetic defects, which are also called charged defect states. These defect states originate from doubly occupied Si dangling bonds (negatively charged) and unoccupied

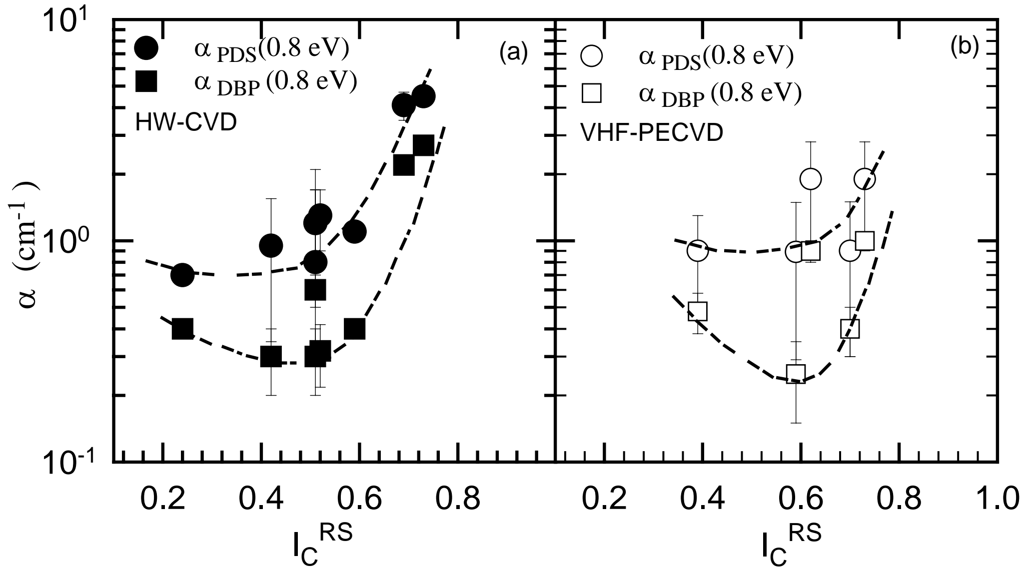

Figure 4.1 The effect of microstructure characterized by the crystalline volume fraction I_C^{RS} on the sub-bandgap absorption coefficient α(0.8 eV) for both HW-CVD and VHF-PECVD μc-Si:H thin films.

Si dangling bonds (positively charged), which are main determining defect in most intrinsic a-Si:H films and affect DBP spectra at high and low bias light intensities [49]. It is known from ESR study that similar defects both in a-Si:H and μc-Si:H are present. Therefore, it could be a possible reason that DBP measurements are also influenced by the non-paramagnetic (charged) defect states. However, in a complicated microstructure of such type intrinsic μc-Si:H non-paramagnetic and ESR active paramagnetic defects are not fully understood yet. The simplest fundamental ESR method also has not identified one of the defect signals at g=2.0043 yet. In the future, more understanding on the microstructure and resulting defects will be advanced and theoretical models will be developed. These experimental results will help in constructing future models for the intrinsic characterization of the intrinsic μc-Si:H thin films.

Furthermore, DBP method has also been used to investigate the inhomogeneity problem of the μc-Si:H thin films. To investigate the effect of inhomogeneity in the α(hν) spectra of μc-Si:H thin films, DBP measurements were also performed for ac light incident through the substrate side. DBP back ac illumination shows that for some films

highly defective layer exist in the film-substrate interface which manifest itself as remaining fringes in the $\alpha(h\nu)$ spectrum. It is also found that some films exhibit remnant fringes in the front ac illumination DBP spectrum. It implies that an inhomogeneous defect layer present near the film surface or through the bulk of the film. However, this is not a systematically observed in all the samples.

In conclusions, DBP method, for both front and back ac illumination, provide very useful information in understanding the optical and electronic properties of intrinsic μc-Si:H thin films and inhomogeneity present throughout the material. Reliable absolute $\alpha(h\nu)$ spectrum is obtained for intrinsic μc-Si:H thin films and correlated with those independently measured from PDS method.

4.1 Future Proposed Research

In this thesis, intrinsic hydrogenated microcrystalline silicon thin films deposited different techniques have been investigated using photothermal deflection spectroscopy and dual beam photoconductivity method. A procedure for calculation of $\alpha(h\nu)$ spectrum from DBP yield spectrum is used and it is found that results are in agreement with those of PDS. However for films have a thickness less than 0.5 μm the accuracy of calculation method becomes less since transmission spectrum in the high-energy region is not free of interference fringes. A more sensitive calculation procedure is a open subject for research. Investigated thin films exhibit an inhomogeneous absorption of light, which manifest themselves as remnant fringes in the spectrum. More investigation are needed to understand the effect of inhomogeneous structure of the material on the $\alpha(h\nu)$ spectrum of the materials. The phase of DBP signal is also serve information about the nature of the defects present in the material. Therefore, a detailed study is necessary to understand the underlying correlation between the phase of signal and the nature of the material. A huge amount of information is hidden in the intensity dependence of DBP on the bias light since it contains information about statistics of occupation of defect states in the bandgap. A detailed numerical and theoretical model remains to be studied in order to obtain information about defect states in the bandgap of these materials.

REFERENCES

1) Vetterl, O., Finger, F., Carius, R., Hapke, P., Houben, L., Kluth, O., Lambertz, A., Mück, A., Rech, B., Wagner, H., Solar Energy Materials & Solar Cells 62 97 (2000)
2) Shah, A.V., Meier, J., Vallat-Sauvain, E., Wyrsch, N., Kroll, U., Droz, C., Graf, U., Solar Energy Materials&Solar Cells 78 (2003) 469-491
3) Kepner, H., Meier, J., Torres, P., Fischer, D., Shah, A., Appl. Phys. A 69, 169-177 (1999)
4) Klein, S., Finger, F., Carius, R., Dylla, T., Rech, B., Grimm, M., Houben, L., Stutzmann, M., Thin Solid Films 430, 202 (2003)
5) Yamamoto, K., Yoshimi, M., Tawada, Y., Fukuda, S., Sawada, T., Meguro, T., Takat, H., Suezaki, T., Koi, Y., Hayashi, K., Suzuki, T., Ichikawa, M., Nakajima, A., Solar Energy Materials and Solar Cells, 74 (2002) 449-455
6) Klein, S., Finger, F., Carius, R., Wagner, H., Stutzmann, M., Thin Solid Films 395, 305 (2001)
7) Schroop, R. E. I., Thin Solid Films, (2003)
8) Veprek, S., Maracek, V., Solid State Electron. 11 (1968) 683.
9) Usui, S., Kikuchi, M., J. Non-Cryst. Solids 34 (1979) 1.
10) Spear, W.E., Willeke, G., LeComber, P.G., Fitzgerald, A.G., J. Phys-Paris 42 (1981) C4.
11) Lucovsky, G., Wang, C., Nemanich, R.J., Williams, M.J., Sol. Cells 30 (1991) 419
12) Faraji, M., Gokhale, S., Choudhari, S.M., Takwle, M.G., Ghaisas, S.V., Appl. Phys. Lett. 60(1992) 3289
13) Flückiger, F., Meier, J., Keppner, H., Kroll, U., Shah, A., Greim, O., Morris, M., Pohl, J., Hapke, P., Carius, R., Proc. Of the 11th EC PV Solar Energy Confernce, Montreux, p.617 (1992)
14) Meier, J., Flcckiger, R., Keppner, H., Shah, A., Appl.Phys. Lett. 65 860 (1994)
15) Finger, F., Hapke, P., Luysberg, M., Carius, R., Wagner, H., and Scheib, M., Appl. Phys. Lett. 65,2588 (1994)

16) Prasad, K., Finger, F., Curtins, H., Shah, A., and Baumann, J., Proc. Mat. Res. Soc. Symp. 164 27 (1989)
17) Rech, B., Roschek, T., Muller, J., Weider, S., and Wagner, H., Solar Energy Materials and Solar Cells 66,267 (2000)
18) Heya, A., Nakat, K., Izumi, A., and Matsumura, H., Mat. Res. Soc. Symp. Proc. 507, 435 (1998)
19) Meier, J., Dubail, S., Platz, R., Torres, P., Kroll, U., Anna Selvan, J.A., Pellaton Vaucher, N., Hof, Ch., Fischer, D., Keppner, H., Shah, A., Efert, K.-D., Giannoules, P., Koehler, J. Solar Energy materials and Solar cells, 49 (1997), 35-44
20) Procceding of the 3rd World Confernce on Phorovoltaic Energy Conversion, Osaka, Japan, 2003
21) Matsuda, A., Journal of Non-Cryst. Solids 59/60 767-747 (1983)
22) Iqbal Z., and Veprek, S., J. Phys. C: Solid State Physics 15, 377 (1982)
23) Hapke, P., Luysberg, M., Carius, R., Tzolov, M., Finger, F., and Wagner, H., J. Non-Crystalline solids 200, 198 (1996)
24) Neto, A. L. B., Dylla, T., Klein, S., Repmann, T., Lambertz, A., Carius, R., and Finger, F., Journal of Non-Cryst. Solids 338-340, 168 (2004)
25) Ray, S., Mukhopadhyay, S., Jana, T., Carius, R., Journal of Non-Cryst. Solids 299-302, 761 (2002)
26) Ossadnik, Ch., Veprek, S., and Gregora, I., Thin Solid Films 337 148 (1999)
27) Carius, R., in Photovoltaic and Photoactive Materials-Properties, Technology and Applications, NATO Science series 2. Vol. 80 p.93
28) Houben, L., Luysberg, M., Hapke, P., Carius, R., and Wagner, H., Philos. Mag. A 77, 1447 (1998)
29) Vetterl, O., Groβ, A., Jana, T., Ray, S., Lambertz, A., Carius, R., Finger, F., Journal of Non-Cryst. Solids 299-302, 772 (2002)
30) Iqbal, Z., Saroot, F.-A., Veprek, S., Solid State Phys. 16 (1983) 2005
31) Vanecek, M., Poruba, A., Remes, Z., Beck, N., Nesladek, M., J. Non-Crys. Solids 227-230 (1998) 967

32) Poruba, A., Fejfar, A., Remes, Z., Springer, J., Vanecek, M., Kocka, J., Meier, J., Torres, P., Shah, A., J. Appl. Phys. 88 (2000) 148.
33) Jun, K. H., Carius, R., and Stiebig, H., Phys. Rev. B 66 (2002) 115301
34) Veprek, S., Iqbal, Z., Kühne, R. O., Capezzuto, P., Sarott, F. A., Gimizewski, J.K., J. Phys. C 16, 6241 (1983)
35) Finger, F., Müller, J., Malten, C., Wagner, H., Philos. Mag. B 77, 805 (1998)
36) Lips, K., Kanschat, P., Fuhs, W., Solar Energy Mat&Solar Cells 78, 513 (2003)
37) Finger, F., Müler, J., Malten, C., Carius, R., and Wagner, H., J. Non-Cryst Solids 266-269, 511 (2000)
38) Carius, R., Finger, F., Backhousen, U., Luysberg, M., Hapke, P., Houben, L., Otte, M., Overhoff, H., Mater. Res. Soc. Symp. Proc. 467, 283 (1997)
39) Ram, S. K., Kumar, S., Vanderhagen, R., Cabarrocas, P. R., J. Non-Cryst. Solids 299-302, 411 (2002)
40) Jackson, W., Amer, N. M., Boccara, A. C., and Fournier, D., Appl. Opt. 20, 1333, (1981)
41) Amer N. M., and Jackson, W. B., In Semiconductors and Semimetals, edited by Pankove, J.J., Academic, New York, Vol. 21b, p. 83 (1984)
42) Jackson W., and Amer, N. M., PPHYS. Rev. B 25 5559 (1982)
43) Poruba, A., Fejfar, A., Salyk, O., Vanevek, M., Kocka, J., J. Non-Crys. Solids 271, 152 (2000)
44) Vanecek, M., Kocka, J., Stucklik, J., Kozisek, Z., Stika, O., and Triska, A., Solar Energy Materials 8, 411 (1983)
45) Vanecek, M., Kocka, J., Poruba A., and Fejfar, A., J. Appl. Phys., 78 6203 (1995)
46) Beck, N., Meier, J., Fric, J., Remes, Z., Poruba A., Fluckiger, R., Pohl, J., Shah, A., Vanecek, M., J. Non-Crys. Solids 198-200, 903 (1996)
47) Wronski, C.R., Abeles, B., Tiedje, T., and Cody, G.D., Solid State Comm. 44, 1423 (1982)
48) Lee, S., Kumar, S., Wronski, C. R., and Maley, N. M., J. Non-Cryst, Solids 114, 316 (1989)
49) Gunes, M., and Wronski, C. R., Appl. Phys. Lett, 61, 678 (1992)

50) Gunes, M., Akdas, D., Goktas, O., Carius, R., Klomfass, J., and Finger, F., J. Mater. Sci: Mat. In Electr.,14, 729 (2003)

51) Ritter, D., and Weiser, K., Opt. Commun. 57, 336 (1986)

52) Rath, J. K., in Photovoltaic and Photoactive Materials-Properties, Technology and Applications, NATO Science series 2. Vol. 80 p.157-170

53) Matsumura, H., Jap. J. Appl. Phys. 25 (1986) L949

54) Mahan, A. H., Carapella, J., Nelson, B. P., Crandall, R. S., Balberg, I., J. appl. Phys. 69 (1991) 6728

55) Akdas, D., MSc thesis, Izmir Institute of Teshnology, Department of Material Science and Enginering, 2002, Izmir

56) Cody, G D., Wronski, C. R., Abeles, B., Stephens, R., and Broks, B., Solar Cells,2,227 (1980)

57) Wiedeman, S., Bennet, M.S., and Newton, J. L., Mat. Res. Soc. Symp. Proc. Vol 95, 145 (1987)

58) Cody, G. D., in: Semiconductors and Semimetals, Vol. 21B, ed. Pankove, J. I., (Academic Press, Newyork, 1984) p. 11.

59) Swanepoel, R., J. Phys. E 16, 1214 (1983)

60) Amato, G., Benedetto, G., Boarino, L., and Sagnolo, R., Appl. Phys. A 50, 503 (1990)

61) Grillo G., and De Angelis, L., J. Non-Cryst. Solids 114, 750 (1989)

62) Mai, Y., Klein, S., Geng, X., and Finger, F., Appl. Phys. Lett (2004)

63) Gross, A., Vetterl, O., Lambertz, A., Finger, F., Wagner, H., and Dasgupta, A., Appl. Phys. Lett. 79, 2841 (2001)

64) Shah, A., Vallat-Sauvain, E., Torres, P., Meier, J., Kroll, U., Hof, C., Droz, C., Goerlitzer, M., Wyrsch, N. and Vanacek, M., Mater. Sci. B, 69/70, 219 (2000)

65) Yamamoto, K., Yoshimi, M., Tawada, Y., Okamoto, Y., Nakajima, A., J. Non-Cryst. Solids 266-269, 1082 (2000)

APPENDIX A

COMPUTER PROGRAM USED FOR DBP MEASUREMENTS

The computer program used for DBP measurements was written in Objectbench software. The program firs written by D. Akdas [55] in the previous thesis study on this system and improved during this thesis study. It used to control lock-in amplifier, monochromator driver, filter driver and for data acquisition between computer and lock-in amplifier. The commands are written in regular fonts and explanations are written in italic fonts.

start: *the main loop*

graphcomment$="Comments about the graph "

sensflag=0:timeflag=0.3:oldflag=0.3

dir$="D: \" *Defines the directory that data willl be stored*

input "sample name",sampname$: filecomment$=sampname$

rem ***********************************

input "data file name",dbs$

format #1,energy["energy=","eV"],average["average current=","A"],avgdevia["angle=",""],-ratio["dc/ac=",""],absorp["absorp. coeff.=",""]

format #2,energy["energy=","eV"],curr[" current=","a"],avgdevia["angle=",""]

format #3,energy["energy=","eV"],Logaverage["average current=","A"],avgdevia["angle=",""],Logratio["dc/ac=",""],Logabsorp["absorp. coeff.=",""]

open #1, file= dir$+dbs$+".dat",desc$,overwrite

rem open #1, file= dbs$+".dat",desc$,overwrite

open #2, file= "v"+dbs$+".dat",desc$,overwrite

open #3, file= "graph_f.dat",desc$,overwrite

open #3, graph= "dualbeam",overwrite

open #3, screen

The files to store data and to use screen are defined

rem ***********************************

input "first value of energy",start *Initial values are defined*

input "step value for energy",step

input "input number of measurements for each energy",n

input "enter dc current dueto bias light(format 1e-5)",dcac

rem **

```
rem ****************************************
gosub fluxRead Flux file will be read and will be used  to normalize raw current
rem*******************************************
Lock-in amplifier will be initialized
gpibwrite(8,"OUTX 1,OVRM 1"):gpibwrite(8,"*RST"):gpibwrite(8,"*CLS"):
gpibwrite(8,"FMOD 0"):gpibwrite(8,"DDEF 1,1,0"):gpibwrite(8,"DDEF 2,1,0"):
gpibwrite(8,"ICPL 0"):gpibwrite(8,"ISRC 2"):gpibwrite(8,"OFSL 3")
gpibwrite(8,"IGND 1"):rem gpibwrite(8,"SENS 23"):gpibwrite(8,"SYNC 1")
gpibwrite(8,"OFLT 9"):gpibwrite(8,"AGAN"):gosub delay4:gosub delay4
gpibwrite(8,"ARSV"):gosub delay4:gosub delay4:gpibwrite(8,"APHS")
gosub delay4:gosub delay4:gosub delay4:gpibwrite(8,"RMOD 1")
gosub delay4:gosub delay4:gosub delay4:
rem
energy=start    the initial energy value is defined

wl=6200/energy: fark=(2.5-start) : fark=fark/(0.02) : bbb$=str$(fark) : z=val(mid$(bbb$,1,2))
loop:           the main loop of the measurement
sum=0: dvsum=0: r=0: z=z+1
rem ********************************
loopa:
r=r+1
The value of CH1 and CH2 will be read
gpibwrite(8,"OUTR? 1") : a$=gpibread$(8) :  gpibwrite(8,"OUTR? 2") : j$=gpibread$(8)
curr=val(mid$(a$,1)) : standdev(r)=curr : ? "current=",curr," A" : devia=val(mid$(j$,1))
angldev(r)=devia : ? devia : sum=sum+curr : dvsum=dvsum+devia

rem *************
write #2 The value of CH1 and CH2 wil be stored for temporary use
if timeflag=0.3 then gosub delay3msec  Here the appropriate delay is set
if timeflag=1 then gosub delay1sec
if timeflag=3 then gosub delay3sec
if timeflag=10 then gosub delay10sec
if timeflag=30 then gosub delay30sec
rem ***********************
```

if r<n then goto loopa *For each energy value n data will be read*

average=sum/n : avgdevia=dvsum/n *The current and phase averaged*

rem ***********************************

b$=str$(wl) : wv=val(mid$(b$,1,5)) : realw=2*wv

ratio=dcac/average *the value of dc current over ac current is calculated*

absorp=average/y(z) *the average raw current is divided to flux value to normalize it*

Logabsorp=0.43429489*log(absorp) *To show data on the screen in log scale*

Logaverage=0.43429489*log(average) *To show data on the screen in log scale*

Logratio=0.43429489*log(ratio) *To show data on the screen in log scale*

Write #1 *The raw current, phase, dc over ac ratio and normalized current is stored*

write #3 *The data is written on the screen in log scale*

if z=94 then goto bitti

Monochromator will be set to next energy value (wavelenght)

energy=energy-step

wl=6200/energy : c$=str$(wl) : wk=val(mid$(c$,1,5)) : filterw=2*wk

kf=wk-wv : d$=str$(kf) : kw=0.5*kf : f$=str$(kw) : wt=val(mid$(f$,1,3))

i$=str$(wt) : kg=0.3*kf : g$=str$(kg) : wy=val(mid$(g$,1,3)) : h$=str$(wy)

rem ------------------------------

if energy=1.86 then gosub ttl *Filters willl be changed*

if energy=1.36 then gosub ttl *Filters willl be changed*

if energy=1.0 then gosub ttl *Filters willl be changed*

gosub delay2

gpibwrite(14,"C") : gpibwrite(14,"E")

if energy>=0.9 then gosub shortw

if energy<0.9 and energy>0.8 then gosub midw

if energy<=0.8 then gosub longw

gosub delay

rem ********************

The fallowing delay is used to wait for saturation of signal after monochromator changed the next energy value

if timeflag=0.3 then gosub delay1sec : if timeflag=0.3 then gosub delay1sec

if timeflag=1 then gosub delay1sec : if timeflag=1 then gosub delay1sec

if timeflag=1 then gosub delay1sec : if timeflag=3 then gosub delay3sec

if timeflag=3 then gosub delay3sec : if timeflag=3 then gosub delay3sec

```
if timeflag=3 then gosub delay3sec : if timeflag=10 then gosub delay10sec
if timeflag=10 then gosub delay10sec : if timeflag=10 then gosub delay10sec
if timeflag=10 then gosub delay10sec : if timeflag=10 then gosub delay10sec
if timeflag=30 then gosub delay30sec : if timeflag=30 then gosub delay30sec
if timeflag=30 then gosub delay30sec : if timeflag=30 then gosub delay30sec
if timeflag=30 then gosub delay30sec
gosub bosoku
```

xxx=1 *The value of ac current will be read to set lock-in amplifier to the appropriate sensitivity and time constant*

```
lopsens:
gpibwrite(8,"OUTR? 1") : a$=gpibread$(8)
gpibwrite(8,"OUTR? 2") : j$=gpibread$(8)
curr=val(mid$(a$,1)) : ? "current=",curr," A"
devia=val(mid$(j$,1)) : average=average+curr
xxx=xxx+1
if xxx<6 goto lopsens
average=average/5
gosub delay : gosub delay
```

Lock-in amplifier will be set to the appropriate sensitivity and time constant will be set depending on the value of signal

```
if 4.9e-7<=average and average<1e-6 then gosub sensita :
if 1.9e-7<=average and average<4.9e-7 then gosub sensitb
if 9e-8<=average and average<1.9e-7 then gosub sensitc
if 4.5e-8<=average and average<9e-8 then gosub sensitd
if 1.5e-8<=average and average<4.5e-8 then gosub sensite
if 8e-9<=average and average<1.5e-8 then gosub sensitf
if 4e-9<=average and average<8e-9 then gosub sensith
if 1.5e-9<=average and average<4e-9 then gosub sensitk
if 7.5e-10<=average and average<1.5e-9 then gosub sensitl
if 3.5e-10<=average and average<7.5e-10 then gosub sensitm
if 1.5e-10<=average and average<3.5e-10 then gosub sensitn
if 7.5e-11<=average and average<1.5e-10 then gosub sensito
if 3.5e-11<=average and average<7.5e-11 then gosub sensitp
```

```
if 1.5e-11<=average and average<3.5e-11 then gosub sensitr
if 7.5e-12<=average and average<1.5e-11 then gosub sensits
if 3.5e-12<=average and average<7.5e-12 then gosub sensitt
if 1.5e-12<=average and average<3.5e-12 then gosub sensitab
if 6.5e-13<=average and average<1.5e-12 then gosub sensitac
if 2.5e-13<=average and average<6.5e-13 then gosub sensitad
if 8e-14<=average and average<2.5e-13 then gosub sensitae
if 1e-14<=average and average<8e-14 then gosub sensitaf
if  average<=1e-14 then gosub sensitag
if sensflag>=15  then gosub tflag300msec : if sensflag=14 then gosub tflag1sec
if sensflag=13 then gosub tflag3sec : if sensflag<13 and sensflag=>10  then gosub tflag10sec
if sensflag<10   then gosub tflag30sec
if sensflag>=15  and oldflag<>timeflag then gosub tcons300msec
if sensflag=14 and oldflag<>timeflag then gosub tcons1sec
if sensflag=13 and oldflag<>timeflag then gosub tcons3sec
if sensflag=12 and oldflag<>timeflag then gosub tcons10sec
if sensflag=11 and oldflag<>timeflag then gosub tcons10sec
if sensflag=10 and oldflag<>timeflag then gosub tcons10sec
if sensflag<10  and oldflag<>timeflag then gosub tcons30sec
rem ****************************
if timeflag=0.3 then gosub delay1sec : if timeflag=0.3 then gosub delay1sec
if timeflag=1 then gosub delay1sec : if timeflag=1 then gosub delay1sec
if timeflag=1 then gosub delay1sec : if timeflag=1 then gosub delay1sec
if timeflag=1 then gosub delay1sec
if timeflag=3 then gosub delay3sec : if timeflag=3 then gosub delay3sec
if timeflag=3 then gosub delay3sec : if timeflag=3 then gosub delay3sec
if timeflag=3 then gosub delay3sec : if timeflag=3 then gosub delay3sec
if timeflag=10 then gosub delay10sec : if timeflag=10 then gosub delay10sec
if timeflag=10 then gosub delay10sec : if timeflag=10 then gosub delay10sec
if timeflag=10 then gosub delay10sec : if timeflag=10 then gosub delay10sec
if timeflag=30 then gosub delay30sec : if timeflag=30 then gosub delay30sec
if timeflag=30 then gosub delay30sec : if timeflag=30 then gosub delay30sec
if timeflag=30 then gosub delay30sec : if timeflag=30 then gosub delay30sec
if timeflag=30 then gosub delay30sec :
```

```
if z<=93 then goto loop
bitti:
gosub delay
? "Wait 30 seconds to finish the experiment"
gosub delay
gosub back    Monochromator will be set to the initial energy value
close #1 : close #3 : stop
read dbs$+".dat",d : print d.time$
if not yesnobox("Okey?") then goto start
stop
bosoku:
gpibwrite(8,"OUTR? 1") : abc$=gpibread$(8) : gpibwrite(8,"OUTR? 2") : jbc$=gpibread$(8)
return
ttl:
gpibwrite(8,"AUXV 1,1.4") : gpibwrite(8,"AUXV 1,0.8")
return
sensita: : gpibwrite(8,"SENS 26") : sensflag=26 : return
sensitb: : gpibwrite(8,"SENS 25") : sensflag=25 : return
sensitc: : gpibwrite(8,"SENS 24") : sensflag=24 : return
sensitd: : gpibwrite(8,"SENS 23") : sensflag=23 : return
sensite: : gpibwrite(8,"SENS 22") : sensflag=22 : return
sensitf: gpibwrite(8,"SENS 21") : sensflag=21 : return
sensith: gpibwrite(8,"SENS 20") : sensflag=20  return
sensitk: gpibwrite(8,"SENS 19") : sensflag=19 : return
sensitl: gpibwrite(8,"SENS 18") : sensflag=18 : return
sensitm: gpibwrite(8,"SENS 17") : sensflag=17 : return
sensitn: gpibwrite(8,"SENS 16") : sensflag=16 : return
sensito: gpibwrite(8,"SENS 15") : sensflag=15 : return
sensitp: gpibwrite(8,"SENS 14") : sensflag=14 : return
sensitr: gpibwrite(8,"SENS 13") : sensflag=13 return
sensits: gpibwrite(8,"SENS 12") : sensflag=12 return
sensitt: gpibwrite(8,"SENS 11") : sensflag=11 : return
sensitab: gpibwrite(8,"SENS 10") : sensflag=10 : return
sensitac: gpibwrite(8,"SENS 9") : sensflag=9 : return
```

```
sensitad: gpibwrite(8,"SENS 8") : sensflag=8 return
sensitae: gpibwrite(8,"SENS 7") : sensflag=7 return
sensitaf: gpibwrite(8,"SENS 6") : sensflag=6 return
sensitag: gpibwrite(8,"SENS 5") : sensflag=5 return
shortw: gpibwrite(14,"V100,S") : gosub delay : gpibwrite(14,"G+"+d$+",S"): return
midw: gpibwrite(14,"V100,S") : gpibwrite(14,"G+"+d$+",S") : return
longw: gpibwrite(14,"V100,S") : gpibwrite(14,"G+"+d$+",S") : return
rem *******************************
tflag300msec: timeflag=0.3 : return
tflag1sec: timeflag=1 : return
tflag3sec: timeflag=3 : return
tflag10sec: timeflag=10 : return
tflag30sec: timeflag=30 : return
tcons300msec: gpibwrite(8,"OFLT 9") return
tcons1sec: oldflag=timeflag : gpibwrite(8,"OFLT 10") return
tcons3sec: oldflag=timeflag : gpibwrite(8,"OFLT 11") : return
tcons10sec: oldflag=timeflag : gpibwrite(8,"OFLT 12") : return
tcons30sec: oldflag=timeflag :gpibwrite(8,"OFLT 13") return
back: gpibwrite(14,"V120,S") : gpibwrite(14,"G-7208,S") :return
rem --------------------------------
delay0: t=time delay01:if time-t<500 then goto delay01 : return
delay: t=time delay0a1:if time-t<1000 then goto delay0a1 : return
rem -------------------------------------
delay3msec: t=time : delay111:if time-t<1000 then goto delay111: return
delay1sec: t=time : delay1sa:if time-t<1000 then goto delay1sa
 return
delay3sec: t=time : delay1:if time-t<3000 then goto delay1 :  return
delay10sec: t=time : delay133:if time-t<10000 then goto delay133 :  return
delay30sec: t=time : delay1a1:if time-t<30000 then goto delay1a1 : return
delay4: t=time : delay5:if time-t<6000 then goto delay5 : return
delay2:  t=time: delay5ed:if time-t<3 then goto delay5ed :  return
delayshort: t=time : delayshrt:if time-t<10000 then goto delayshrt :  return
delaymidle: t=time : delaymid:if time-t<60000 then goto delaymid :  return
delaylong: t=time : delayl:if time-t<150000 then goto delayl :return
```

```
arabek: t=time : delayl123:if time-t<6000 then goto delayl123 :return
fluxRead: flux file is to be read into y variable
dim y(94) : m=0 : read "D:\data2004\fx\Fx27july.dat",oku
k=0 : okut: k=k+1 : y(k)=oku(k,3) :rem print "y(",k,")",y(k)
if k<94 then goto okut : return
```

APPENDIX B

COMPUTER PROGRAM FOR CALCULATION OF α(hν) SPECTRUM

This program was written in Objectbench software and is used to calculate absolute absorption coefficient from DBP yield spectrum. It calculates the absorption coefficient based on the procedure discussed in Chapter 2.

```
filecomment$="Comments about the data"
input "data file name",dbs$ : input "tickness of the film",d
format #1,energy["energy","eV"],alfa["absolute alfa","cm^-1 "], abstr["absolute tr", " "]
open #1,file="C:\folder name\"+dbs$+".dat",desc$,overwrite
format #2, energy["energy","eV"],absalfa["absolute alfa","cm^-1 "], abstr["absolute tr", " "]
open #2,file="alfatr.dat",desc$,overwrite
format #3, energy["energy","eV"],alfalog["absolute alfa","cm^-1 "], abstr["absolute tr", " "]
open #3,file="g123.dat",desc$,overwrite
open #3, graph= "alfa tr",overwrite
Rxf=0.41: Tx=0.08
gosub troku
gosub dbpoku
maxbul:
dim z(94) : temp=0 : trmax=0 : k=0 : kars:
k=k+1
t(k)=oku(k,4)
if t(k)>trmax then gosub degistir
if k<boyut then goto kars
absolutetr:
k=0 : trfark=1000 : tx=0.08
kkk2:
k=k+1
t(k)=t(k)*0.92/trmax : fark=abs(t(k)-tx)
if fark<trfark then gosub exbul
if k<boyut then goto kkk2
Ax=1-Tx-Rxf
```

```
gosub absoltealfa
gosub alfahesapfront
gosub dosyayaz
stop
alfahesapfront: r2=0.10 : dim alfa(boyutdbp)
k=0 :
hh:
k=k+1
alfa(k)=(1/d)*(ln(0.5*((1-r2)*(1+Alf(k)/T(k))+sqrt((1-r2)*(1-
r2)*(1+Alf(k)/T(k))*(1+Alf(k)/T(k))+4*r2))))
if k<boyutdbp then goto hh
return
degistir:
trmax=t(k)
return
troku:
m=0
read "*.*",oku
boyut=oku.rows
input akl$
dim t(boyut)
dim z(boyut)
k=0
okut:
k=k+1
t(k)=oku(k,4)
rem print k,t(k)
if k<boyut then goto okut
return
dbpoku:
read "C:\OB\Data\ *.*",okudbp
boyutdbp=okudbp.rows
input akl$
dim A(boyutdbp)
```

```
k=0
okut23:
k=k+1
A(k)=okudbp(k,5)
if k<boyutdbp then goto okut23
return
exbul:
trfark=fark
ex=k
return
absoltealfa:
dim Alf(boyutdbp)
k=0
c=ex
okut23c:
k=k+1
Alf(k)=A(k)*Ax/A(c)
if k<boyutdbp then goto okut23c
return
dosyayaz:
k=0
kkk123:
k=k+1
energy=okudbp(k,1)
absalfa=Alf(k)
abstr=t(k)
alfa=alfa(k)
write #1
alfalog=log(alfa(k))
write #2
write #3
if k<boyutdbp then goto kkk123
return
```